Year : 2021

The role of EPHB2 in Ewing sarcoma

Rucci Beatrice

UNIL | Université de Lausanne
Faculté de biologie
et de médecine

UNIVERSITE DE LAUSANNE - FACULTE DE BIOLOGIE ET DE MEDECINE
Département de la Formation et Recherche
Service de Pathologie Expérimentale

The role of EPHB2 in Ewing sarcoma

THESE

préparée sous la direction du Professeur Ivan Stamenkovic
avec la collaboration du Professeur Nicolò Riggi
et de la Docteure Tugba Keskin

et présentée à la Faculté de biologie et de médecine de
l'Université de Lausanne pour l'obtention du grade de

DOCTEUR EN MEDECINE

par

Beatrice RUCCI

Médecin diplômée de la Confédération Suisse
Originaire de Lûterkofen-Ichertswil (Solothurn)

Lausanne
2021

UNIL | Université de Lausanne
Faculté de biologie
et de médecine

UNIVERSITE DE LAUSANNE - FACULTE DE BIOLOGIE ET DE MEDECINE
Département de la Formation et Recherche
Service de Pathologie Expérimentale

The role of EPHB2 in Ewing sarcoma

THESE

préparée sous la direction du Professeur Ivan Stamenkovic
avec la collaboration du Professeur Nicolò Riggi
et de la Docteure Tugba Keskin

et présentée à la Faculté de biologie et de médecine de
l'Université de Lausanne pour l'obtention du grade de

DOCTEUR EN MEDECINE

par

Beatrice RUCCI

Médecin diplômée de la Confédération Suisse
Originaire de Lûterkofen-Ichertswil (Solothurn)

Lausanne
2021

UNIL | Université de Lausanne
Faculté de biologie et de médecine

Ecole Doctorale
Doctorat en médecine

Imprimatur

Vu le rapport présenté par le jury d'examen, composé de

Directeur.trice de thèse	Prof. **Ivan Stamenkovic**
Co-Directeur.trice de thèse	
Expert.e	Prof. **Michel Duchosal**
Vice-Directeur de l'Ecole doctorale	Prof. **John Prior**

la Commission MD de l'Ecole doctorale autorise l'impression de la thèse de

Madame Beatrice Rucci

intitulée

The role of EPHB2 in Ewing sarcoma

Lausanne, le 7 octobre 2021

pour Le Doyen
de la Faculté de Biologie et de Médecine

Monsieur le Professeur John Prior
Vice-Directeur de l'Ecole doctorale

Résumé

Le sarcome d'Ewing (SE) est le deuxième cancer des os et tissus mous le plus fréquent chez les enfants et les jeunes adultes. Il s'agit d'une tumeur rare mais hautement agressive ; lorsque localisée, la survie à 5 ans dépasse le 70%, cependant ce pourcentage s'écroule à moins de 25% lorsque la tumeur devient métastatique. C'est pour cette raison que des nouvelles options thérapeutiques, idéalement ciblées contre les cellules les plus agressives et métastatiques, sont nécessaires.

Au cours de notre dernier travail (Keskin et al., 2021, joint à page 59), le récepteur Ephrin type B2 (EPHB2), membre de la famille des récepteurs tyrosines kinases, a été identifié comme étant non seulement un marqueur de mauvais pronostic chez les patients atteints du SE, mais aussi un facteur pro-métastatique au sein des cellules primaires extraites de cette tumeur. Dans ce travail, nous explorons les voies par lesquelles EPHB2 confère aux cellules du SE la capacité d'envahir.

En travaillant sur les lignées cellulaires, afin d'avoir un modèle stable et reproductible, nous avons observé que les cellules du SE ayant une perte ou une baisse d'expression d'EPHB2, perdent partiellement leur capacité d'adhésion et forment des sphères en suspension. Au vu de ces phénomènes, nous avons exploré les voies de signalisation de FAK et AKT et avons observé des changements essentiels qui varient en fonction de la lignée cellulaire utilisée.

Nous avons ensuite estimé la capacité d'invasion *in vitro* des cellules et analysé comment cette dernière change en fonction du niveau d'EPHB2, en observant que les cellules déficientes en EPHB2 ont une capacité inférieure à envahir, quelle que soit la lignée cellulaire testée. Par la suite, nous avons corrélé ce changement à une variation d'expression des gènes responsables de la transition épithélio-mésenchymateuse (TEM), qui varient en fonction de la lignée cellulaire utilisée, en acquérant soit un génotype plus épithélial, soit un génotype plus mésenchymateux, suite au knockdown d'EPHB2.

Dans l'ensemble, ces résultats soulignent l'importance de l'hétérogénéité inter-tumorale du SE et nous montrent des directions à explorer, afin de développer de nouvelles thérapies qui puissent cibler les cellules les plus agressives et diminuer idéalement le poids de la mortalité liée aux SE métastatiques.

Table of contents

List of figures

List of abbreviations

CSCs: Cancer stem cells

ECM: Extracellular matrix

EMT: Epithelial to mesenchymal transition

EPHA1: Ephrin type-A receptor 1

EPHA4: Ephrin type-A receptor 4

EPHB2: Ephrin type-B receptor 2

EPHB4: Ephrin type-B receptor 4

ETS transcription factor: Erythroblast transformation specific transcription factor

EwS: Ewing sarcoma

FAK: Focal adhesion kinase

FGFRs: Fibroblast growth factor receptors

GAP: GTPase activating protein

GEF: Guanine-exchange factor

HERs: Human epidermal growth factor receptors

HGFs: Hepatocyte growth factor receptors

IGF-1R: Insulin-like growth factor 1 receptor

MET: Mesenchymal to epithelial transition

MSCs: Mesenchymal stem cells

mTOR: Mechanistic target of rapamycin

PDGFRs: Platelet-derived growth factor receptors

PI3K: Phosphatidylinositol 3-kinase

PLC: Phospholipase C

RBPs: RNA-binding proteins

RTK: Receptor tyrosine kinase

shRNAs: short hairpin RNAs

TET family: TAF15, EWS, and TLS/FUS family

totAkt: total Akt

totFAK: total FAK

Summary

Ewing sarcoma (EwS), the second most frequent bone and soft tissue cancer in children and young adults, is a rare but highly aggressive malignancy. Local disease is currently associated with a five-year survival rate of more than 70%, but this percentage drops to less than 25% when metastases are present. For this reason, there is the necessity to find new therapies targeting the most aggressive and invasive cells.

In recent work (Keskin et al., 2021, attached at page 59), we identified the Ephrin type-B receptor 2 (EPHB2), a member of receptor tyrosine kinase (RTK) family, as a poor prognostic biomarker in EwS patients and as a strong pro-metastatic factor in primary EwS cells. In the present follow-up work, we explore the pathways that EPHB2 exploits to increase the invasiveness and metastatic proclivity of EwS cells.

Using EwS cell lines in order to rely on a well-established and stable model, we observed that, upon EPHB2 depletion, EwS cells lose their ability to attach to substrate and form clumps and spheres in suspension. In light of these observations, we explored FAK and AKT pathways and observed marked changes following *EPHB2* knockdown, with the emergence of different phenotypes according to the used cell line.

We then assessed the invasive capability of the cells *in vitro* and observed decreased spreading in each *EPHB2* knockdown model. This change correlated with a shift in the expression of genes implicated in epithelial to mesenchymal transition (EMT), which also varied according to the cell line, by adopting a predominantly epithelial or mesenchymal profile upon EPHB2 depletion.

Taken together, these results underline the importance of inter-tumor heterogeneity in EwS and point to relevant landscapes to be explored toward developing more specific therapies that could target the most aggressive and invasive cells and ideally lower the burden of metastatic EwS mortality.

Introduction

1. Ewing sarcoma (EwS)

1.1 Background

Pediatric cancer mortality is constantly decreasing thanks to improvements in therapeutic regimens and strategies. Nevertheless, tumors remain the most common cause of disease-related death in children and young adults in developed countries (1,2). These malignancies, similar to their adult counterparts, are driven by genetic mutations that transform cells and provide them with the capacity to divide indefinitely and deregulate their own biological properties. However, in contrast to adult malignancies, which are defined by multiple different mutations that accumulate over years, pediatric cancers are characterized by a small number of mutations that suffice to orchestrate cell functions required for transformation and subsequent tumor growth (3,4).

In Ewing sarcoma (EwS), the second most frequent bone and soft tissue cancer in children and young adults, the pathognomonic mutation is represented by a unique reciprocal chromosomal translocation, which in 85-90% of cases is t(11;22)(q24;q12) and leads to the fusion of *EWSR1* and *FLI1* genes. The resulting chimeric protein, EWS-FLI-1, leads to transformation of permissive cells, primarily by modifying their epigenetic status, which, in turn, activates a series of events, explained in the following sections, that promote tumor maintenance, growth and progression (5).

1.2 Pathogenesis and intra-tumor heterogeneity

As mentioned above, the mutational burden in EwS is among the lowest in all malignancies. A few mutations, including *STAG2* and *TP53* occur at late stages in a minority of tumors (6,7), but in as many as a third of EwS, the translocation leading to the *EWSR1-FLI1* fusion is the only detectable genetic event. The fusion itself may display several alternative forms, as both *EWSR1* and *FLI1* have several genomic breakpoints. Among them, the type 1

translocation, composed of the first seven exons of *EWSR1* and exons 6-9 of *FLI1,* is the most common. The second most prevalent translocation, type 2, includes exon 5 of *FLI1*. The type 3 translocation, which has a minimal prevalence, comprises the first ten exons of *EWSR1* fused to exons 6-9 of *FLI1* (Fig. 1) (8–10).

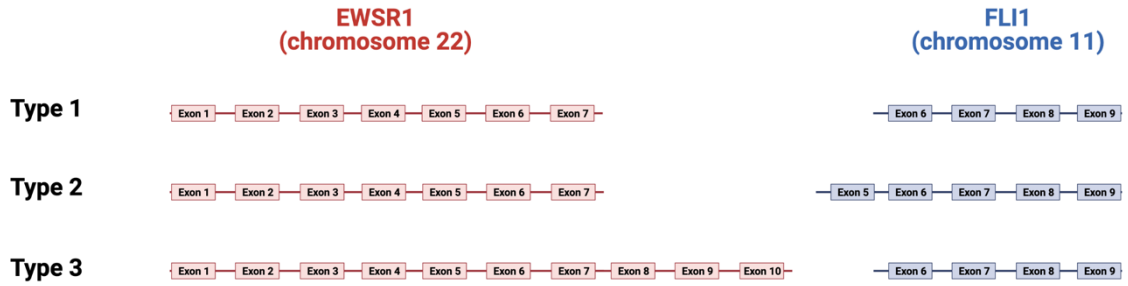

Figure 1: The three main translocation types in EwS

The three most prevalent possibilities of translocation are shown. *EWSR1* exons are presented in red, *FLI1* exons are presented in blue.

Although the majority of Ewing sarcomas are generated by the *EWSR1-FLI1* fusion gene, a minority of tumors arise as a result of other translocations. The elemental structure of these translocations is the union between a TET gene family member and a gene coding for an ETS transcription factor. TET gene family products, among which EWS is the best characterized, are implicated in both physiological and pathological events by playing an important role in cell self-renewal and meiosis (11). They are also RNA-binding proteins (RBPs), suggesting a direct implication in the regulation of RNA metabolism (12,13) that includes stability, transport and splicing. In Ewing sarcoma, the most frequently implicated TET gene family member is *EWSR1* but the FUS RNA-binding protein can be observed in less than 1% of cases (Fig. 2) (14).

Whereas the TET gene family is almost always represented by *EWSR1* within the fusion gene, the ETS factor-encoding partners are more variable. The ETS family is composed of a large number of transcription factors implicated in numerous functions, differentiation and cell cycle control being among the most prominent. Not surprisingly, their action has been associated with the development of a variety of cancers, including acute pre-B

lymphoblastic leukemia and prostate cancer (15,16). The most prevalent ETS factor in Ewing sarcoma is FLI1 (85%), followed by ERG (10%) and in a minor percentage, ETV1-4, E1AF and FEV (Fig. 2) (17–21).

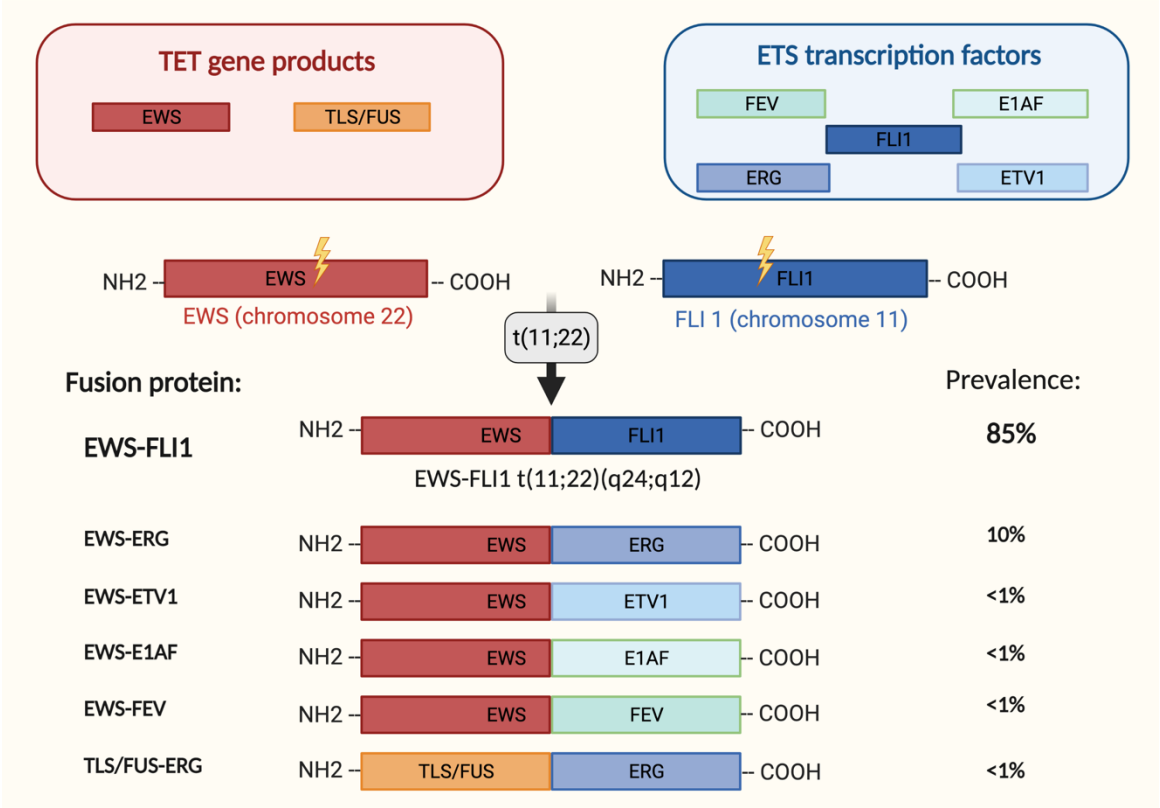

Figure 2: TET and ETS fusion proteins in EwS - adapted from reference (5)

TET and ETS family members that generate the aberrant fusion protein are shown with their respective relative frequency.

As foretold, the aberrant fusion protein is the primary driving force in EwS pathogenesis. Because of its prevalence, we will focus on the mechanisms of action of EWS-FLI-1. It has been shown that the EWS-FLI-1 fusion protein can directly activate and repress DNA transcription by modifying the chromatin state (22). To better understand such mechanisms, we need to take a step back to summarize key concepts of epigenetics.

Epigenetic regulation constitutes a powerful mechanism of transcriptional control, based on modifications that adjust chromatin structure, DNA accessibility and therefore gene expression, without changing any element in the nucleotide sequence (23). This higher-

order structure regulation justifiably attracted a great deal of scientific attention during the past few decades, as it is heritable, influenced by the environment and exploited by cancer cells. Its importance therefore cannot be overstated (24,25). Epigenetic events can lead to transcriptional changes by at least three different mechanisms: DNA methylation, histone modification (with consequent nucleosome structure adjustment), and regulatory control by non-coding RNAs (ncRNAs) (Fig. 3).

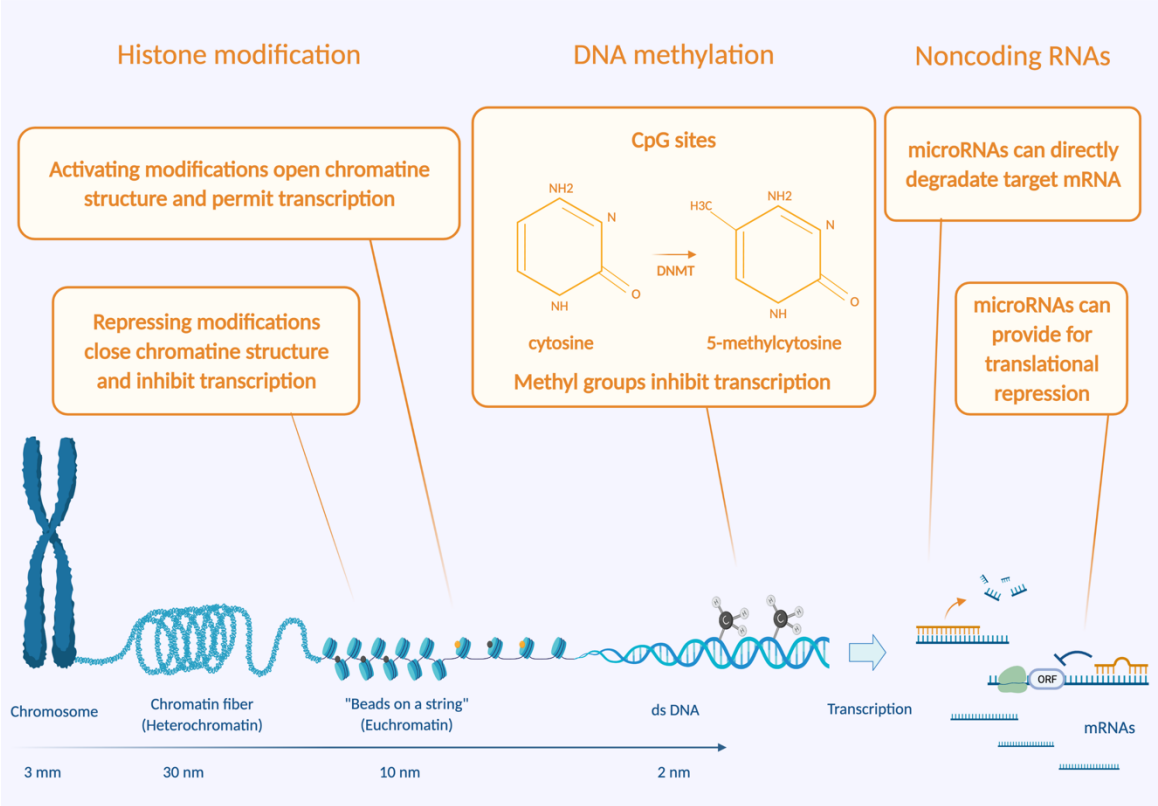

Figure 3: Epigenetic regulation of gene expression

Epigenetic regulation controls gene expression by alterations of histone modifications, DNA methylation and noncoding RNA expression.

In Ewing sarcoma, EWS-FLI-1 has been shown to alter the epigenetic status of permissive cells by using each of the above-mentioned strategies (22,26–29). EWS-FLI-1 recognizes the core GGAA motif but has markedly divergent effects according to whether it binds GGAA microsatellite repeats or single GGAA sites. Upon binding to GGAA repeats, the aberrant protein relaxes chromatin in transcriptionally silent regions of the genome to induce *de novo* enhancers that stimulate expression of oncogenes. Conversely, upon

recognizing single GGAA sequences, EWS-FLI-1 displaces wild-type resident ETS factors and closes the local chromatin structure, preventing enhancer access and leading to the silencing of the corresponding genes (22). In addition to altering chromatin structure, EWS-FLI-1 can reduce DNA methylation at the promoters of selected genes, resulting in their activation (26–28). EWS-FLI-1 also represses miRNAs implicated in cell differentiation, including miRNA-145 (29), influencing cell pluripotency. The resulting reconfiguration of a portion of the genome leads to the establishment of an oncogenic gene expression profile whose overall effect is to transform permissive cells and lead to the full-blown phenotype of EwS.

To orchestrate these major modifications of the epigenetic landscape, EWS-FLI-1 requires permissive cellular environment. Mesenchymal stem/stromal cells (MSCs) provide such a permissive context, in which the aberrant protein can successfully exert its biological properties to achieve transformation (30,31). These cells originate in the mesenchyme, the mesodermal part of the embryo that evolves into connective and skeletal tissues (32). It has been shown that MSCs harbor a loose chromatin structure at repetitive GGAA regions, which can be exploited by EWS-FLI-1. In most differentiated cells, these regions are associated with heterochromatin and are thereby inaccessible to transcription factors. In such conditions, EWS-FLI-1 cannot find an available binding site to fulfill its oncogenic role (33).

Because EWS-FLI-1-mediated modification of chromatin spreads across a sizeable portion of the genome, the expression of hundreds of genes is affected and it appears to be clear that no single EWS-FLI-1 target gene alone bears responsibility for the emergence of EwS. Instead, the transcriptome resulting from the structural reconfiguration of parts of the genome in permissive cells initiates the oncogenic program. Nevertheless, the contribution of several Individual genes toward EWS-FLI-1-mediated tumorigenesis has been elucidated (34). Thus, *SOX-2,* which plays a prominent role in the maintenance of pluripotency in normal stem cells, has been shown to participate in the transformation of MSCs toward EwS. More specifically, SOX-2 at least partially reiterates its physiological function by providing the transformed cells with a degree of pluripotency that gives them attributes of cancer stem cells (CSCs). Expression of SOX2 in transformed MSCs is induced by at least

two mechanisms: directly by EWS-FLI-1 and by the repression of mi-RNA145 (29). The transformed MSC-derived CSCs give rise to a heterogeneous tumor mass composed of cells with diverse properties and varying degrees of differentiation most of which no longer display tumorigenic properties. The CSCs, however, express high levels of *OCT4* and *NANOG*, allowing them to maintain pluripotency as well as to initiate and sustain tumor growth. In EwS, these cells express the CD133-Prominin-1 marker, and represent 4-15% of the tumor cell mass (31).

1.3 Clinical features

Children and young adults affected by EwS may present a painful local swelling, often initiated by minor trauma. The level of pain varies depending on patients - it can be mild, increased at night or by exercise whereas some patients don't even experience pain at all. In such patients, the only sign may be the discovery of a firm mass, often surrounded by erythema (5,35). This mass can occur in any part of the skeleton but has a predilection for the pelvis and proximal long bones. Although primary soft tissue localization is limited to a small fraction of the tumors (20%), Ewing sarcoma has been documented in numerous organs (Fig. 4). In advanced disease, local symptoms may be accompanied by constitutional signs, such as fever, fatigue and weight loss (5,35). Biological tests may show elevated levels of non-specific inflammation markers, including serum lactate dehydrogenase (36). Stronger hints leading to the diagnosis include three typical radiologic findings in the involved bone: the "moth-eaten" appearance, constituted by multiple lytic and confluent lesions; Codman's triangle and the onion peel image, representing respectively the displaced periosteum and its consequent regenerative reaction due to the sub-periosteal tumor growth (Fig. 4). Moreover, a pathologic fracture can be observed in 10-15% of cases (5,35).

Definitive diagnosis is provided by histological and molecular examination of tissue specimens obtained by biopsy or following surgery. Ewing sarcoma morphology is characterized by sheaths of poorly differentiated small round blue cells with a prominent nucleus and scant cytoplasm that sometimes led to misdiagnosis as lymphoma prior to the discovery of the chromosomal translocations that are unique to Ewing sarcoma (Fig. 4). It

is the detection of these pathognomonic translocations (*EWSR1-FLI1* and others, discussed above) by fluorescence in situ hybridization (FISH) of by polymerase chain reaction (PCR) that allows the definitive diagnosis (5,11).

Several factors influence prognosis. Among them, presence of metastases at the time of diagnosis plays the most important role: local disease treated by multimodal therapy currently has a five-year survival rate of more than 70%. In contrast, when metastasis is present, this percentage drops to less than 25%. Metastases occur most frequently in the lungs, bone and bone marrow (5,37). Novel treatment strategies should therefore focus on targeting cells that are more prone to spread and metastasize.

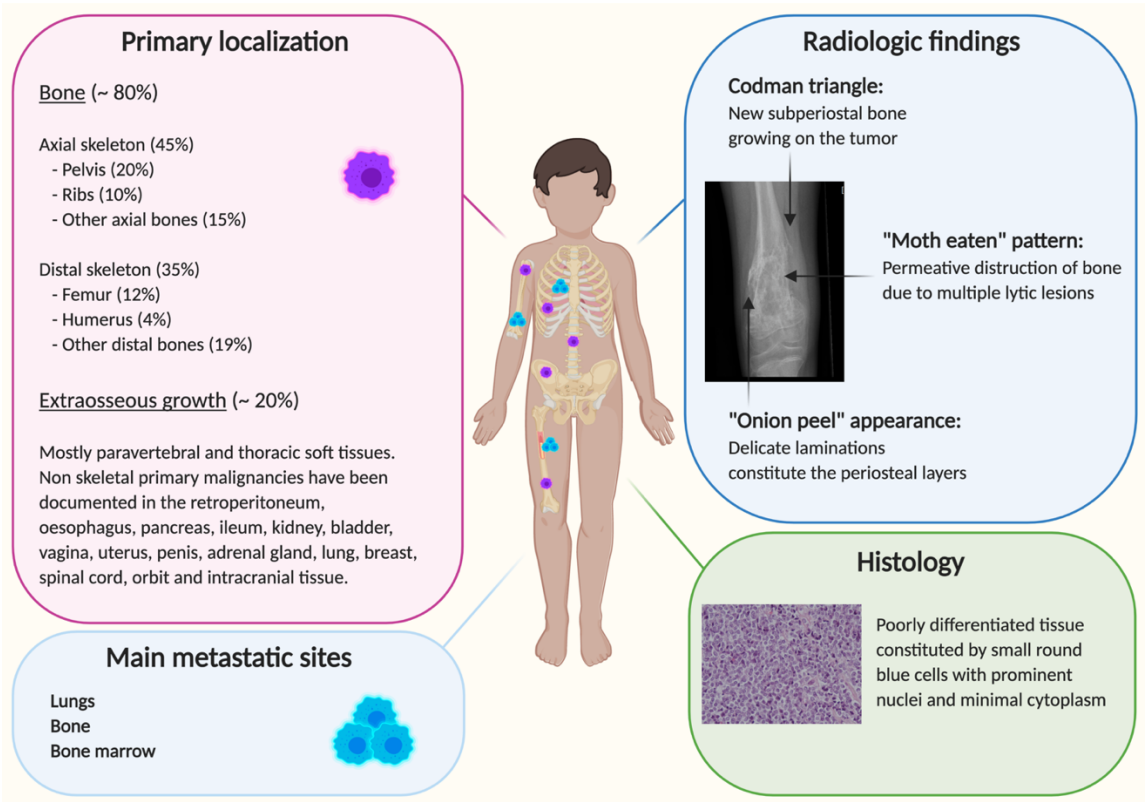

Figure 4: Clinical features of EwS - adapted from reference (5)

Most common primary and metastatic EwS sites are shown, along with radiologic patterns and histologic features (hematoxylin and eosin).

Multidisciplinary treatment for Ewing sarcoma currently involves surgery, chemotherapy and radiotherapy. Despite the fact that most patients present local disease at the time of

diagnosis, the majority present recurrence. These tumors are always considered to have subclinical metastasis, for which neoadjuvant and adjuvant chemotherapy is given. Regimens include doxorubicin, etoposide, cyclophosphamide, vincristine and ifosfamide, with different doses, combinations and schedules, according to a variety of protocols. Local treatment is based on surgery and/or radiotherapy, according to feasibility (5,38).

Frontline therapy is then limited and although local disease has largely taken advantage of improved strategies, treatment for relapsing and metastatic cases clearly remains unsatisfactory. Several potential targeted therapies have been studied during last 50 years, including the attempt to directly target the fusion protein, the use of PARP inhibitors, insulin-like growth factor 1 receptor (IGF-1R) antibodies and mechanistic target of rapamycin (mTOR) pathway blockade. No striking results have been observed with any of these approaches. Arguably, the most disappointing observation is that the fusion protein itself cannot be targeted with current means because of its structural features (39). Immunotherapy, also appears not to be a relevant option based on the observation that EwS is poorly immunogenic (5,40).

The lack of success of targeted therapies thus far and the unresponsiveness of relapsed and metastatic tumors to conventional therapy call for a revision of our perspective and our approach. A potentially important lead is the discovery of intra-tumor heterogeneity, dictated, at least in part by CSCs. As only a fraction of cells in EwS appears to harbor tumor initiating properties, a seemingly rational approach would be to identify the biological features of these cells that are amenable to neutralizing therapy.

2. A reporter system to identify the most relevant cells in terms of tumor initiation and maintenance

To identify the cells that have tumor initiating and disseminating properties and thereby constitute the driving force of the tumor, we designed a functional live cell reporter system. Current identification of CSC in most tumors relies on the expression of single or a combination of cell surface markers (CD133 in EwS, colon carcinoma, glioblastoma; $CD44^{high}/CD24^{low}$ in breast carcinoma, etc.) none of which are specific. Moreover, cell

populations expressing these markers are typically only enriched in CSCs but most likely do not encompass all of the cells with tumor initiating properties. Furthermore, marker expression may change during *in vitro* culture. Robust identification of the most relevant cells in any tumor should therefore rely on a functional attribute that reflects their behavior, independent of any loosely associated cell surface marker. To this end we developed a functional live cell reporter system based on the expression of miRNA-145, which my lab has previously shown to be implicated in the maintenance of EwS tumor initiating cells (29). MiRNA-145 is repressed in normal stem cells and its expression increases with differentiation, to which it contributes by repressing genes associated with pluripotency (29). We therefore expressed in primary EwS cells a green fluorescent protein (GFP) sequence with a 3' untranslated region (UTR) designed to contain 5 miRNA-145 recognition motifs. In cells expressing miRNA-145, the GFP should be silenced whereas it should be fully expressed in cells with very low on no miRNA-145 expression. The reporter should therefore allow relatively straightforward separation of pluripotent tumor initiating cells expressing GFP from more differentiated and poorly tumorigenic "dark" (GFP-negative) cells. Indeed, this turned out to be the case and we could readily characterize the biological properties and the transcriptome of the GFP positive cells. Details of this work can be found in the attached publication (page 59). Importantly, characterization of GFP positive cells led to the identification of the EphrinB2 receptor expressed on their surface, which we then showed to play a pivotal role in the ability of these cells to disseminate and form metastases. In the follow-up of this work, which constitutes my MD thesis, I addressed the mechanisms by which EphrinB2 expression might facilitate EwS metastasis.

3. EPHB2 receptor

3.1 Eph receptors biology and their role in cancer

Eph receptors belong to the receptor tyrosine kinase (RTK) family. This large family is composed of heterogeneous cell surface receptors most of which bind soluble cytokines, growth factors and hormones with high affinity although some RTKs recognize other cell surface receptors as ligands.

In essence, when the ligand binds to the extracellular region of the RTK, it induces receptor oligomerization that initiates kinase activity. The downstream signals triggered by this interaction regulate diverse physiological processes, including the cell cycle, metabolism, differentiation, adhesion and migration (41). It is therefore not surprising that RTKs play an important role in cancer development. Mutations in the kinase but also the extracellular domain can cause them to become constitutively active and promote cell proliferation, migration, invasion but also drug resistance in a ligand-independent manner (42).

The role of several RTKs in EwS development has been widely interrogated. Several studies have shown that IGF-1R activation is required for transformation of permissive cells and confers to EwS cells the capacity to withstand anticancer drug toxicity. Not surprisingly, IGF-1R is upregulated in the large majority of EwS (43–45), in addition to fibroblast growth factor receptors (FGFRs), human epidermal growth factor receptor (EGFR) and platelet-derived growth factor receptors (PDGFRs). All these receptors have been targeted in pre-clinical and clinical studies but only partial and transient responses were observed (46).

Eph receptors are the largest and arguably the most convoluted sub-group of the RTK family and their complexity may be one reason why they have not been extensively explored in the context of EwS pathogenesis. The first property that confers their intricacy to Eph receptors is their ability to orchestrate bidirectional signaling: an Ephrin ligand-expressing cell provides a forward signal to an Eph receptor-expressing cell, which depends on Eph kinase activity; in parallel, the latter provides a reverse signal, which takes advantage of Src family kinase action (47). Once these signals are initiated, downstream

changes in the activity of small GTPases trigger cytoskeletal rearrangements and promote cell-cell adhesion or repulsion. For these reasons, Eph receptor signaling is critical for physiological neuron migration, vascular remodeling and bone development. Because many cell types require adhesion to substrate in order to grow, regulation of their adhesiveness is one mechanism by which Eph receptors signaling controls cell proliferation and survival (48).

Their capability to control cell adhesion makes Eph receptors ideal candidate executors of tumor cell needs. In fact, numerous Eph receptors are expressed in most cancer cells but their presence has been linked to both cancer progression and quiescence (Fig. 5) (49). Moreover, both increased and decreased Eph receptor expression has been associated with tumor aggressiveness (49). Thus, *EPHA2* expression correlates with increased aggressiveness and poor clinical outcome in diverse cancer types (50) and *EPHB4* expression is linked to tumor progression (51). Conversely, poor survival in colorectal cancers is associated with downregulation of *EPHA1* (52) and metastatic lung tumors express less *EPHB6* than non-metastatic counterparts (53). Moreover, Eph receptor expression seems to decrease in late tumor stages, as if the malignancy calibrates Eph receptor use up to a critical point of necessity (49). Several studies exploring the relationship between tumorigenicity and Eph receptor signals underline the importance not only of their expression in malignant cells, but also in the tumor microenvironment (54). For example, EPHA2 signaling in endothelial cells has been shown to improve VEGF-mediated angiogenesis (55), whereas EPHA3 inhibition leads to stromal microenvironment disruption with consequent tumor growth inhibition (56).

a

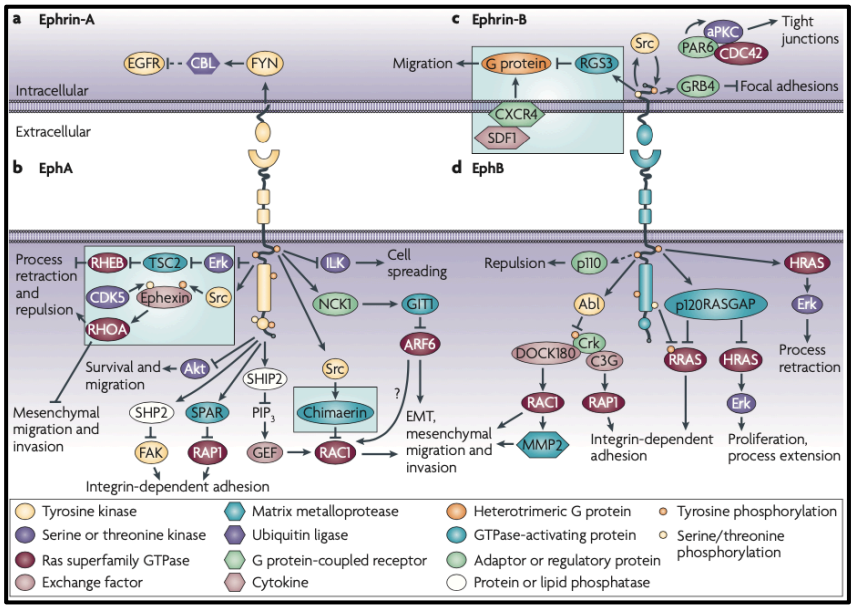

b

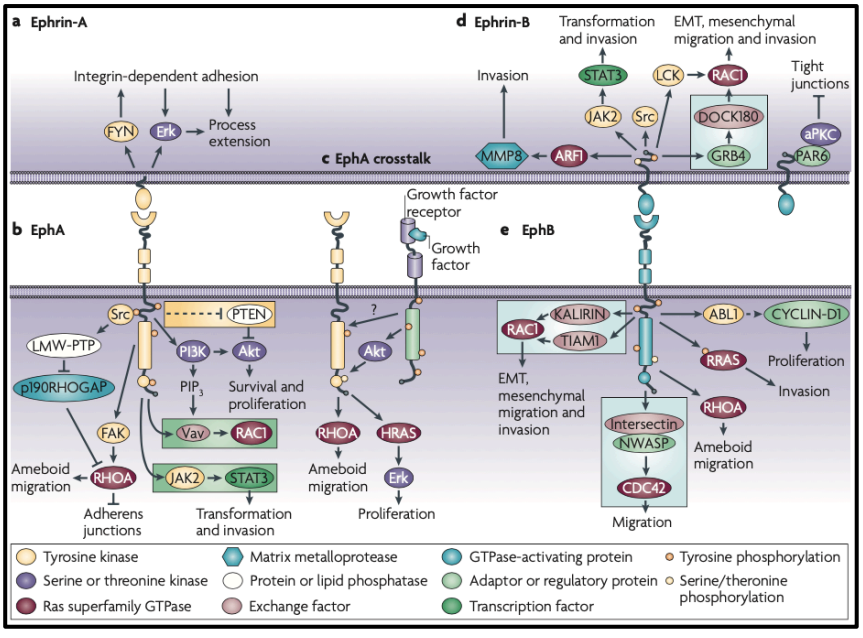

Figure 5: Tumor suppression (a) and tumor promotion (b) through EPH receptor bidirectional signaling – from reference (49)

The complexity of bidirectional pathways is shown for both cancer progression and suppression.

3.2 EPHB2

EPHB2 is a transmembrane receptor that has been largely studied in neural pathophysiology. Its significance in cancer development remains relatively obscure, with several contradictory observations, according to cancer type. For example, in colon cancer, EPHB2 cytoplasmic signaling has been shown to promote proliferation by inducing cyclin D1 activity via c-Abl, while repressing migration through an independent pathway (57). *EPHB2* expression has also been directly correlated with cell proliferation in ependymoma (58). In contrast, EPHB2 decreases proliferation but promotes invasiveness in cholangiocarcinoma (59). Similarly, invasion seems to be increased by *EPHB2* expression in cervical cancer (60), medulloblastoma (61) and glioblastoma (62,63), whereas in skin squamous cell carcinoma, *EPHB2* knockdown does not seem to change cell viability or migration, but leads to increased Epithelial to Mesenchymal Transition (EMT) (64). This tumor type-dependent dichotomy in EPHB2 behavior underlines the necessity for a deeper understanding of its physiopathology in cancer as well as of the landscape in which the receptor is operating. Downstream pathways of EPHB2 signaling in cancer that are relevant to tumor cell migration, adhesion and invasion include focal adhesion kinase (FAK) activation (59,62), which will be introduced in the next section.

4 Integrin mediated cell adhesion: the central role of FAK

4.1 Integrins and FAK biology

To fulfill their physiological needs, cells need to communicate with the extracellular matrix (ECM), a substrate composed of a multitude of elements, including collagens, and a host of diverse glycoproteins and enzymes that provide structural and nutritional support to cells (65). Cell interaction with the ECM is mediated primarily by integrins, a large family of cell surface adhesion receptors.

Integrins are heterodimeric transmembrane receptors that grant, as their name suggests, the integration between extracellular ligand-initiated signals and cytoskeletal adaptor protein effector functions (66). Once they are stimulated by external signals, integrins

activate several intracellular pathways that support cell-matrix adhesion, actin filament polymerization and guanine-exchange factor (GEF) as well as GTPase activating protein (GAP) activity (65).

A major player in the coordination of integrin-mediated signals is Focal Adhesion Kinase (FAK), a large cytoplasmic tyrosine kinase that orchestrates the establishment and implementation of a complex signaling platform (Fig. 6). Once integrins are activated by their ligands, the adaptor proteins paxillin and talin are instructed to recruit FAK to the cell membrane, with the help of vinculin (67). FAK activation is reflected by the phosphorylation of multiple residues, the key being Tyr397 autophosphorylation, which recruits Src family kinases and initiates phospholipase C (PLC) and phosphatidylinositol 3-kinase (PI3K) activity; and Tyr576/577 phosphorylation that guarantees maximal catalytic activation. At least two more residues that undergo phosphorylation deserve to be mentioned: Tyr925, responsible for the activation of the Grb2/Ras/MAPK pathway and Tyr861, which allows p130Cas binding to proline-rich regions (68).

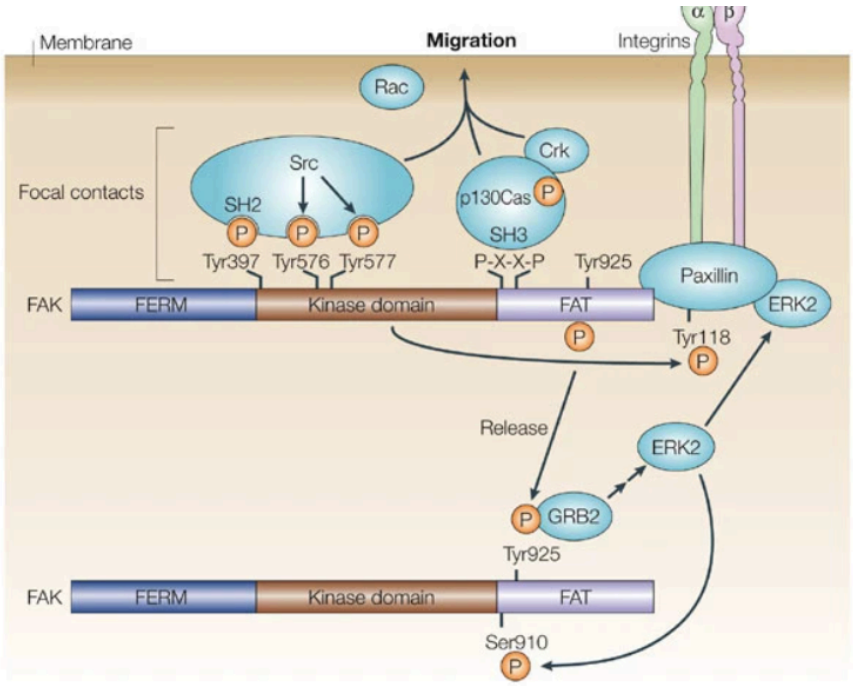

Figure 6: FAK signals that regulate cell's migration – from reference (67)

A schematic view of FAK interactions and main phosphorylation sites.

The activation of this complex machinery is essential for several key intracellular physiologic events, including microtubule stabilization that maintains cell polarity and appropriate turnover of membrane components that ensure its integrity (67). Arguably, the most relevant aspect of FAK downstream signaling in cancer development lies in its role in cell adhesion and motility, but possibly also in survival (67,69).

4.2 Cancer cell adhesion and the role of FAK

The balance between adhesion and detachment needs to be finely regulated in cancer cells. On the one hand tumor cells require attachment to the ECM for proliferation and invasion, whereas on the other they must be able to detach from the substrate to disseminate. The importance of FAK in tumor development and progression therefore cannot be overstated.

Cancer cells have been widely shown to take advantage of the FAK signaling hub for adhesion and migration. Initially, FAK expression was shown to be increased in invasive epithelial neoplasms (70) and in high grade and metastatic sarcomas (71). Several studies in various malignancies showed a direct correlation between FAK expression and poor prognosis (72). Subsequently, research focused on Tyr397 autophosphorylation and on how its disruption might inhibit tumor growth (73–77).

FAK phosphorylation and activity have been addressed in EwS pathogenesis and it has been shown that different EwS cell lines display divergent FAK phosphorylation levels (78). Moreover, in recent years, FAK has been shown to confer pro-migratory and antiapoptotic properties in both EwS cell lines and primary tumors (79) that can be thwarted by FAK inhibitors (80–82). Taken together, these results point to a potentially interesting pathway to target in EwS therapy.

4.3 FAK and PI3K/AKT/mTOR pathway

Among the cardinal pathways that lead to cell survival, in both physiological and malignant conditions, a central role is played by PI3K/AKT/mTOR signaling, which is also key in the regulation of cell growth, metabolism, and cytoskeletal structure organization (83). Under physiological conditions, FAK and AKT cooperate in the regulation of adhesion mechanisms and mechanical signals in cells from all tissues, including bone (84,85). In tumor cells, they have been shown to collaborate for promoting migration and invasion (86–88) . This cooperation has been studied in EwS cell lines, where inhibition of the FAK pathway led to the loss of AKT phosphorylation and induced both cell cycle arrest and inhibition of invasion (81). The AKT pathway is therefore activated downstream of the FAK machinery and may constitute a potentially attractive target in EwS cells. Exploration of the downstream effects of FAK/AKT activation revealed an association with Epithelial to Mesenchymal Transition (EMT) (89,90), which will be treated in the following chapter.

5 EMT: an important step for metastatic spread

5.1 EMT

When studying tumor dissemination and metastasis, it is essential to mention EMT and its importance in the context of tumor cell migration and invasion. In order to detach from the primary mass and spread to the circulation and distant organs, the cancer cell needs to orchestrate structural and functional changes that allow its passage through blood and lymphatic vessels. A tumor cell of epithelial origin first needs to lose its static epithelial features and adopt more motile properties that are typically associated with mesenchymal cells. This means decreasing intercellular adhesion and expressing receptors and intracellular machinery related to migratory properties, which together facilitate detachment from the primary site and penetration of as well as survival within the systemic circulation. At a later time, when the cell extravasates into a secondary site following immobilization on capillary endothelium, these mesenchymal features must be reconverted into epithelial ones to allow the cell to divide and create its own new colony. The latter mechanism is known as Mesenchymal to Epithelial Transition (MET) and

illustrates the transience and reversibility of EMT, which plays an essential role in normal development and wound healing.

The complex phenotypic changes that constitute EMT are driven by a cluster of transcription factors, including SNAIL, SLUG, TWIST, ZEB and several others (91). Activity of these factors ensures appropriate gene expression changes that repress epithelial features, including expression of E-cadherin and cytokeratins and apico-basal polarity, while inducing expression of vimentin, N-cadherin, migration-promoting integrins and a variety of proteolytic enzymes, including MMP-2, MMP-9 and several other.

5.2 EMT in EwS

EMT-related phenomena have been widely studied and understood in adult epithelial neoplasms but also in pediatric malignancies (91,92). However, the relevance of EMT in sarcomas may be subject to scrutiny. Because the origin of these malignancies is by definition mesenchymal, it seems surprising that such cells might adopt an even more marked mesenchymal state. This field of study is evolving and results are suggesting that sarcoma cells show bi-phenotypic morphology within the epithelial/mesenchymal spectrum, which depends, in part, on the degree of tumor progression, particularly as related to metastases (92–94).

In Ewing sarcoma, single cell transcriptome analysis has suggested that the *EWSR1-FLI1* expression level may be directly related to the EMT/MET balance. High *EWSR1-FLI1* expression has been linked to a more epithelial phenotype, induced when high proliferation is needed. Conversely, low *EWSR1-FLI1* expressing cells adopt a more mesenchymal phenotype that provides for increased motility and invasion (95). Moreover, inter-tumoral heterogeneity has been shown among different EwS patient samples regarding epithelial and mesenchymal gene expression, with contrasting prognostic value (96).

Because tumor invasiveness seems to be the main obstacle toward EwS patient survival, the downregulation of genes associated with the mesenchymal phenotype in EwS cells may appear as a possible strategy to decrease cell migration and improve outcome. Among encouraging pre-clinical results, Zeb2 depletion led to a reduced metastatic potential of EwS cell lines injected into mice (97). In the same direction, in EwS tumor xenografts in mice, TWIST1 knockdown promoted metastasis suppression, while its overexpression activated invasion. In this study, TWIST 1 expression was directly linked to metastatic capability, without affecting primary tumor growth (98).

6. Aim of study

In the present project, which stemmed from our recent work briefly introduced above (Keskin et al., 2021), we aimed to explore the abovementioned pathways in the relation to EPHB2 expression in EwS pathogenesis. In the publication, to which I contributed as 2nd author and generated data that are depicted in Figures 6 and 7, we reported a direct correlation between EPHB2 expression and poor prognosis of EwS, as well as a functional implication of EPHB2 in inducing a pro-metastatic state in primary EwS cells. Here, we investigated the mechanisms by which EPHB2 contributes to the biology of EwS and show that its expression may lead to increased invasiveness. We believe that the discovery of EPHB2 signaling as a means to promote EwS metastasis provides a significant contribution to the EwS field by identifying a potentially important therapeutically targetable mechanism of tumor aggressiveness.

Results

1. *EPHB2* expression in EwS

As discussed in the introduction, metastatic cases of EwS have a 5-year survival rate of less than 25%, which underlines the necessity to find functionally relevant pro-metastatic markers that could be targeted to inhibit or prevent malignant spread. Therefore, we addressed the possible correlation between *EPHB2* expression and survival of EwS patients. We found that patients with higher *EPHB2* expression have poorer prognosis for both event-free and overall survival (Fig. 7).

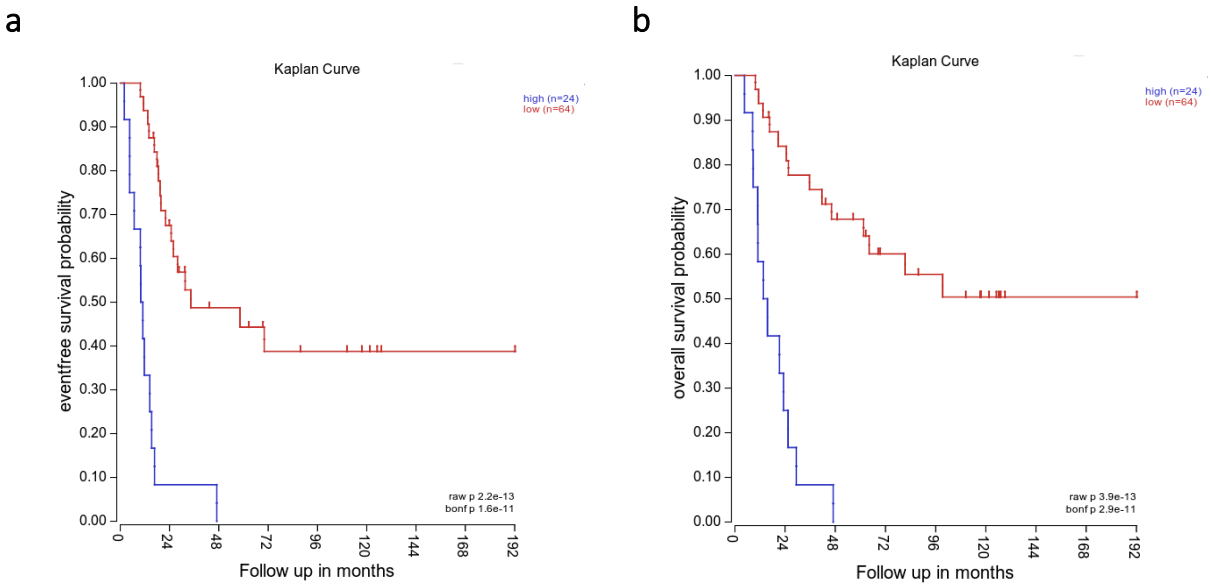

Figure 7: EPHB2 expression correlation with survival in EwS patients

Event-free (a) and overall survival (b) probability according to EPHB2 expression are shown.

In our recent work (Keskin et al., 2021), we discovered that EPHB2 is an independent marker of tumor cell aggressiveness in EwS and showed that its expression strongly promotes their metastatic capability. Once we observed the impressive difference in metastatic proclivity between high and low *EPHB2* expressing cells, we assessed the function of primary EwS cells depleted of and overexpressing *EPHB2*. We observed an impaired ability of EPHB2-depleted cells to initiate tumor growth *in vivo* and the capability to form macro-metastasis *de novo* of EPHB2 overexpressing cells.

In the present work, we therefore interrogated the mechanisms by which EPHB2 confers pro-metastatic power to cells and explored a panel of available EwS cell lines to establish a stable model to help define such mechanisms. We first assessed EPHB2 expression in several EwS cell lines (Fig. 8). We found that among different tested cell lines, TC71 have the highest EPHB2 expression level, followed by RDES, A673 and SK-N-MC (Fig. 8). We proceeded with the study of EPHB2 function in TC71 cells.

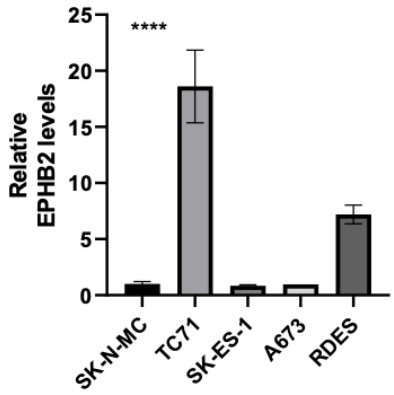

Figure 8: *EPHB2* relative expression in EwS cell lines

EPHB2 relative expression was assessed by qPCR, GAPDH expression was used as internal control. Error bars indicate standard deviations.

2. *EPHB2* knockdown leads to phenotypic and protein changes in TC71 cells

First, we succeeded at obtaining partial EPHB2 depletion using lentiviral vectors carrying 2 different *EPHB2*-specific short hairpin RNAs (shRNAs, sh1 and sh2) in TC71 cells, and we confirmed the knockdown at both the RNA and protein levels (Fig. 9 a, b). Compared to controls, cells depleted of EPHB2 showed decreased capability to adhere to culture dishes and began growing in suspension by forming clumps and spheres (Fig. 9 c).

a

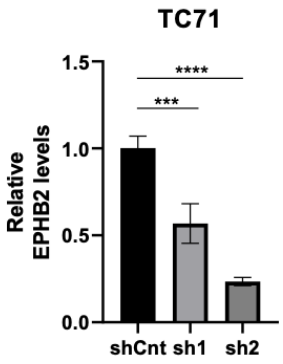

b

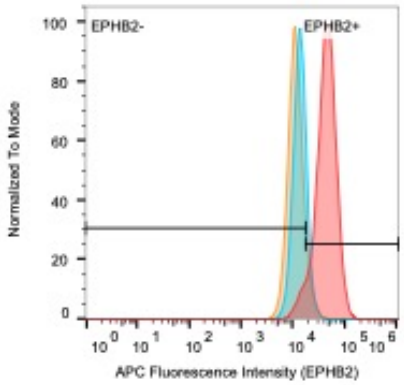

Sample Name	EPHB2- :: Freq. of Parent	EPHB2+ :: Freq. of Parent	EPHB2+ :: Median : FL6-A
TC71 shCnt	4.59	95.4	45656
TC71 sh1	76.8	23.2	19002
TC71 sh2	87.2	12.8	19458

c

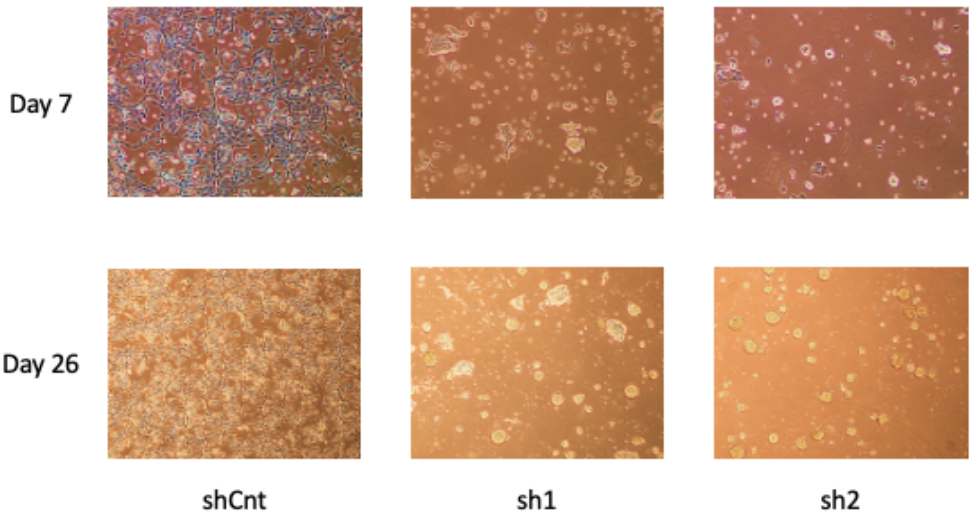

Figure 9: Knockdown confirmation and phenotypic changes upon EPHB2 depletion in TC71 cells

9a: Knockdown confirmation at the transcription level by qPCR, GAPDH expression was used as an internal control. Error bars indicate standard deviations. 9b: Knockdown confirmation at the protein level by FACS. 9c: TC71 cells detach from the culture plate surface and form spheres upon EPHB2 depletion. Images taken at 10x magnification on day 7 (Day 7, top) and day 26 (Day 26, bottom) after infection.

Considering the key role of integrins in adhesion and the consequent FAK activation, we hypothesized that EPHB2 activity, like that of other RTKs, may lead to FAK activation and therefore provide for increased adhesiveness. We therefore analyzed the FAK phosphorylation profile in TC71 cells and found that FAK Tyr397phosphorylation was completely lost upon EPHB2 depletion, whereas the total FAK content was only slightly decreased (Fig. 10 a). To verify that the loss of phosphorylation was due to EPHB2 depletion and not merely to the suspended state of cells, we cultured TC71 cells in suspension and used them as a control sample. Control cells grown in suspension showed decreased FAK phosphorylation, but not the complete loss observed upon EPB2 depletion (Fig. 10 a).

Next, we assessed the activation of the AKT pathway. The interactions between FAK and AKT have been shown to increase upon cell adhesion (81). We found decreased phosphorylation of AKT Ser473 (a marker of AKT activation) upon EPHB2 depletion (Fig. 10 b), whereas suspension growth conditions did not affect AKT Ser473 phosphorylation (Fig. 10 b). Therefore, we can conclude that the dramatic reduction in AKT Ser473 phosphorylation level is due to EPHB2 depletion in TC71 cells.

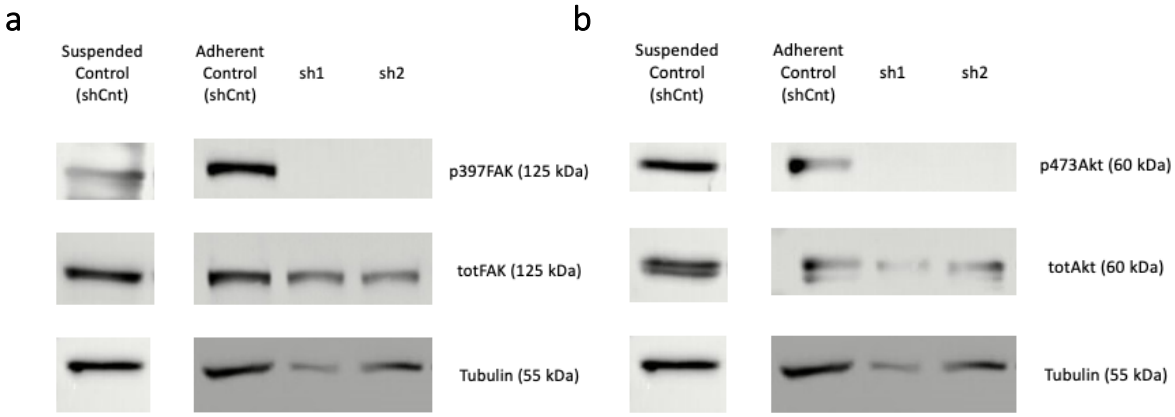

Figure 10: FAK and AKT pathways changes following EPHB2 depletion in TC71 cells

10a: Total FAK protein (totFAK) and its phosphorylation at tyrosine 397, as tested by Western Blot. 10b: Total AKT protein (totAKt) and its phosphorylation at serine 473, as tested by Western Blot.

3. From adhesion to invasion: EPHB2 depletion decreases migration of TC71 cells and leads to Mesenchymal to Epithelial Transition (MET)

In light of the decreased adhesion observed upon EPHB2 depletion, as well as of decreased activation of FAK and AKT pathways, we investigated whether EPHB2 depletion affects the invasion capacity of the cells. We cultured TC71 cells in serum-free medium in the upper chamber of a Matrigel® invasion device while the lower chamber contained serum-supplemented medium, in which the serum serves as a chemoattractant. After 44hr, cells that had migrated to lower chamber through Matrigel® membrane were counted (Fig. 11 a). We found that Ephb2 depletion markedly impaired the invasion capacity of TC71 cells (Fig. 11 b).

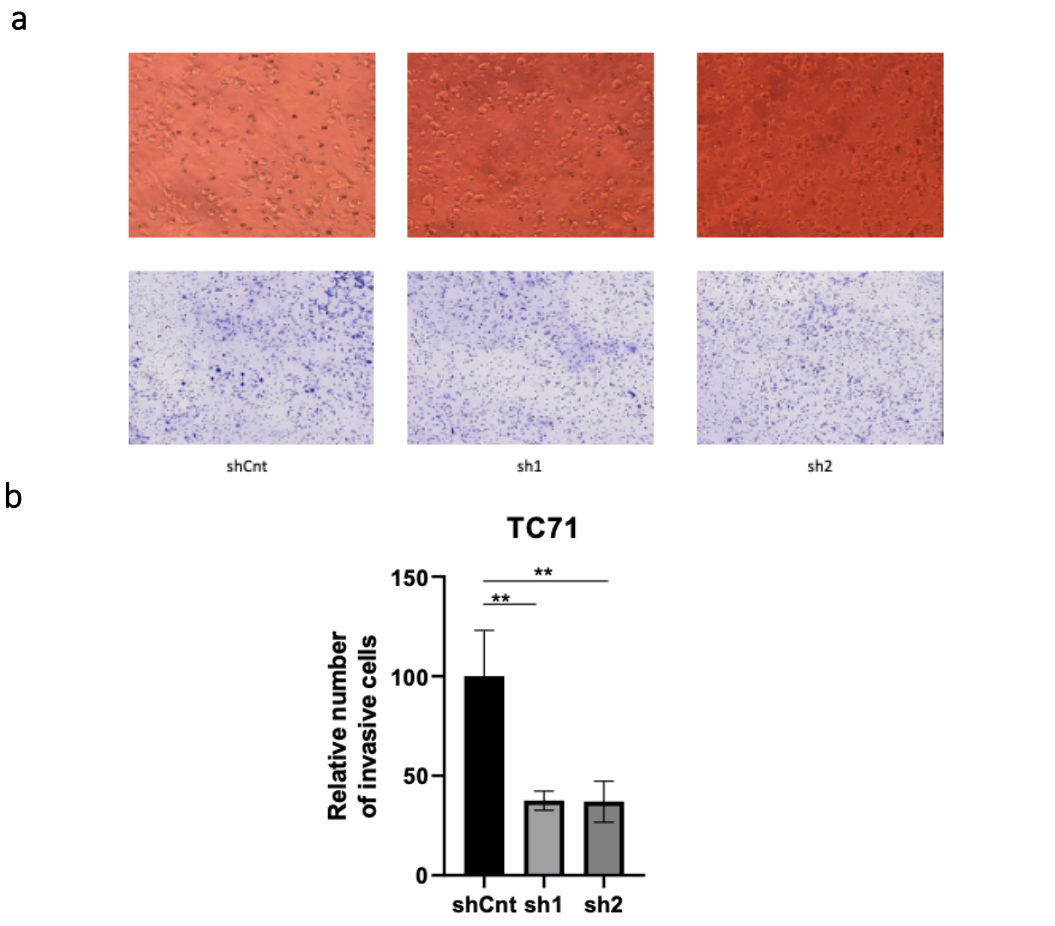

Figure 11: EPHB2 depletion reduces invasion capability of TC71 cells

11a: Matrigel® invasion chambers before (top) and after (bottom) staining at 4x magnification. 11b: Relative invasion capability for knocked-down cells with both shRNAs compared to control. Error bars indicate standard deviations.

We further investigated the mechanisms by which EPHB2 may confer an invasive phenotype to cells and found striking differences between EPHB2-depleted and control cells in terms of EMT gene expression. *EPHB2* knockdown decreased the expression of *N-cadherin*, *Snail1*, *MMP2*, *Zeb1*, *Zeb2*, while increasing the expression of *E-cadherin* (Fig. 12). To exclude the possibility that the expression of these genes changed merely as a result of growth in suspension of EPHB2-depleted cells, we grew wild type TC71 cells (wt TC71) in two different conditions (adherent plate and suspension flask) and assessed the expression of the EMT gene panel. Both growth conditions showed similar profiles for each tested EMT gene (Fig. 13).

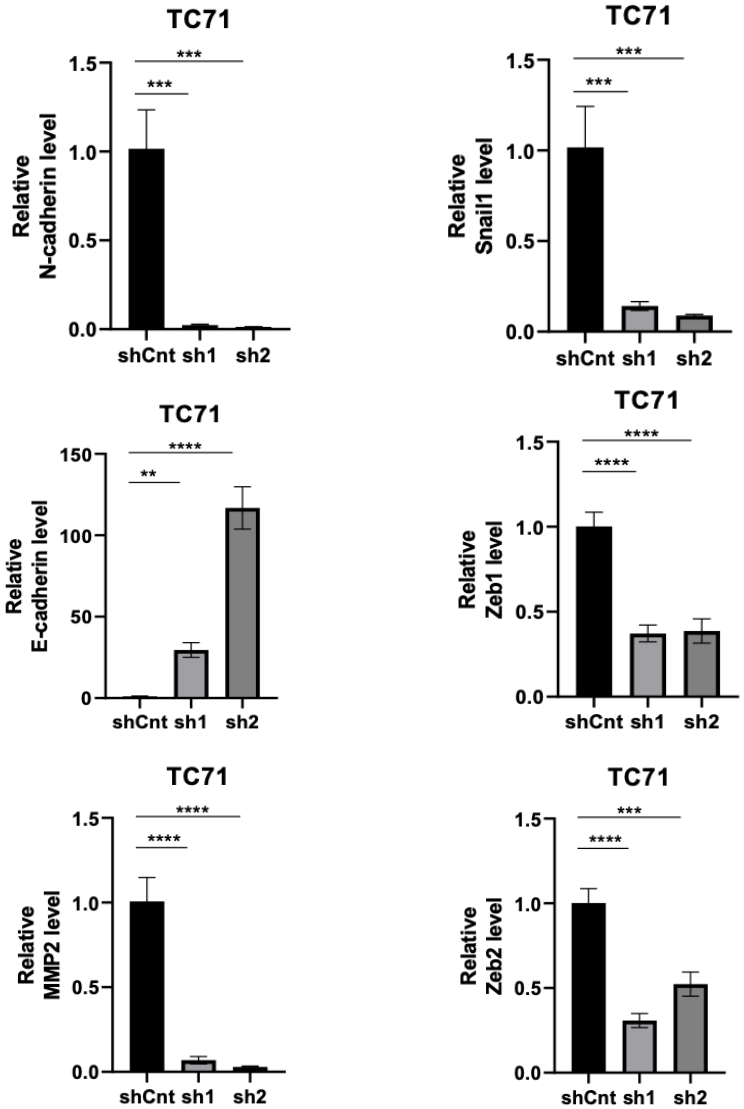

Figure 12: *EPHB2* knockdown changes EMT gene profile in TC71 cells
TC71 cells show a MET upon EPHB2 depletion with both shRNAs (decreased N-cadherin, Snail1, MMP2, as well as Zeb1 and Zeb2, whereas E-cadherin is increased). GAPDH expression was used as an internal control. Error bars indicate standard deviations.

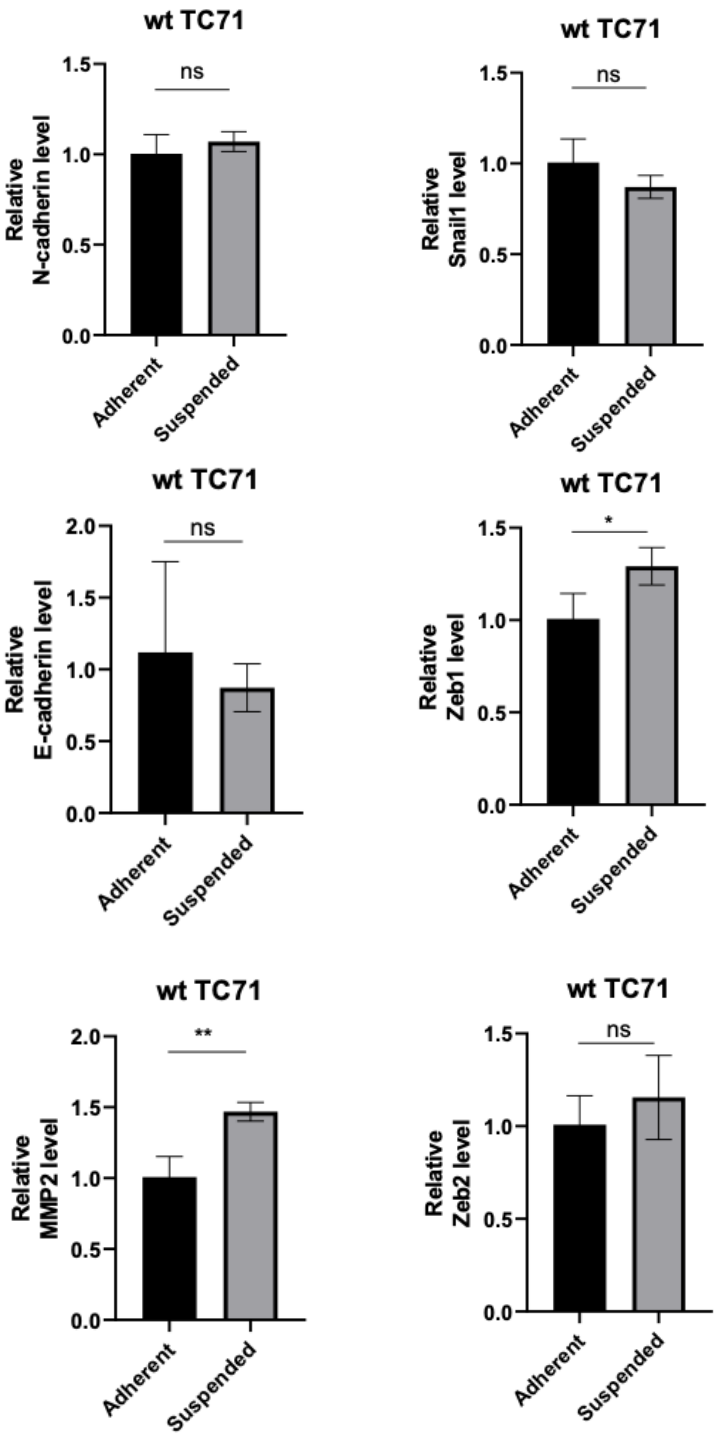

Figure 13: EMT gene expression in suspended and adherent conditions

EMT genes expression doesn't change according to growing conditions in wt TC71 cells (adherent versus suspended). A slight modification is observed for *ZEB1* and *MMP2* but in the opposite direction. GAPDH expression was used as internal control. Error bars indicate standard deviations.

4. *EWSR1-FLI1* expression and its trouble-shooting clue: the pathognomonic translocation

As the EWS-FLI1 protein plays the central role in EwS pathogenesis, we asked whether EPHB2 could have an impact on *EWSR1-FLI1* expression. Surprisingly, we observed that wild type (wt) TC71, as well as TC71 control cells displayed a double-peaked melting curve for *EWSR1-FLI1* gene amplification in qPCR analyses (Fig. 14 a). We assumed that two products of two different sizes were amplified and tested our hypothesis by running qPCR products on agarose gel (Fig. 14 b). As expected, two distinct products appeared on the gel; moreover, the larger product (corresponding to the higher temperature peak) was almost completely abrogated in TC71 cells depleted of EPHB2 (Fig. 14 a, b).

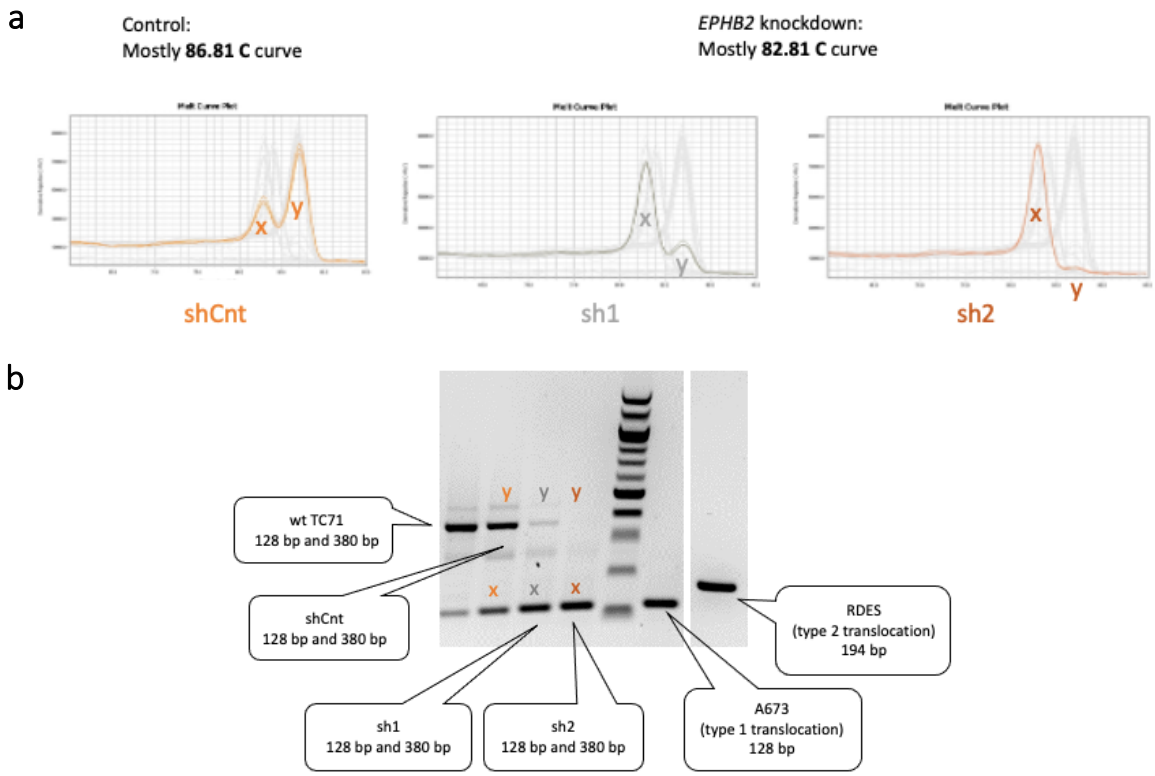

Figure 14: Our trouble-shooting clue: the pathognomonic translocation

14a: *EWSR1-FLI1* amplification gives two different melting curves for TC71 control and *EPHB2* knockdown (x and y). The larger product (y) is prevalent in TC71 control, while the smaller one (x) becomes dominant in EPHB2-depleted cells. 14b: Amplification product run on agarose gel; according to calculations based on the primers used, the larger product (y) corresponds to type 3 *EWSR1-FLI1* translocation (380 bp length).

To investigate whether these two different *EWSR1-FLI1* products were translated, we assessed the presence of the EWS-FLI-1 protein by Western Blot. We observed two bands of different size corresponding to type 1 and type 3 *EWSR1-FLI1* translocation (Fig. 15).

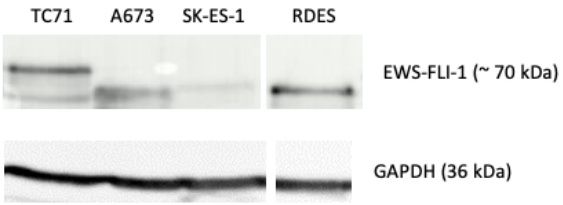

Figure 15: EWS-FLI-1 protein in EwS cell lines

EWS-FLI-1 protein tested by Western Blot. While the other tested cell lines show a unique product, TC71 cells show two different proteins, corresponding to type 1 and type 3 translocation fusion proteins.

A plausible explanation for these observations is that we were dealing with a mix of cell lines. By troubleshooting our data, we realized that in all probability we were using a batch composed of two different EwS cell lines that displayed different sensitivity to EPHB2 depletion: whereas "type 1 translocation cells" resisted EPHB2 depletion, "type 3 translocation population" disappeared upon EPHB2 knockdown. We sent our TC71 cell samples for cell authentication and a mixed population of two distinct EwS cell lines was indeed confirmed. The source of the cells was laboratory in the USA, where TC71 cells were inadvertently mixed with another EwS cell line bearing a type 3 translocation.

This mixed population was nevertheless instructive by revealing marked inter-tumor heterogeneity with respect to sensitivity to EPHB2 depletion. Whereas the type 3 translocation cells were dependent on EPHB2 expression and could not survive in its absence, the type 1 translocation cells, which were confirmed to be TC71, underwent a phenotypic change but survived. Because TC71 cells are adherent, the observed phenotypic change could not be explained by the simple selection of one cell line over the other as a result of EPHB2 depletion. TC71 cells clearly lost adhesiveness and appeared to undergo a MET. However, we could not rely on a mixed cell population to pursue our studies and keeping our hypothesis regarding the mechanism by which EPHB2 regulates EwS cell aggressiveness in mind, we sought other cell lines in which to test it (Fig. 16 a). We

interrogated EPHB2 expression results using DepMap online tool generated data (Fig. 16 b) and selected two cell lines with an adherent phenotype and clearly detectable EPHB2 expression: RDES and A673.

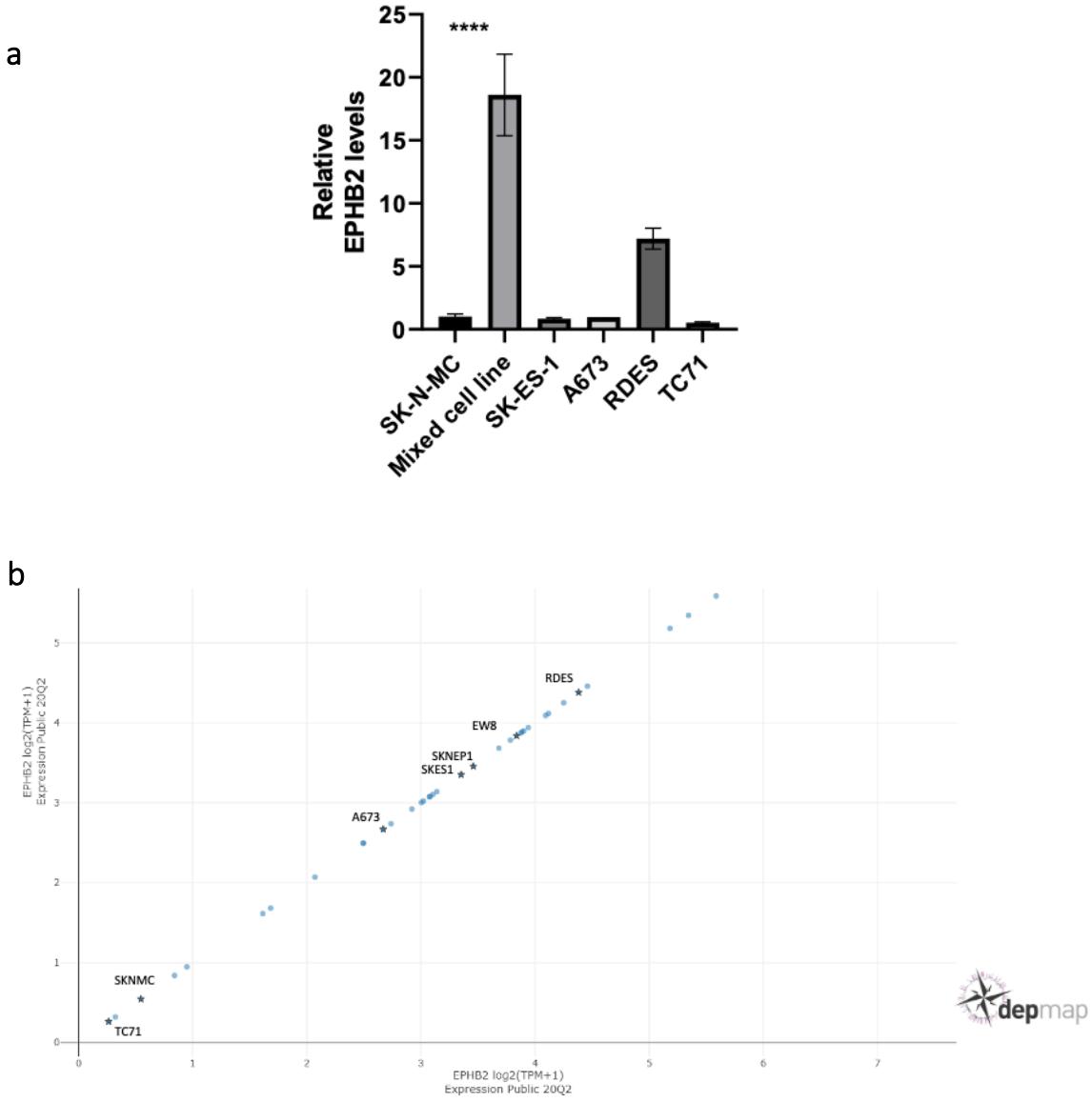

Figure 16: *EPHB2* relative expression in EwS cell lines (II)

16a: *EPHB2* relative expression assessed by qPCR, GAPDH expression was used as an internal control. Error bars indicate standard deviations. "Mixed cell line" is representing the above-called "TC71", while "TC71" is the authentic cell line that we reordered from commercial source. 16b: Graph showing *EPHB2* expression in several EwS cell lines, generated by online tool DepMap.

5. EPHB2 knockdown in A673 and RDES cell lines: two different paths leading to the same outcome

Before proceeding with experiments, we confirmed EPHB2 knockdown at RNA and protein levels (Fig. 17 a, b).

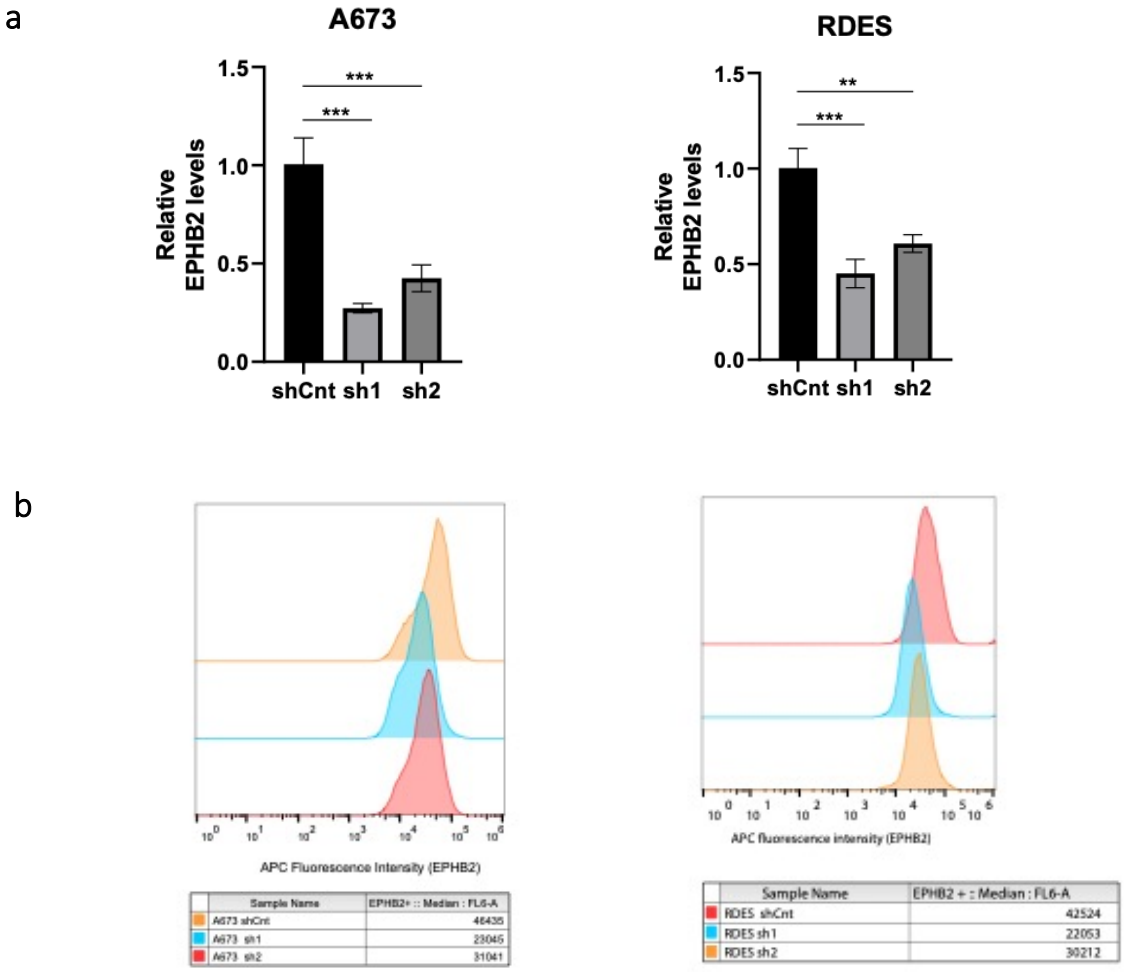

Figure 17: *EPHB2* knockdown confirmation in A673 and RDES cell lines

17a: RNA levels were tested by qPCR, GAPDH expression is used as internal control. Error bars show standard deviations. 17b: Protein levels were tested by FACS.

We observed phenotypic changes in both cell lines upon EPHB2 depletion: A673 cells showed detachment upon EPHB2 depletion, with evident sphere formation (Fig. 18 a), whereas RDES cells display slower growth and clump-forming propensity (Fig. 18 b).

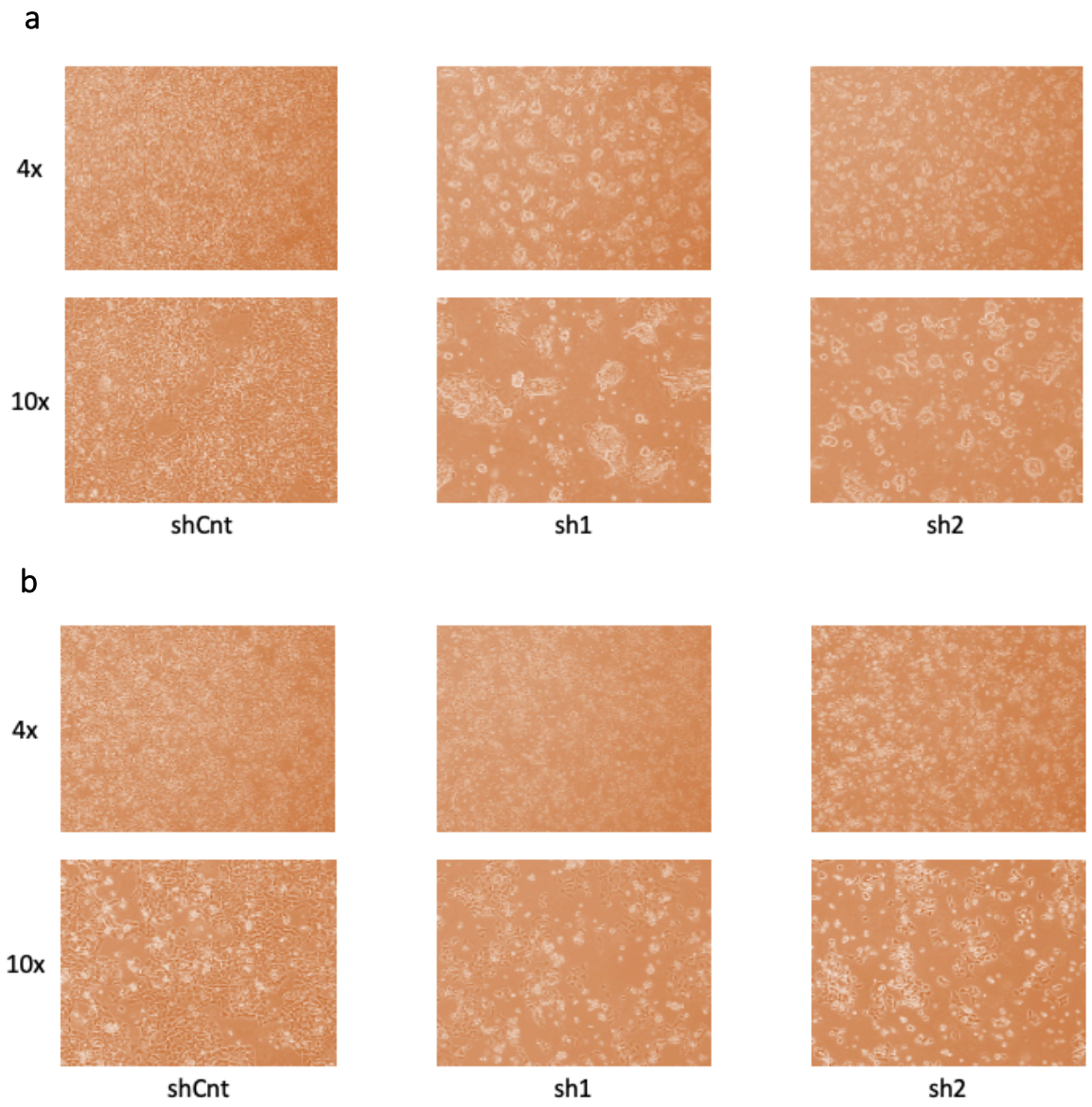

Figure 18: Cell phenotype upon EPHB2 depletion

18a: A673 phenotype after *EPHB2* knockdown (images taken on day 7 after infection). 18b: RDES phenotype after *EPHB2* knockdown (images taken on day 7 after infection).

As both detachment and slow growth are linked to FAK and AKT activity, we assessed protein phosphorylation: A673 displayed decrease in both FAK Tyr397 and AKT Ser473 phosphorylation (Fig. 19 a), whereas RDES displayed an unchanged FAK profile and increased AKT Ser473 phosphorylation (Fig. 19 b).

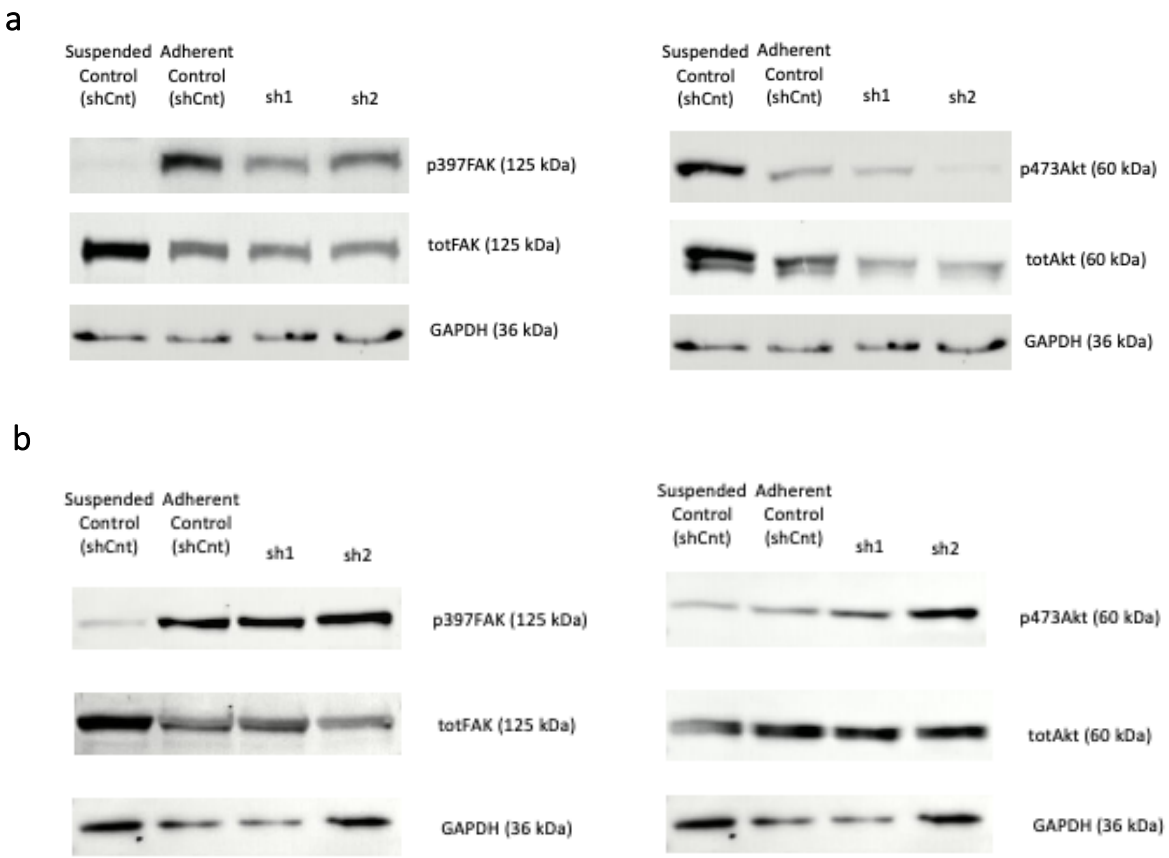

Figure 19: FAK and AKT pathways changes following EPHB2 depletion in A673 and RDES cells

19a: FAK protein and its phosphorylation at tyrosine 397 as well as AKT protein and its phosphorylation at serine 473 as tested by Western Blot in A673. 19b: FAK protein and its phosphorylation at tyrosine 397 as well as AKT protein and its phosphorylation at serine 473 as tested by Western Blot in RDES.

This divergent behavior was also observed in EMT gene analysis: A673 showed a decreased EMT gene profile (MMP2 and N-cadherin reduction and E-cadherin gain) in EPHB2-depleted cells (Fig. 20 a), contrary to RDES, which presented a striking increment of N-cadherin and a decrease in E-cadherin in EPHB2 knocked-down cells (Fig. 20 b).

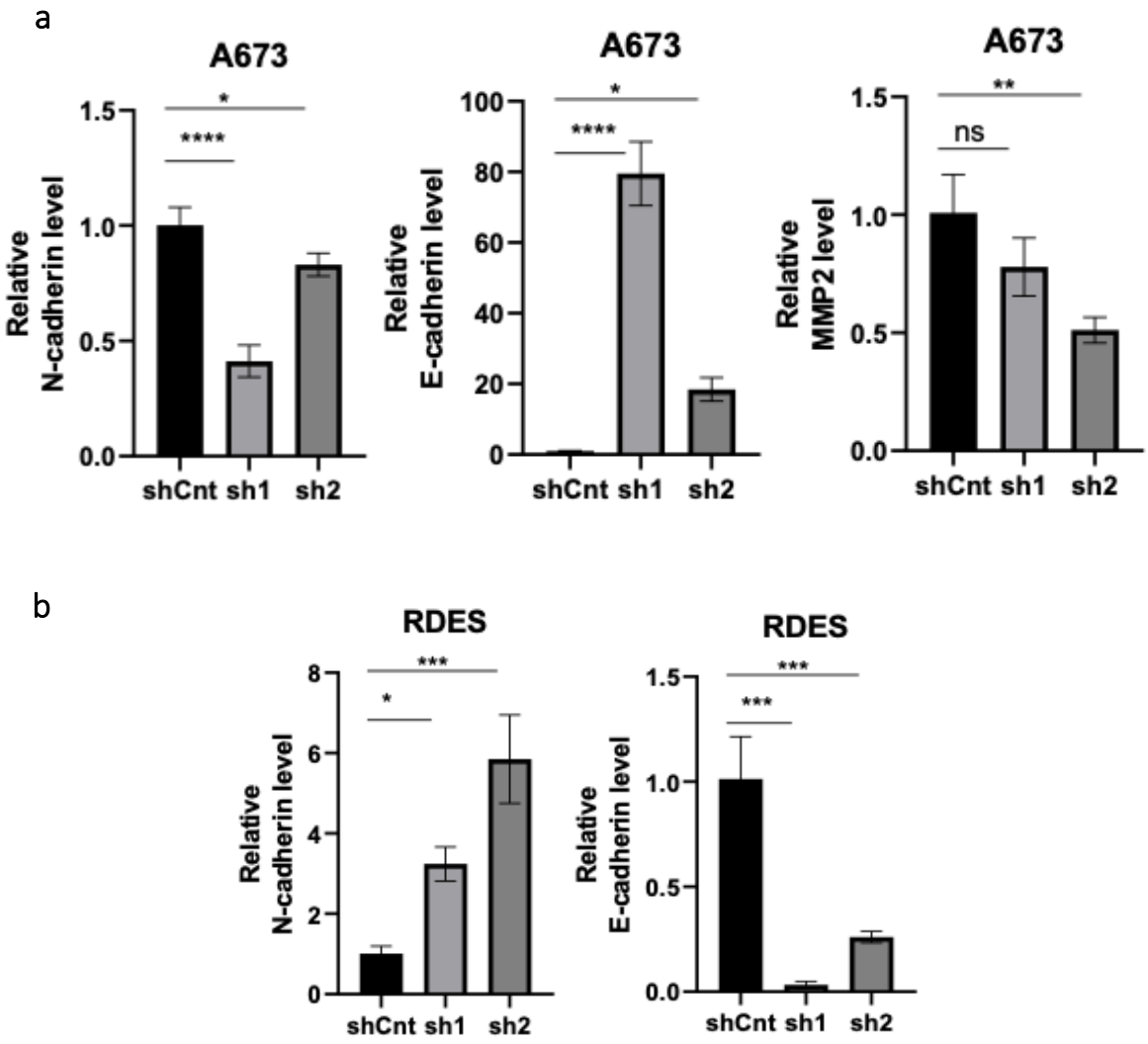

Figure 20: *EPHB2* knockdown changes EMT gene profile in A673 and RDES cells
20a: A673 are going to a MET upon EPHB2 depletion. RNA levels are tested by qPCR, GAPDH expression is used as internal control. Error bars show standard deviations. 20b: RDES are going to a EMT upon EPHB2 depletion. RNA levels are tested by qPCR, GAPDH expression is used as internal control. Error bars show standard deviations.

An intriguing result is that, despite the fact that these two cell lines displayed mirror-image behavior at both the gene and protein expression levels, invasive capability of both was decreased upon EPHB2 depletion (Fig. 21 a-d).

a

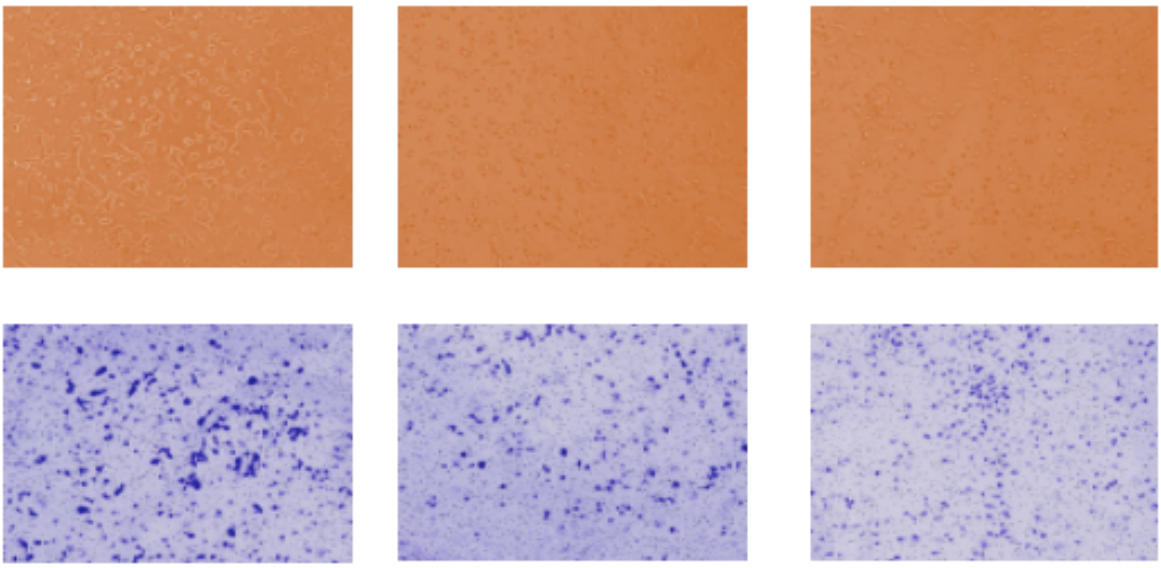
shCnt
sh1
sh2

b

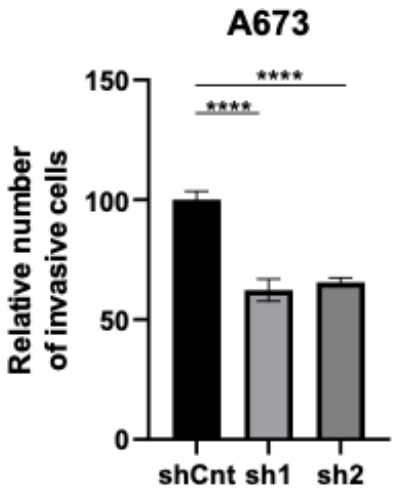
A673
Relative number of invasive cells
150
100
50
0
****
****
shCnt
sh1
sh2

c

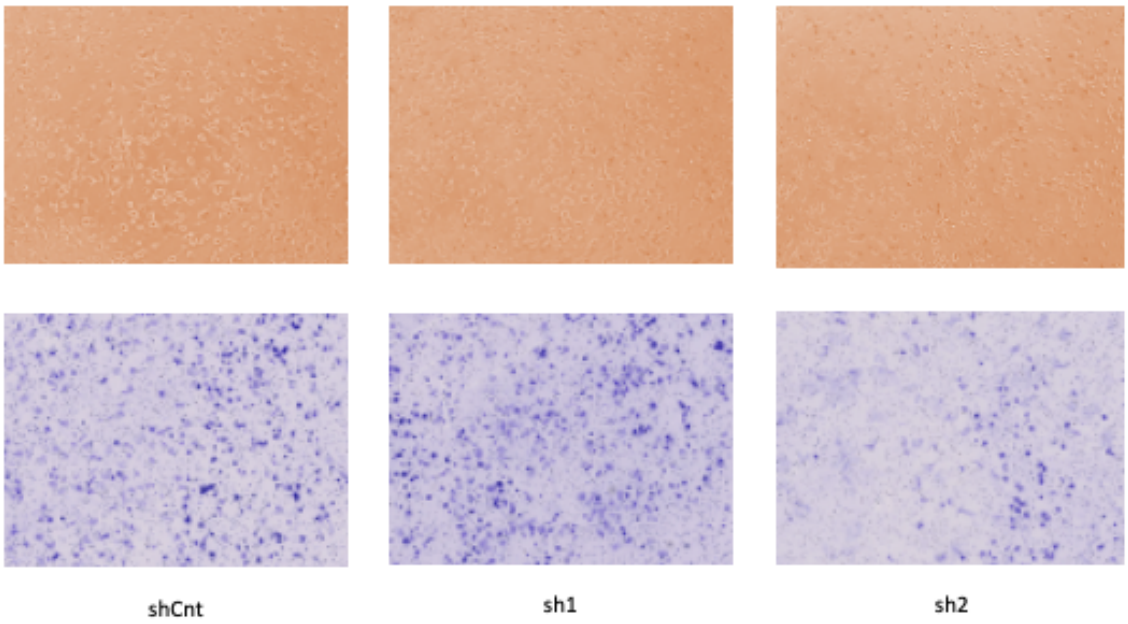

d

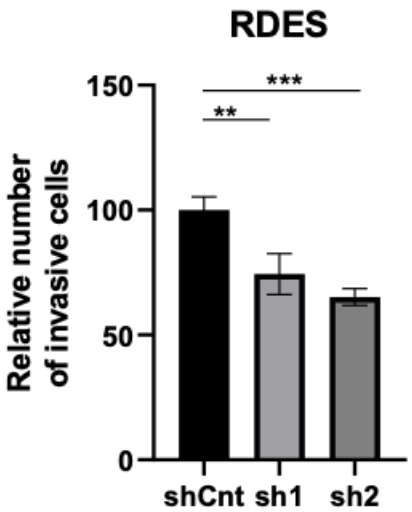

Figure 21: *EPHB2* expression is directly correlated to invasion capability in A673 and RDES cells

21a: Matrigel® invasion chambers before (top) and after (bottom) staining in A673 cells at 4x magnification. 21b: Relative invasion capability for knocked-down cells with both shRNAs compared to control in A673 cells. Error bars indicate standard deviations. 21c: Matrigel® invasion chambers before (top) and after (bottom) staining in RDES cells at 4x magnification. 21d: Relative invasion capability for knocked-down cells with both shRNAs compared to control in RDES cells. Error bars indicate standard deviations.

Discussion and perspectives

Our quest to determine how EPHB2 might contribute to EwS metastasis revealed that the receptor promotes EwS cell invasion but that the mechanisms by which it does so differ among tumor cell lines. Sensitivity of EwS cell lines to loss of EPHB2 expression also appeared to be widely divergent, with at least one cell line appearing to depend on EPHB2 for survival.

The mixed cell culture, composed of two distinct EwS cell lines that could be distinguished by virtue of a different chromosomal translocation (type 1 versus the rare type 3), was highly instructive and provided unbiased insight into the scope of EPHB2-dependent effects on EwS cell behavior. Depletion of EPHB2 led to cell detachment from the culture plate and formation of spheroids in suspension that could be attributed to FAK inactivation, a decrease in AKT activity and MET. However, these features appeared to affect only the type 1 translocation-bearing cell line (TC71) because the type 3 translocation bearing cells were no longer detectable, as evidenced by the disappearance of the corresponding fusion gene in qRT-PCR assays. This observation suggests that at one end of the spectrum, EwS cells, or subpopulations thereof, may depend on EPHB2 signaling for survival, possibly because EPHB2 in these particular cells may play a dominant role in maintaining AKT activity with its corresponding survival promoting functions.

Other EwS cells (exemplified by the type 1 translocation-bearing TC71 cells in the mixed culture) can survive upon EPHB2 depletion but display a marked MET that alters their functions with respect to adhesion and migration resulting in decreased invasiveness. We confirmed our initial observations on the mixed cell culture using A673 cells, which displayed a similar, albeit slightly less marked effect of EPHB2 depletion.

An unexpected observation was made using RDES cells. Depletion of EPHB2 in these cells had an opposite effect to that in TC71 and A673 cells in that it promoted EMT. However, despite accentuating EMT, EPHB2 depletion decreased RDES invasion. Although it may appear paradoxical that increased EMT translates into reduced invasiveness, it must be

remembered that EMT is important for normal and malignant epithelial cell migration and invasion. As discussed in the introduction, the importance of EMT in mesenchymal tumor invasion remains to be defined. What appears clear from our observations in RDES cells is that invasiveness is not directly linked to EMT and that EPHB2 may control RDES cell invasion by other mechanisms. Taken together, our observations suggest that EPHB2 is implicated in controlling EwS cell invasion and/or survival but that it may do so by cell context-dependent mechanisms.

EPHB2 has been shown to play a role in tumor cell adhesion and has been suggested to interact with FAK (62). Its activation may lead to paxillin and FAK phosphorylation (99), which are linked to EMT. However, the role of EPHB2 in EMT remains to be fully elucidated.

In our work on the miRNA reporter system (Keskin et al., 2021), we observed widely varying *EPHB2* expression levels among EwS patient samples, which could possibly explain the different responses to EPHB2 depletion that we found in the present study. However, the relationship between these different responses and the *EPHB2* expression level does not appear to straightforward. The mixed cell culture expressed the highest level of the gene, namely 17 times more than A673, but this was most likely due to the type 3 translocation-bearing cell line, as TC71 expresses less EPHB2 that A673 (Fig.16). It is possible that high expression of EPHB2 reflects cell dependence on its signaling for survival, as was the case for the type 3 translocation-bearing cells, but additional highly expressing cell lines or populations would need to be tested to provide support for this notion. A673, which appears to express 3 times more EPHB2 than TC71 behaves in same way as the latter, with marked detachment, MET, and downregulation of both FAK and AKT pathways upon EPHB2 depletion. In contrast, RDES cells, which express an intermediate level of EPHB2 (6 times more than A673), display decreased proliferation, EMT, and AKT pathway activation upon EPHB2 depletion. In the absence of a direct correlation between the EPHB2 expression level and cell behavior in response to its depletion, it would appear that other factors influence the behavior of different tumor cell populations. One possibility that we did not test is that the different cells that we used as well as their microenvironment may express different repertoires of EPH receptors and Ephrin ligands. As different EPH receptors and their ligands expressed in the same cells may modulate each other's function (49,54),

depending on the inherent tumor cell autonomous or microenvironmental EPH receptor and Ephrin ligand expression, the response to EPHB2 depletion may indeed be highly divergent. Thus cells with different Ephrin receptor-ligand repertoires may display markedly different behavior in the same microenvironment. Conversely, cells placed in two different habitats could employ different EPHB2 signaling pathways to promote invasion and dissemination. Given the importance of bidirectional signaling of Ephrin/Eph receptors coupled to our observations on the role of EPHB2 in EwS cell invasion and metastasis, exploring Ephrin expression repertoires in EwS cells should be a worthwhile endeavor.

As with any potential therapeutic target, the question arises as to the possible effectiveness of EPHB2 neutralization in EwS cells. First, not all EwS cells express EPHB2, such that the putative tumor inhibitory effect of EPHB2 targeting may be limited to only a fraction of EwS. Consistent with this notion, our laboratory has recently discovered that about 10% of EwS are exquisitely dependent on the RNA binding protein LIN28B (100). Depletion of LIN28B in these tumors leads to their deconstruction and complete loss of oncogenic properties. However, only 10% of EwS fall within that category. Furthermore, is the observed inhibition of invasiveness in response to EPHB2 depletion a lasting or a transient effect? Because of the marked plasticity that constitutes a hallmark of most malignant cells, it is possible that, over time, cells depleted of EPHB2 adapt and restore their initial invasiveness by relying on other mechanisms. Bearing these potential caveats in mind, the discovery of any candidate therapeutic target in a pediatric cancer whose relapsed and metastatic forms have no effective therapy should be explored to the point of determining its potential in the clinic even if it may benefit only a fraction of patients. The current work, in extension of the attached study (Keskin et al., 2021), places EPHB2 in the spotlight as a candidate therapeutic target to investigate in EwS and sets the stage to address a series of key questions that will determine its potential utility.

Future directions

As discussed above, our study has led to the point of designing a set of experiments to dissect the mechanisms by which EPHB2 regulates EwS cell invasiveness and determine under what conditions its targeting may be beneficial.

The first set of experiments should elucidate the relationship between EPHB2 expression and the response to its depletion, which, as discussed above, does not appear straightforward based on the limited number of cell lines that we have tested. A larger panel of cell lines with a range of naturally occurring EPHB2 expression levels should be assessed for their response to EPHB2 depletion. If a pattern emerges – for example, dependence on high EPHB2 expression levels for survival and on lower levels for invasion – the observations should be conformed in primary samples grown as organoids.

The next set of experiments should assess the repertoire of EPH receptors and Ephrin ligands in cells lines with divergent responses to EPHB2 depletion. Once the repertoire of each cell line is known, it can be modulated and the effect of EPHB2 depletion determined. For example, a cell line may express EPHB2 and EPHA4. Abrogation of EPHA4 expression may alter the response to EPHB2 depletion. Systematic assessment of the EPH/Ephrin ligand repertoire in EwS cell lines and the effects of its modulation should help predict which constellation will benefit most from EPHB2 depletion. This can then be transposed to primary samples grown as organoids.

Additional pathways to explore include FAK and AKT inhibitors, which could provide powerful tools to test our findings upon EPHB2 depletion. These experiments could be done in combination with reconstruction strategies, which would help determine whether the phenotypic, transcriptomic and protein changes are reversible upon EPHB2 overexpression. To test such putative reversibility, UTR targeting shRNAs are needed. We generated two different shRNAs (sh3, sh4) and tested their efficiency (Fig. 22), which was found to be comparable to our previously used shRNAs (Fig. 10 a).

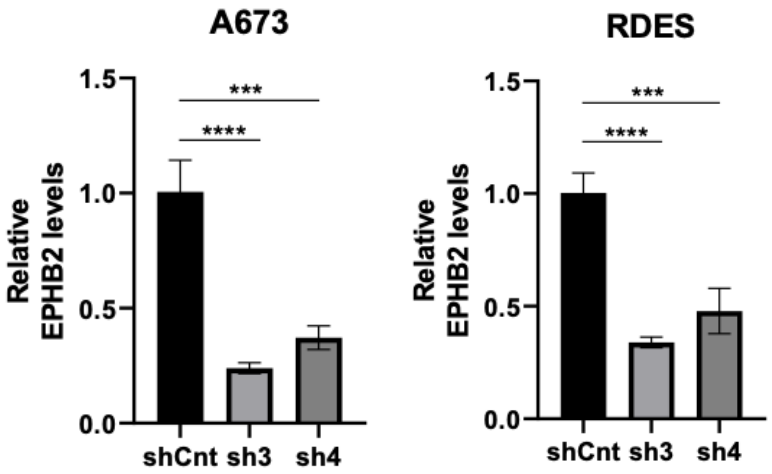

Figure 22: *EPHB2* knockdown confirmation with UTR targeting shRNAs in A673 and RDES cells

EPHB2 relative expression is assessed by qPCR, GAPDH expression is used as internal control. Error bars show standard deviations.

Finally, the relationship between EPHB2 and EMT should be further explored and as a first step, the effect of EPHB2 depletion of EMT transcription factor expression should be assessed.

If EPHB2 is confirmed to be an attractive candidate therapeutic target, even for a fraction of EwS patient, small molecule inhibitors can be screened for and/or designed and tested in *vitro* and *in vivo*.

Materials and methods

Cell culture

We cultured HEK 293T cells (from ATCC) in DMEM (Gibco), supplemented with 10% FBS (PAN, Biotec), 1% penicillin-streptomycin (Gibco) and 1% MEM NEAA (Gibco). We cultured A673 cells (from ATCC) in DMEM (Gibco), and RDES cells in RPMI (Gibco), both supplemented with 10% FBS (PAN, Biotec) and 1% penicillin-streptomycin (Gibco). TC71 mixed cells from our lab batch, as well as pure TC71 cells (from DSMZ), were cultured in IMDM (Gibco) supplemented with 10% FBS (PAN, Biotec) and 1% penicillin-streptomycin (Gibco). We used humified culture chambers, at 37C, with 5% CO_2.

Lentiviral transduction

We provided for lentiviral production by using HEK 293T cells (from ATCC), which were transfected using FuGENE® 6 Transfection Reagent (Promega). We used envelope plasmid pMD2G (from ADDGENE, # 12259) and packaging plasmid pCMVΔR8.74 (from ADDGENE, # 12263). We harvested lentivirus using Lenti-X Concentrator (from TAKARA). We provided for EPHB2 knockdown by using two different shRNAs from RNAi Consortium (sh1 ref: TRCN0000006423; sh2 ref: TRCN0000006425). We also tested two UTR targeting shRNAs (sh3 ref: TRCN0000425463; sh4 ref: TRCN0000422938). We selected transduced cells with puromycin, 1 mg/ml and 0.5 mg/ml for A673 and RDES respectively, for 48 hours.

RNA Isolation, Reverse Transcriptase PCR and Real Time qPCR

We performed RNA extraction with RNeasy Mini Kit (from QIAGEN, # 74106). cDNA samples were subsequently amplified with M-MLV Reverse Transcriptase (from Promega). We used Power SYBR® Green PCR Master Mix (from Applied Biosystems) for qPCR amplification, by using QuantStudio™ 5 System (from Thermo Fischer).

PCR steps were:

- 50° for 2 min (initial step)
- 95° 10 min, 95° for 15 sec, 60° C for 1 min (40 cycles)

GAPDH amplification was used as endogenous control. We used the $2^{-\Delta\Delta Ct}$ method for quantifying gene relative expression.

Following primer sequences were selected according to PrimerBank (http://pga.mgh.harvard.edu/primerbank):

EPHB2 (PrimerBank ID: 111118977c1)

Forward: 5'-AGAAACGCTAATGGACTCCACT-3'

Reverse: 5'-GTGCGGATCGTGTTCATGTT-3'

N-cadherin (PrimerBank ID: 215422305c2)

Forward: 5'-AGCCAACCTTAACTGAGGAGT-3'

Reverse: 5'-GGCAAGTTGATTGGAGGGATG-3'

E-cadherin (PrimerBank ID: 169790842c2)

Forward: 5'-ATTTTTCCCTCGACACCCGAT-3'

Reverse: 5'-TCCCAGGCGTAGACCAAGA-3'

Following primer sequences were selected according to literature:

MMP2 from reference (99)

Forward: 5'-CGGCCGCAGTGACGGAAA-3'

Reverse: 5'-CATCCTGGGACAGACGGAAG-3'

Snail1 from reference (100)

Forward: 5'-GCTGCAGGACTCTAATCCAGA-3'

Reverse: 5'-ATCTCCGGAGGTGGGATG-3'

Zeb1 from reference (100)

Forward: 5'-GGGAGGAGCAGTGAAAGAGA-3'

Reverse: 5'-TTTCTTGCCCTTCCTTTCTG-3'

Zeb2 from reference (100)

Forward: 5'-AAGCCAGGGACAGATCAGC-3'

Reverse: 5'-CCACACTCTGTGCATTTGAACT-3'

EWSR1-FLI1 from reference (101)

Forward: 5'-AGCAGCCTCCCACTAGTTAC-3'

Reverse: 5'-CCAAGCTCCTCTTCTGACTG-3'

GAPDH from reference (101)

Forward: 5'-GGTCTCCTCTGACTTCAACA-3'

Reverse: 5'-GTGAGGGTCTCTCTCTTCCT-3'

Fluorescence-Activated Cell Sorting (FACS)

EPHB2 levels were assessed by labeling cells with APC Mouse Anti-Human EPHB2 (from BD Parmingen). We labeled control cells with APC Mouse IgG1, K isotype antibody (from BD Parmingen). We detected alive cells with Calcein violet 450 AM (from Thermofisher) labeling dye. We acquired APC and AM intensity with Gallios cytometer (B43618, Beckman Coulter), with FL6 and FL9, respectively.

Immunoblotting

Western Blot analyses were performed according to standard procedures, with some shrewdness to avoid phosphorylation's loss: adherent cells were collected by directly pouring liquid nitrogen on washed plate, while suspension cells were collected by a gentle centrifuge at 800 rpm for 3 min of washed cells. Phosphatase inhibitors Cocktail 2 and Cocktail 3 (Sigma) were added to lysis buffer, blocking buffer, primary and secondary antibody solutions. Images were collected with FusionCapt Advance FX7 software. We used anti-FAK and anti-phosphoFAK(Tyr397) antibodies from Cell Signaling Technology (# 9330), anti-AKT and anti-phosphoAKT(Ser397) antibodies from BioConcept (# 4691S and # 4060S, respectively), anti-GAPDH antibody from Sigma-Aldrich (# G9295), anti-tubulin antibody from Calbiochem (# CP06), anti-FLI1 antibody from Abcam (ab133485) and anti-rabbit secondary antibody from Dako (# P0448).

Invasion assay

We followed Corning® BioCoat™ Matrigel® Invasion Chamber Protocol (Corning, #354480), optimized with the following modifications: cells number was increased to 50'000 and incubation time was expanded to 44 hours.

Statistical analysis and used software

Kaplan-Meier survival curves were created with https://hgserver1.amc.nl/cgi-bin/r2/main.cgi. We created graphs and performed one-way ANOVA and Student's T test analyses with Graphad Prism program (version 7). qPCRs and invasion assays were performed by using three replicates per each condition. P values less than 0.0001 are shown with four asterisks (****), P values less than 0.001 are shown with three asterisks (***), P values less than 0.01 are shown with two asterisks (**), P values less than 0.05 are shown with one asterisk (*), P values higher than 0.05 are shown as non-significant (ns). We collected qPCR results with QuantStudio Design and Analysis software (v1.4.2) and analyzed them with Excel program. We used FlowJo program (v10) for FACS data analyses. We analyzed Matrigel® Invasion Chamber images with AperioImageScope (v12.1.0.5029). Figures were created with BioRender.com.

Acknowledgements

First of all, thank you to Professor Ivan Stamenkovic, the greatest mentor I could ever meet. It has been an honor to work with you during these years and I am grateful for the immensity of knowledge that you convey all around you.

Thank you to Nicolò Riggi, for sharing with me a part of your amazing sharpness, applied in each field of research and life.

Thank you so much to Tugba Keskin, your flawless rigor and your unlimited kindness will be etched in my memory forever. Thank you for teaching me new things every single day and for being the perfect co-worker during this project.

Thank you to Carlo Fusco and Luisa Cironi, thank you for constantly helping me with any of lab and life issues and for our Italian chats that I will miss so much.

Thank you to Patricia Martin for your precious collaboration in technical procedures and for all the much appreciated lunch breaks and tea moments.

Thank you to each lab member, it has been a great experience working with you all.

Thank you to Alexis, my never-ending driving force, and to my parents for believing in me, always.

I dedicate this work to my daughter, growing in my belly while I was growing in the wonderful world of research.

Bibliography

1. Bhakta N, Force LM, Allemani C, Atun R, Bray F, Coleman MP, et al. Childhood cancer burden: a review of global estimates. Lancet Oncol. 2019 Jan 1;20(1):e42–53.
2. Barr RD, Ferrari A, Ries L, Whelan J, Bleyer WA. Cancer in Adolescents and Young Adults: A Narrative Review of the Current Status and a View of the Future. JAMA Pediatr. 2016 May 1;170(5):495–501.
3. Gröbner SN, Worst BC, Weischenfeldt J, Buchhalter I, Kleinheinz K, Rudneva VA, et al. The landscape of genomic alterations across childhood cancers. Nature. 2018 Mar;555(7696):321–7.
4. Filbin M, Monje M. Developmental origins and emerging therapeutic opportunities for childhood cancer. Nat Med. 2019 Mar;25(3):367–76.
5. Riggi N, Suvà ML, Stamenkovic I. Ewing's Sarcoma. N Engl J Med. 2021 Jan; 384:154-164
6. Brohl AS, Solomon DA, Chang W, Wang J, Song Y, Sindiri S, et al. The Genomic Landscape of the Ewing Sarcoma Family of Tumors Reveals Recurrent STAG2 Mutation. PLoS Genet. 2014 Jul 10.
7. Tirode F, Surdez D, Ma X, Parker M, Le Deley MC, Bahrami A, et al. Genomic landscape of Ewing sarcoma defines an aggressive subtype with co-association of STAG2 and TP53 mutations. Cancer Discov. 2014 Nov;4(11):1342–53.
8. Kovar H. Progress in the Molecular Biology of Ewing Tumors. Sarcoma. 1998 Mar;2(1):3–17.
9. Lin PP, Brody RI, Hamelin AC, Bradner JE, Healey JH, Ladanyi M. Differential transactivation by alternative EWS-FLI1 fusion proteins correlates with clinical heterogeneity in Ewing's sarcoma. Cancer Res. 1999 Apr 1;59(7):1428–32.
10. González I, Vicent S, de Alava E, Lecanda F. EWS/FLI-1 oncoprotein subtypes impose different requirements for transformation and metastatic activity in a murine model. J Mol Med Berl Ger. 2007 Sep;85(9):1015–29.
11. Riggi N, Stamenkovic I. The Biology of Ewing sarcoma. Cancer Lett. 2007 Aug 28;254(1):1–10.
12. Riggi N, Cironi L, Suvà M-L, Stamenkovic I. Sarcomas: genetics, signalling, and cellular origins. Part 1: The fellowship of TET. J Pathol. 2007 Sep;213(1):4–20.
13. Arvand A, Denny CT. Biology of EWS/ETS fusions in Ewing's family tumors. Oncogene. 2001 Sep;20(40):5747–54.
14. Shing DC, McMullan DJ, Roberts P, Smith K, Chin S-F, Nicholson J, et al. FUS/ERG gene fusions in Ewing's tumors. Cancer Res. 2003 Aug 1;63(15):4568–76.
15. Peeters P, Raynaud SD, Cools J, Wlodarska I, Grosgeorge J, Philip P, et al. Fusion of TEL, the ETS-variant gene 6 (ETV6), to the receptor-associated kinase JAK2 as a result of t(9;12) in a lymphoid and t(9;15;12) in a myeloid leukemia. Blood. 1997 Oct 1;90(7):2535–40.
16. Tomlins SA, Rhodes DR, Perner S, Dhanasekaran SM, Mehra R, Sun X-W, et al. Recurrent fusion of TMPRSS2 and ETS transcription factor genes in prostate cancer. Science. 2005 Oct 28;310(5748):644–8.
17. Delattre O, Zucman J, Plougastel B, Desmaze C, Melot T, Peter M, et al. Gene fusion with an ETS DNA-binding domain caused by chromosome translocation in human tumours. Nature. 1992 Sep 10;359(6391):162–5.

18. Dunn T, Praissman L, Hagag N, Viola MV. ERG gene is translocated in an Ewing's sarcoma cell line. Cancer Genet Cytogenet. 1994 Aug;76(1):19–22.
19. Jeon IS, Davis JN, Braun BS, Sublett JE, Roussel MF, Denny CT, et al. A variant Ewing's sarcoma translocation (7;22) fuses the EWS gene to the ETS gene ETV1. Oncogene. 1995 Mar 16;10(6):1229–34.
20. Urano F, Umezawa A, Hong W, Kikuchi H, Hata J. A novel chimera gene between EWS and E1A-F, encoding the adenovirus E1A enhancer-binding protein, in extraosseous Ewing's sarcoma. Biochem Biophys Res Commun. 1996 Feb 15;219(2):608–12.
21. Peter M, Couturier J, Pacquement H, Michon J, Thomas G, Magdelenat H, et al. A new member of the ETS family fused to EWS in Ewing tumors. Oncogene. 1997 Mar 13;14(10):1159–64.
22. Riggi N, Knoechel B, Gillespie SM, Rheinbay E, Boulay G, Suvà ML, et al. EWS-FLI1 utilizes divergent chromatin remodeling mechanisms to directly activate or repress enhancer elements in Ewing sarcoma. Cancer Cell. 2014 Nov 10;26(5):668–81.
23. Bonasio R, Tu S, Reinberg D. Molecular signals of epigenetic states. Science. 2010 Oct 29;330(6004):612–6.
24. Dawson MA, Kouzarides T. Cancer epigenetics: from mechanism to therapy. Cell. 2012 Jul 6;150(1):12–27.
25. Suvà ML, Riggi N, Bernstein BE. Epigenetic reprogramming in cancer. Science. 2013 Mar 29;339(6127):1567–70.
26. Sheffield NC, Pierron G, Klughammer J, Datlinger P, Schönegger A, Schuster M, et al. DNA methylation heterogeneity defines a disease spectrum in Ewing sarcoma. Nat Med. 2017 Mar;23(3):386–95.
27. Stadler MB, Murr R, Burger L, Ivanek R, Lienert F, Schöler A, et al. DNA-binding factors shape the mouse methylome at distal regulatory regions. Nature. 2011 Dec;480(7378):490–5.
28. Tomazou EM, Sheffield NC, Schmidl C, Schuster M, Schönegger A, Datlinger P, et al. Epigenome Mapping Reveals Distinct Modes of Gene Regulation and Widespread Enhancer Reprogramming by the Oncogenic Fusion Protein EWS-FLI1. Cell Rep. 2015 Feb 24;10(7):1082–95.
29. Riggi N, Suvà M-L, De Vito C, Provero P, Stehle J-C, Baumer K, et al. EWS-FLI-1 modulates miRNA145 and SOX2 expression to initiate mesenchymal stem cell reprogramming toward Ewing sarcoma cancer stem cells. Genes Dev. 2010 May;24(9):916–32.
30. Riggi N, Cironi L, Provero P, Suvà M-L, Kaloulis K, Garcia-Echeverria C, et al. Development of Ewing's Sarcoma from Primary Bone Marrow–Derived Mesenchymal Progenitor Cells. Cancer Res. 2005 Dec 15;65(24):11459–68.
31. Suvà M-L, Riggi N, Stehle J-C, Baumer K, Tercier S, Joseph J-M, et al. Identification of cancer stem cells in Ewing's sarcoma. Cancer Res. 2009 Mar 1;69(5):1776–81.
32. Lv F-J, Tuan RS, Cheung KMC, Leung VYL. Concise review: the surface markers and identity of human mesenchymal stem cells. Stem Cells Dayt Ohio. 2014 Jun;32(6):1408–19.
33. Gomez NC, Hepperla AJ, Dumitru R, Simon JM, Fang F, Davis IJ. Widespread Chromatin Accessibility at Repetitive Elements Links Stem Cells with Human Cancer. Cell Rep. 2016 01;17(6):1607–20.
34. Riggi N, Suvà M-L, Suvà D, Cironi L, Provero P, Tercier S, et al. EWS-FLI-1 expression triggers a Ewing's sarcoma initiation program in primary human mesenchymal

stem cells. Cancer Res. 2008 Apr 1;68(7):2176–85.
35. Widhe B, Widhe T. Initial symptoms and clinical features in osteosarcoma and Ewing sarcoma. J Bone Joint Surg Am. 2000 May;82(5):667–74.
36. Biswas B, Shukla NK, Deo SVS, Agarwala S, Sharma DN, Vishnubhatla S, et al. Evaluation of outcome and prognostic factors in extraosseous Ewing sarcoma. Pediatr Blood Cancer. 2014;61(11):1925–31.
37. Cotterill SJ, Ahrens S, Paulussen M, Jürgens HF, Voûte PA, Gadner H, et al. Prognostic factors in Ewing's tumor of bone: analysis of 975 patients from the European Intergroup Cooperative Ewing's Sarcoma Study Group. J Clin Oncol Off J Am Soc Clin Oncol. 2000 Sep;18(17):3108–14.
38. Anderson JL, Denny CT, Tap WD, Federman N. Pediatric sarcomas: translating molecular pathogenesis of disease to novel therapeutic possibilities. Pediatr Res. 2012 Aug;72(2):112–21.
39. Boulay G, Sandoval GJ, Riggi N, Iyer S, Buisson R, Naigles B, et al. Cancer-Specific Retargeting of BAF Complexes by a Prion-like Domain. Cell. 2017 Sep 21;171(1):163-178.e19.
40. Hoang NT, Acevedo LA, Mann MJ, Tolani B. A review of soft-tissue sarcomas: translation of biological advances into treatment measures. Cancer Manag Res. 2018 May 10;10:1089–114.
41. Lemmon MA, Schlessinger J. Cell signaling by receptor tyrosine kinases. Cell. 2010 Jun 25;141(7):1117–34.
42. Du Z, Lovly CM. Mechanisms of receptor tyrosine kinase activation in cancer. Mol Cancer. 2018 Feb 19;17(1):58.
43. Toretsky JA, Helman LJ. Cytogenetics and experimental models. Curr Opin Oncol. 1997 Jul;9(4):342–7.
44. Asmane I, Watkin E, Alberti L, Duc A, Marec-Berard P, Ray-Coquard I, et al. Insulin-like growth factor type 1 receptor (IGF-1R) exclusive nuclear staining: a predictive biomarker for IGF-1R monoclonal antibody (Ab) therapy in sarcomas. Eur J Cancer Oxf Engl 1990. 2012 Nov;48(16):3027–35.
45. Mora J, Rodríguez E, de Torres C, Cardesa T, Ríos J, Hernández T, et al. Activated growth signaling pathway expression in Ewing sarcoma and clinical outcome. Pediatr Blood Cancer. 2012 Apr;58(4):532–8.
46. Wook Jin. The Role of Tyrosine Kinases as a Critical Prognostic Parameter and Its Targeted Therapies in Ewing Sarcoma. Front. Cell Dev. Biol., 2020 Jul; Vol 8 Art 613.
47. Kania A, Klein R. Mechanisms of ephrin–Eph signalling in development, physiology and disease. Nat Rev Mol Cell Biol. 2016 Apr;17(4):240–56.
48. Pasquale EB. Eph-ephrin bidirectional signaling in physiology and disease. Cell. 2008 Apr 4;133(1):38–52.
49. Pasquale EB. Eph receptors and ephrins in cancer: bidirectional signaling and beyond. Nat Rev Cancer. 2010 Mar;10(3):165–80.
50. Ireton RC, Chen J. EphA2 receptor tyrosine kinase as a promising target for cancer therapeutics. Curr Cancer Drug Targets. 2005 May;5(3):149–57.
51. Noren NK, Pasquale EB. Paradoxes of the EphB4 receptor in cancer. Cancer Res. 2007 May 1;67(9):3994–7.
52. Herath NI, Doecke J, Spanevello MD, Leggett BA, Boyd AW. Epigenetic silencing of EphA1 expression in colorectal cancer is correlated with poor survival. Br J Cancer. 2009 Apr 7;100(7):1095–102.

53. Müller-Tidow C, Diederichs S, Bulk E, Pohle T, Steffen B, Schwäble J, et al. Identification of metastasis-associated receptor tyrosine kinases in non-small cell lung cancer. Cancer Res. 2005 Mar 1;65(5):1778–82.
54. McCarron JK, Stringer BW, Day BW, Boyd AW. Ephrin expression and function in cancer. Future Oncol Lond Engl. 2010 Jan;6(1):165–76.
55. Cheng N, Brantley DM, Liu H, Lin Q, Enriquez M, Gale N, et al. Blockade of EphA Receptor Tyrosine Kinase Activation Inhibits Vascular Endothelial Cell Growth Factor-Induced Angiogenesis11 NIH Grants HD36400 and DK47078; JDF grant I-2001-519; DOD grant BC010265; American Heart Association Grant 97300889N; ACS Institutional Research Grant IN-25-38 (to J. Chen); Vascular Biology Training Grant T32-HL-07751-06 and American Heart Association Fellowship 0120147B (to D. Brantley); Cancer training Grant T-32 CA09592 (to N. Cheng); and a core facilities Grant 2P30CA68485 to the Vanderbilt-Ingram Cancer Center. Mol Cancer Res. 2002 Nov 1;1(1):2–11.
56. Vail ME, Murone C, Tan A, Hii L, Abebe D, Janes PW, et al. Targeting EphA3 inhibits cancer growth by disrupting the tumor stromal microenvironment. Cancer Res. 2014 Aug 15;74(16):4470–81.
57. Genander M, Halford MM, Xu N-J, Eriksson M, Yu Z, Qiu Z, et al. Dissociation of EphB2 signaling pathways mediating progenitor cell proliferation and tumor suppression. Cell. 2009 Nov 13;139(4):679–92.
58. Chen P, Rossi N, Priddy S, Pierson CR, Studebaker AW, Johnson RA. EphB2 activation is required for ependymoma development as well as inhibits differentiation and promotes proliferation of the transformed cell. Sci Rep. 2015;
59. Khansaard W, Techasen A, Namwat N, Yongvanit P, Khuntikeo N, Puapairoj A, et al. Increased EphB2 expression predicts cholangiocarcinoma metastasis. Tumour Biol J Int Soc Oncodevelopmental Biol Med. 2014 Oct;35(10):10031–41.
60. Gao Q, Liu W, Cai J, Li M, Gao Y, Lin W, et al. EphB2 promotes cervical cancer progression by inducing epithelial-mesenchymal transition. Hum Pathol. 2014 Feb;45(2):372–81.
61. Sikkema AH, den Dunnen WFA, Hulleman E, van Vuurden DG, Garcia-Manero G, Yang H, et al. EphB2 activity plays a pivotal role in pediatric medulloblastoma cell adhesion and invasion. Neuro-Oncol. 2012 Sep;14(9):1125–35.
62. Wang SD, Rath P, Lal B, Richard J-P, Li Y, Goodwin CR, et al. EphB2 receptor controls proliferation/migration dichotomy of glioblastoma by interacting with focal adhesion kinase. Oncogene. 2012 Dec;31(50):5132–43.
63. Qiu W, Song S, Chen W, Zhang J, Yang H, Chen Y. Hypoxia-induced EPHB2 promotes invasive potential of glioblastoma. Int J Clin Exp Pathol. 2019 Feb 1;12(2):539–48.
64. Inagaki Y, Tokunaga T, Yanai M, Wu D, Huang J, Nagase H, et al. Silencing of EPHB2 promotes the epithelial-mesenchymal transition of skin squamous cell carcinoma-derived A431 cells. Oncol Lett. 2019 Apr;17(4):3735–42.
65. Stephan Huveneers, Erik H. J. Danen. Adhesion signaling – crosstalk between integrins, Src and Rho | Journal of Cell Science. J Cell Sci (2009) 122 (8): 1059–1069.
66. Hynes RO. Integrins: Bidirectional, Allosteric Signaling Machines. Cell. 2002 Sep 20;110(6):673–87.
67. Mitra SK, Hanson DA, Schlaepfer DD. Focal adhesion kinase: in command and control of cell motility. Nat Rev Mol Cell Biol. 2005 Jan;6(1):56–68.
68. Lim Y, Han I, Jeon J, Park H, Bahk Y-Y, Oh E-S. Phosphorylation of Focal Adhesion

Kinase at Tyrosine 861 Is Crucial for Ras Transformation of Fibroblasts*. J Biol Chem. 2004 Jul 9;279(28):29060–5.
69. Tapial Martínez P, López Navajas P, Lietha D. FAK Structure and Regulation by Membrane Interactions and Force in Focal Adhesions. Biomolecules. 2020 Feb; 10(2): 179.
70. Owens LV, Xu L, Craven RJ, Dent GA, Weiner TM, Kornberg L, et al. Overexpression of the focal adhesion kinase (p125FAK) in invasive human tumors. Cancer Res. 1995 Jul 1;55(13):2752–5.
71. Weiner TM, Liu ET, Craven RJ, Cance WG. Expression of growth factor receptors, the focal adhesion kinase, and other tyrosine kinases in human soft tissue tumors. Ann Surg Oncol. 1994 Jan;1(1):18–27.
72. Fu W, Hall JE, Schaller MD. Focal adhesion kinase-regulated signaling events in human cancer. Biomol Concepts. 2012 Jun 1;3(3):225–40.
73. Golubovskaya VM, Figel S, Ho BT, Johnson CP, Yemma M, Huang G, et al. A small molecule focal adhesion kinase (FAK) inhibitor, targeting Y397 site: 1-(2-hydroxyethyl)-3, 5, 7-triaza-1-azoniatricyclo [3.3.1.1(3,7)]decane; bromide effectively inhibits FAK autophosphorylation activity and decreases cancer cell viability, clonogenicity and tumor growth in vivo. Carcinogenesis. 2012 May;33(5):1004–13.
74. O'Brien S, Golubovskaya VM, Conroy J, Liu S, Wang D, Liu B, et al. FAK inhibition with small molecule inhibitor Y15 decreases viability, clonogenicity, and cell attachment in thyroid cancer cell lines and synergizes with targeted therapeutics. Oncotarget. 2014 Sep 15;5(17):7945–59.
75. Heffler M, Golubovskaya VM, Dunn KMB, Cance W. Focal adhesion kinase autophosphorylation inhibition decreases colon cancer cell growth and enhances the efficacy of chemotherapy. Cancer Biol Ther. 2013 Aug;14(8):761–72.
76. Golubovskaya VM, Huang G, Ho B, Yemma M, Morrison CD, Lee J, et al. Pharmacologic blockade of FAK autophosphorylation decreases human glioblastoma tumor growth and synergizes with temozolomide. Mol Cancer Ther. 2013 Feb;12(2):162–72.
77. Michael L. Megison et al. FAK Inhibition Abrogates the Malignant Phenotype in Aggressive Pediatric Renal Tumors. Mol Cancer Res; April 2014;12(4)
78. Moritake H, Sugimoto T, Kuroda H, Hidaka F, Takahashi Y, Tsuneyoshi M, et al. Newly established Askin tumor cell line and overexpression of focal adhesion kinase in Ewing sarcoma family of tumors cell lines. Cancer Genet Cytogenet. 2003 Oct 15;146(2):102–9.
79. Steinestel K, Trautmann M, Jansen E-P, Dirksen U, Rehkämper J, Mikesch J-H, et al. Focal adhesion kinase confers pro-migratory and antiapoptotic properties and is a potential therapeutic target in Ewing sarcoma. Mol Oncol. 2020 Feb;14(2):248–60.
80. Wang S, Hwang EE, Guha R, O'Neill AF, Melong N, Veinotte CJ, et al. High-throughput Chemical Screening Identifies Focal Adhesion Kinase and Aurora Kinase B Inhibition as a Synergistic Treatment Combination in Ewing Sarcoma. Clin Cancer Res Off J Am Assoc Cancer Res. 2019 Jul 15;25(14):4552–66.
81. Moritake H, Saito Y, Sawa D, Sameshima N, Yamada A, Kinoshita M, et al. TAE226, a dual inhibitor of focal adhesion kinase and insulin-like growth factor-I receptor, is effective for Ewing sarcoma. Cancer Med. 2019 Dec;8(18):7809–21.
82. Megison ML, Gillory LA, Stewart JE, Nabers HC, Mrozcek-Musulman E, Beierle EA. FAK inhibition abrogates the malignant phenotype in aggressive pediatric renal tumors.

Mol Cancer Res MCR. 2014 Apr;12(4):514–26.
83. Noorolyai S, Shajari N, Baghbani E, Sadreddini S, Baradaran B. The relation between PI3K/AKT signalling pathway and cancer. Gene. 2019 May 25;698:120–8.
84. Boccafoschi F, Mosca C, Bosetti M, Cannas M. The role of mechanical stretching in the activation and localization of adhesion proteins and related intracellular molecules. J Cell Biochem. 2011 May;112(5):1403–9.
85. Thompson WR, Rubin CT, Rubin J. Mechanical regulation of signaling pathways in bone. Gene. 2012 Jul 25;503(2):179–93.
86. Tzeng H-E, Chen J-C, Tsai C-H, Kuo C-C, Hsu H-C, Hwang W-L, et al. CCN3 increases cell motility and MMP-13 expression in human chondrosarcoma through integrin-dependent pathway. J Cell Physiol. 2011 Dec;226(12):3181–9.
87. Wu MH, Lo J-F, Kuo C-H, Lin JA, Lin Y-M, Chen L-M, et al. Endothelin-1 promotes MMP-13 production and migration in human chondrosarcoma cells through FAK/PI3K/Akt/mTOR pathways. J Cell Physiol. 2012 Aug;227(8):3016–26.
88. Jiang H, Wang X, Miao W, Wang B, Qiu Y. CXCL8 promotes the invasion of human osteosarcoma cells by regulation of PI3K/Akt signaling pathway. APMIS Acta Pathol Microbiol Immunol Scand. 2017 Sep;125(9):773–80.
89. Joerg Schwock, Neesha Dhani, David W Hedley. Targeting focal adhesion kinase signaling in tumor growth and metastasis. Expert Opin Ther Targets. 2010 Jan; 14(1):77-94.
90. Chen P-C, Tai H-C, Lin T-H, Wang S-W, Lin C-Y, Chao C-C, et al. CCN3 promotes epithelial-mesenchymal transition in prostate cancer via FAK/Akt/HIF-1α-induced twist expression. Oncotarget. 2017 Sep 26;8(43):74506–18.
91. Bakir B, Chiarella AM, Pitarresi JR, Rustgi AK. EMT, MET, Plasticity, and Tumor Metastasis. Trends Cell Biol. 2020 Oct;30(10):764–76.
92. Ehnman M, Chaabane W, Haglund F, Tsagkozis P. The Tumor Microenvironment of Pediatric Sarcoma: Mesenchymal Mechanisms Regulating Cell Migration and Metastasis. Curr Oncol Rep. 2019 15;21(10):90.
93. Sannino G, Marchetto A, Kirchner T, Grünewald TGP. Epithelial-to-Mesenchymal and Mesenchymal-to-Epithelial Transition in Mesenchymal Tumors: A Paradox in Sarcomas? Cancer Res. 2017 01;77(17):4556–61.
94. Yang J, Du X, Wang G, Sun Y, Chen K, Zhu X, et al. Mesenchymal to epithelial transition in sarcomas. Eur J Cancer. 2014 Feb 1;50(3):593–601.
95. Franzetti G-A, Laud-Duval K, van der Ent W, Brisac A, Irondelle M, Aubert S, et al. Cell-to-cell heterogeneity of EWSR1-FLI1 activity determines proliferation/migration choices in Ewing sarcoma cells. Oncogene. 2017 Jun 22;36(25):3505–14.
96. Machado I, López-Guerrero JA, Navarro S, Alberghini M, Scotlandi K, Picci P, et al. Epithelial cell adhesion molecules and epithelial mesenchymal transition (EMT) markers in Ewing's sarcoma family of tumors (ESFTs). Do they offer any prognostic significance? Virchows Arch Int J Pathol. 2012 Sep;461(3):333–7.
97. Wiles ET, Bell R, Thomas D, Beckerle M, Lessnick SL. ZEB2 Represses the Epithelial Phenotype and Facilitates Metastasis in Ewing Sarcoma. Genes Cancer. 2013 Nov;4(11–12):486–500.
98. Choo S, Wang P, Newbury R, Roberts W, Yang J. Reactivation of TWIST1 contributes to Ewing sarcoma metastasis. Pediatr Blood Cancer. 2018 Jan;65(1).
99. Jørgensen C, Sherman A, Chen GI, Pasculescu A, Poliakov A, Hsiung M, et al. Cell-specific information processing in segregating populations of Eph receptor ephrin-

expressing cells. Science. 2009 Dec 11;326(5959):1502–9.
100. Keskin T, Bakaric A, Waszyk P, Boulay G, Torsello M, Cornaz-Buros S, et al. LIN28B Underlies the Pathogenesis of a Subclass of Ewing Sarcoma. Cell Rep. 2020 Mar 31;30(13):4567-4583.e5.
101. Cells Tissues Organs | Karger Journal. [cited 2021 Mar 30]; Available from: https://www.karger.com/Journal/Home/224197
102. Milano A, Mazzetta F, Valente S, Ranieri D, Leone L, Botticelli A, et al. Molecular Detection of EMT Markers in Circulating Tumor Cells from Metastatic Non-Small Cell Lung Cancer Patients: Potential Role in Clinical Practice. Anal Cell Pathol. 2018 Feb 27;2018:e3506874.

CANCER

A live single-cell reporter assay links intratumor heterogeneity to metastatic proclivity in Ewing sarcoma

Tugba Keskin[1], Beatrice Rucci[1], Sandrine Cornaz-Buros[1], Patricia Martin[1], Carlo Fusco[1], Liliane Broye[1], Katarina Cisarova[2], Elizabeth M. Perez[3,4,5], Igor Letovanec[6,7], Stefano La Rosa[7], Stephane Cherix[8], Manuel Diezi[9], Raffaele Renella[9], Paolo Provero[10], Mario L. Suvà[3,4], Ivan Stamenkovic[1]*†, Nicolò Riggi[1†]

Targeting of the most aggressive tumor cell subpopulations is key for effective management of most solid malignancies. However, the metastable nature of tumor heterogeneity, which allows cells to transition between strong and weak tumorigenic phenotypes, and the lack of reliable markers of tumor-promoting properties hamper identification of the most relevant cells. To overcome these obstacles, we designed a functional microRNA (miR)–based live-cell reporter assay to identify highly tumorigenic cells in xenotransplants of primary Ewing sarcoma (EwS) 3D cultures. Leveraging the inverse relationship between cell pluripotency and miR-145 expression, we successfully separated highly tumorigenic, metastasis-prone (miR-145^{low}) cells from poorly tumorigenic, non-metastatic (miR-145^{high}) counterparts. Gene expression and functional studies of the two cell populations identified the EPHB2 receptor as a prognostic biomarker in patients with EwS and a major promoter of metastasis. Our study provides a simple and powerful means to identify and isolate tumor cells that display aggressive behavior.

INTRODUCTION

One of the greatest challenges to cancer therapy is the effective targeting of cells that provide the driving force to the growth and progression of any given tumor. Despite the long-standing notion that solid tumors are heterogeneous, most of the conventional cytotoxic drug–based strategies, which still dominate anticancer treatment, do not account for target cell heterogeneity and have reached their limit in terms of efficacy. Identification and detailed molecular characterization of tumor-driving cells along with in-depth understanding of the dynamics that govern their phenotype therefore appear to be inescapable requirements for the design of effective anticancer treatment.

Several mechanisms underlie the heterogeneity that characterizes solid malignancies, most prominent among which are clonal selection and hierarchical organization of tumor cells along with the effects of microenvironmental cues (*1*–*3*). Tumor cell plasticity renders the heterogeneity dynamic by allowing cells that drive tumor growth to differentiate and lose their tumorigenic properties in addition to providing the means for nontumorigenic cells to regain tumor-initiating capability (*2*–*4*). It is also key to tumor cell adaptation and resistance to treatment (*2*, *4*, *5*). Comprehensive identification of individual cells and cell subpopulations endowed with the ability to initiate and maintain tumor growth and progression is hampered by their lack of reliable biological markers. Although some cell surface receptors have been useful in isolating cell populations enriched in tumor-initiating cells (*1*, *6*), their ability to identify the full spectrum of cells that drive any given tumor remains limited. Moreover, because cancer cells, at least in some tumor types, may transition between tumorigenic and nontumorigenic phenotypes (*1*, *7*), it stands to reason that any unbiased approach designed to capture them in their tumorigenic state should exploit mechanisms underlying their plasticity in the most appropriate models available.

The recent development of three-dimensional (3D) culture technologies has facilitated assessment of tumor heterogeneity and drug sensitivity in a relevant preclinical setting. Under appropriate culture conditions, tumor-derived primary cells can generate spheroids that retain the native tissue heterogeneity or, as observed in a variety of carcinomas, organoids, which recapitulate both the heterogeneity and architecture of the tissue of origin (*8*–*10*). Primary 3D cultures derived from a variety of cancer types have helped identify major determinants of tumor heterogeneity and uncover therapeutic vulnerabilities that went unrecognized in standard 2D models (*10*, *11*). Moreover, patient-derived tumor 3D culture xenografts (PDXs) currently provide the closest in vivo mimics of the corresponding native tumors (*12*) and are particularly valuable for the study of cancers that lack genetically engineered mouse models. A case in point is Ewing sarcoma (EwS), the second most common bone malignancy in children and young adults (*13*).

EwS is a highly aggressive tumor with a marked tendency to relapse following therapy as well as high metastatic proclivity (*14*). Although multimodal therapy has improved survival of patients with localized disease, metastatic lesions at diagnosis markedly worsen prognosis, reducing the 5-year survival to 25%. EwS is caused by one of several reciprocal chromosomal translocations leading to the formation of a fusion a gene that encodes an aberrant transcription factor, the most common, found in 85 to 90% of tumors, being EWS-FLI1 (*15*). The chromosomal translocation is the only detectable genetic event in about 25% of EwS, suggesting that the resulting fusion protein bears dominant, if not sole, responsibility for their

[1]Experimental Pathology Service, Centre Hospitalier Universitaire Vaudois, University of Lausanne, Lausanne, Switzerland. [2]Department of Computational Biology, University of Lausanne, Lausanne, Switzerland. [3]Department of Pathology and Center for Cancer Research, Massachusetts General Hospital and Harvard Medical School, Boston, MA, USA. [4]Broad Institute of MIT and Harvard, Boston, MA, USA. [5]Department of Systems Biology, Harvard Medical School, Boston, MA, USA. [6]Department of Histopathology, Central Institute, Valais Hospital, Sion, Switzerland. [7]Institute of Pathology, Centre Hospitalier Universitaire Vaudois, University of Lausanne, Lausanne, Switzerland. [8]Department of Orthopedics, Faculty of Biology and Medicine, Centre Hospitalier Universitaire Vaudois, Lausanne, Switzerland. [9]Department Woman-Mother-Child, Division of Pediatrics, Centre Hospitalier Universitaire Vaudois, University of Lausanne, Lausanne, Switzerland. [10]Department of Neurosciences Rita Levi Montalcini, University of Turin, Center of Omics Sciences, Ospedale San Raffaele IRCSS, Milan, Italy.
*Corresponding author. Email: ivan.stamenkovic@chuv.ch
†These authors share senior authorship.

pathogenesis. EWS-FLI1 behaves as an aberrant transcriptional regulator that orchestrates major chromatin remodeling and functions as a pioneer factor to establish de novo active enhancers at GGAA microsatellite repeats (*16*). It promotes cell plasticity by deregulating microRNA (miRNA) maturation (*17*) and by directly decreasing miR-145 expression, which plays a prominent role in limiting cell pluripotency in both normal development and cancer (*18*, *19*). Repression of miR-145 contributes to the emergence and maintenance of poorly differentiated cells, which not only initiate primary and metastatic tumor growth but also differentiate into nontumorigenic progeny, thereby fueling tumor heterogeneity (*17*–*19*).

Here, we devised an experimental approach combining the power of miRNA reporter technology with primary 3D models of EwS to identify tumor cell subpopulations endowed with high tumorigenic and prometastatic properties. We leveraged the relationship between down-regulation of miR-145 and increased tumor cell pluripotency in EwS (*18*) to generate an inducible reporter system and isolate live primary miR-145^{high} and miR-145^{low} tumor cells in vivo. Functional analyses showed miR-145^{low} cells to be far more tumorigenic than their miR-145^{high} counterparts and to display a distinct gene expression signature comprising several oncogenes, including the receptor tyrosine kinase (RTK) EPHB2 (Ephrin type-B receptor 2). Current databases show EPHB2 expression to be associated with poor survival among patients with EwS, and our functional assays revealed that EPHB2 plays a critical role in promoting metastasis in EwS. On the basis of the role played by miR-145 in the emergence of undifferentiated and aggressive cells in other tumors, we anticipate our inducible in vivo reporter assay to be widely applicable to diverse cancer types and to facilitate the design of mechanism-based strategies to defeat tumor heterogeneity.

RESULTS

Detection of miR-145 activity in primary EwS cells

Our working strategy is summarized in Fig. 1A. Briefly, primary 3D tumor cell cultures from EwS removed at surgery were engineered to express the miR-145 reporter. Following validation of reporter activity in vitro, the 3D culture–derived tumor cells were transplanted into immunocompromised mice, the resulting tumors were removed, and cells were sorted based on reporter activity. Cells with high and low miR-145 expression could then be assessed for gene expression, clonogenicity, and tumor-initiating capacity following reinjection into mice.

To develop an inducible miR-145 responsive reporter (mirRep145), we engineered a green fluorescent protein (GFP)–encoding sequence containing five consecutive miR-145 recognition motifs in its 3′ untranslated region (3′UTR) and inserted it into the pINDUCER20 plasmid, downstream of the TRE2 promoter (Fig. 1A and fig. S1A) (*20*). An inducible, tetracycline-activated (Tet-On) expression system was chosen to minimize the potential sponge effect of exogenous miRNA binding site overexpression. Administration of doxycycline (Dox) to the cells harboring mirRep145 induced transcription of the GFP reporter sequence, and GFP expression levels were directly dependent on the intrinsic miR-145 activity (by binding to its target sequences, miR-145 suppresses the translation or transcription of the corresponding gene), providing an unbiased means to identify miR-145^{low} (GFP$^+$) and miR-145^{high} (GFP$^-$) cells (Fig. 1A). miR-145 target sequences were substituted by an unrelated DNA sequence to generate a mirReporter-Control vector (mirRepC) (fig. S1B).

mirRep145 was tested in HeLa cells, which express low levels of miR-145. Induction of GFP expression in cells harboring mirRep145 occurred within 48 hours of treatment with Dox, as assessed by confocal microscopy (Fig. 1B and fig. S1C, bottom), and neither mirRep145- nor mirRepC-containing cells expressed GFP in the absence of Dox (Fig. 1B and fig. S1C, top). To validate the specific dependency of our reporter system on miR-145 activity, we tested the effect of unrelated miRNAs on HeLa cells bearing mirRep145 using expression plasmids containing the red fluorescent protein (RFP)–puromycin resistance fusion protein (rPuro), which allows simultaneous assessment of infection efficiency by RFP expression and selecting for puromycin resistance (Fig. 1C, middle). Immunofluorescence microscopy of Dox-treated HeLa mirRep145 cells infected with a mock miRNA sequence (an unrelated sequence matching miR-145 length), let7a-, or miR-145–containing vectors revealed reduced GFP expression only in cells expressing miR-145 (Fig. 1C, right), indicating specific targeting of the reporter GFP construct by miR-145.

We then assessed mirRep145 function in two EwS 3D cultures, EwS1 and EwS2 (*21*–*23*), derived, respectively, from a metastatic lung lesion removed after chemotherapy and an untreated primary tumor (table S1). Both 3D cultures, which appeared as spheroids, retained the hierarchical cellular organization of the primary tumors from which they were derived (*21*, *22*). EwS1 and EwS2 cells infected with a lentivirus containing the mirRep145 were maintained as 3D cultures in medium supplemented with Dox for 48 hours and assessed for GFP expression by flow cytometry and fluorescence microscopy 2 (D2), 5 (D5), and 10 (D10) days following Dox removal (fig. S1, D to G). Fluorescence-activated cell sorting (FACS) revealed that 47 and 38% of the EwS1- and EwS2-mirRep145 cell populations, respectively, were GFP$^+$ after Dox-mediated induction (fig. S1, D and F). GFP expression decreased rapidly following Dox removal and was undetectable after 10 days of Dox-free culture. Neither Dox nor its removal affected 3D spheroid formation in vitro (fig. S1, E and G).

Purification of primary EwS cell subpopulations based on miR-145 expression

We previously showed that EwS cells with low miR-145 expression have clonogenic and tumor-initiating capacity, giving rise to tumors that phenocopy the original tumor, whereas cells with high miR-145 expression from the same tumor were poorly tumorigenic (*17*, *18*). To address the properties of miR-145^{low} EwS cells and identify candidate predictive markers of tumor aggressiveness, we transplanted mirRep145-expressing EwS1 and EwS2 3D culture–derived cells into the subcapsular renal compartment of nonobese diabetic severe combined immunodeficient γ (NSG) mice whose diet was supplemented with appropriate doses of Dox. Upon reaching 1 cm^3, the tumors were removed at autopsy and dissociated, and GFP expression of the cells was assessed by flow cytometry. Both EwS 3D culture–derived tumors displayed induction of GFP expression in vivo, with approximately 21% of EwS1 and 15% of EwS2 cells being GFP$^+$ (Fig. 1D).

Next, we verified that mirRep145 allows separation of tumor cells based on their intrinsic miR-145 expression by quantitative polymerase chain reaction (qPCR) assessment of miR-145 transcripts in sorted GFP$^-$ and GFP$^+$ subpopulations. Consistent with its mechanism of action, expression of miR-145 was almost threefold lower in GFP$^+$ than in GFP$^-$ cells (Fig. 1E). Immunohistochemistry (IHC) using anti-GFP antibody on tumor tissue sections revealed no GFP signal in control tumors but strong expression in a fraction of cells

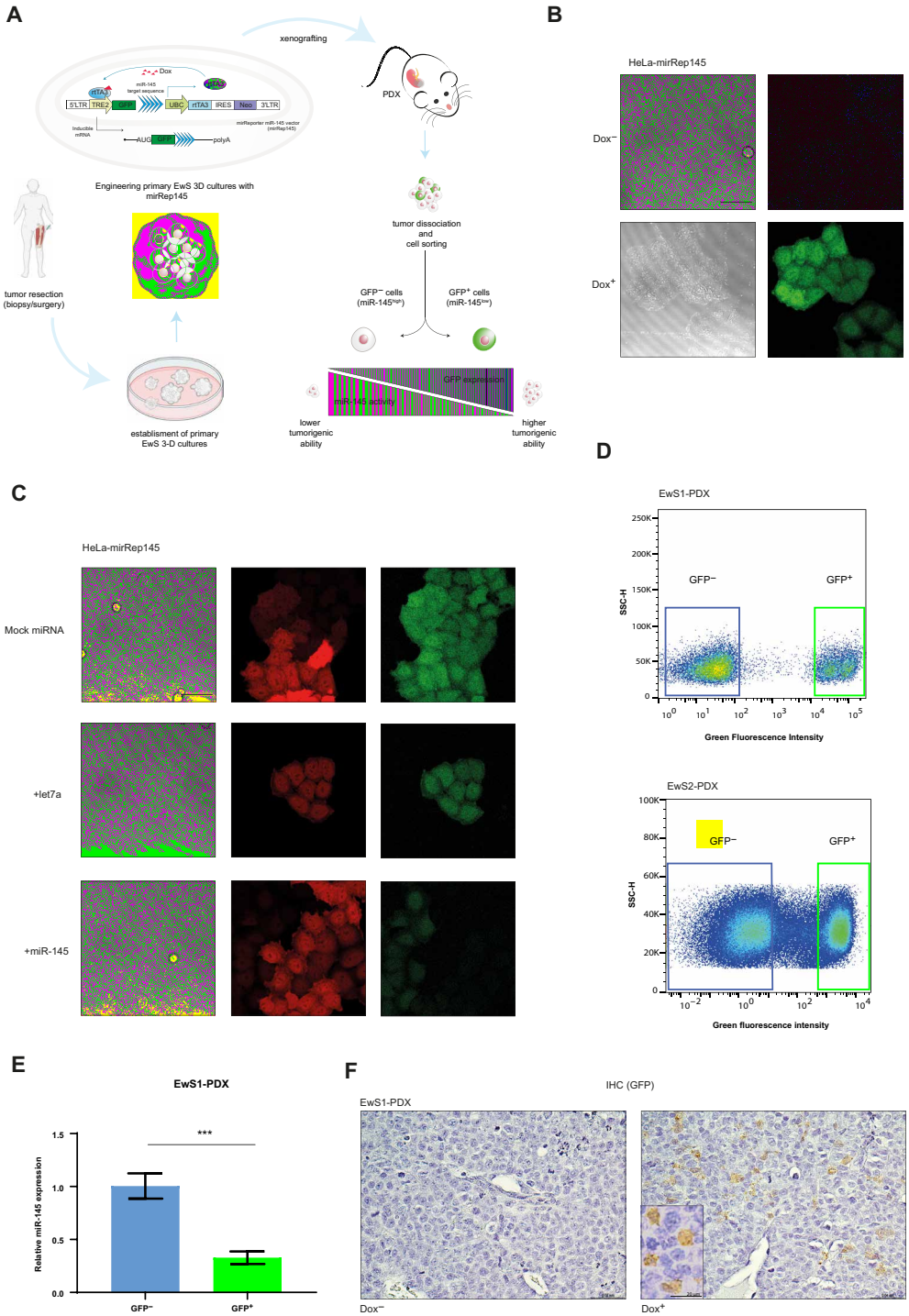

Fig. 1. In vitro and in vivo implementation of the mirReporter assay. (**A**) Schematic overview of the experimental design (Dox, doxycycline; GFP, green fluorescent protein; IRES, internal ribosome entry site; LTR, long terminal repeat; Neo, neomycin; rtTA3, reverse tetracycline-controlled transactivator 3; PDX, patient-derived xenograft; TRE2, Tet response element 2; UBC, ubiquitin C promoter; 5′cap = ●—). (**B**) Representative confocal microscopy images of induced GFP (green) expression in HeLa-mirRep145 cells treated with Dox (1 μg/ml, 48 hours) (bottom) compared to phosphate-buffered saline (PBS)–treated control cells (Dox^-) (top) (40× objective; scale bar, 50 μm). (**C**) Representative confocal microscopy images showing decreased GFP expression (green) in Dox-treated HeLa-mirRep145 cells overexpressing miR-145 compared to HeLa-mirRep145 cells overexpressing mock miRNA and let7a [middle: red fluorescent protein (RFP) expression (red); right: GFP expression (green); 40× objective; scale bar, 50 μm]. (**D**) Fluorescence-activated cell sorting (FACS) based on GFP expression in mirRep145-bearing EwS1-PDX (top) and EwS2-PDX (bottom) cells. (**E**) Quantitative real-time polymerase chain reaction (qRT-PCR) assessment of mature miR-145 expression in GFP^+ and GFP^- subpopulations of EwS1-PDX carrying mirRep145 after in vivo induction, tumor dissociation, and cell sorting. (Mean ± SD values of three technical replicates are shown. Statistical analysis was done by unpaired *t* test; $^{***}P \leq 0.001$.) (**F**) Immunohistochemical assessment of GFP expression in tumor tissues of a EwS1-PDX-mirRep145–injected control mouse (Dox^-) and a Dox-treated mouse (Dox^+) (scale bars, 40 μm; inset scale bar, 20 μm).

in tumors from Dox-fed mice (Fig. 1F and fig. S1H). Dox penetration of the tumor tissue appeared to be adequate, as GFP$^+$ cells were observed throughout the tumor and not merely around blood vessels. miR-145 expression was significantly higher in both EwS1- and EwS2-derived PDXs compared to their corresponding in vitro culture models, confirming the ability of primary 3D culture–derived cells to generate more differentiated progeny in vivo (fig. S1I). On the basis of our earlier observations that miR-145 regulates the pluripotency-associated gene *SOX2* in EwS cells (*18*), we compared *SOX2* expression between bulk EwS1 cells and their GFP$^+$ and GFP$^-$ fractions. Consistent with our previous results, GFP$^+$ cells expressed higher levels of *SOX2* than their GFP$^-$ counterparts (fig. S1J).

Low miR-145 activity as a marker of primary EwS cells in a highly tumorigenic state

We then assessed miR-145^{high} and miR-145^{low} cell tumorigenicity in vivo. MirRep145-infected EwS1 and EwS2 3D culture–derived cells were transplanted beneath the kidney capsule of NSG mice, and tumor growth was monitored by ultrasonography weekly. Mice bearing tumors of about 1 cm^3 were given Dox for 96 hours, after which they were euthanized and tumors were removed. Following dissociation and mouse cell depletion, tumor cells were sorted into GFP$^-$ and GFP$^+$ subpopulations, which were then retransplanted beneath the kidney capsule of NSG mice. Unsorted bulk tumor cells (induced bulk, IB) from Dox-treated animals were transplanted into a third group of mice and tumor growth in all animals was monitored by ultrasonography (Fig. 2A).

Self-renewal of GFP$^-$, GFP$^+$, and bulk cells from Dox-treated (IB) and untreated (control bulk) mice was assessed by clonogenic assays in which sphere formation was scored after 4 weeks of culture. Both EwS1 and EwS2 PDX–derived GFP$^+$ cells displayed higher self-renewal than either batch of bulk or GFP$^-$ cells (Fig. 2B). Consistent with their higher self-renewal, EwS1 and EwS2 GFP$^+$ cells were more tumorigenic than their GFP$^-$ counterparts (Fig. 2, C to G).

To verify mirRep145 stability, aliquots of cells derived from first-round xenografts, including IB, GFP$^+$, and GFP$^-$ cells, were cultured in vitro in the presence of geneticin and Dox. The three cell populations retained resistance to neomycin, whereas only GFP$^+$ and IB tumor–derived populations expressed GFP in response to Dox (fig. S2). MirRep145 therefore remained stably expressed and functional throughout in vivo tumor growth, demonstrating the feasibility of using miR-145 expression as a functional reporter to isolate subpopulations of cells with divergent tumorigenic capacity from a heterogeneous tumor cell population.

A dual-color mirReporter to monitor the evenness of cell infection

To ensure that GFP$^-$ and GFP$^+$ subpopulations reflect endogenous differences in miR-145 expression rather than uneven cell infection, we generated a second mirReporter to monitor infection homogeneity. The RFP-puromycin vector (rPuro, described above) provides both an antibiotic selection marker and the means to track infected cells by monitoring RFP expression. We thus established a miR-145–responsive dual-color reporter assay (Dual mirRep145) in which green fluorescence indicates miR-145 expression and red fluorescence reflects infection homogeneity (Fig. 3A).

Dual mirRep145 expression in HeLa cells (Fig. 3B) revealed that RFP expression was independent of Dox treatment, confirming successful cell infection, and that GFP expression was induced upon Dox administration. Similarly, EwS1 and EwS2 cells harboring Dual mirRep145 expressed RFP and, upon treatment with Dox for 48 hours, initiated GFP while maintaining RFP expression (fig. S3A). Following removal of Dox, EwS1 and EwS2 cells lost GFP expression within 10 days but retained RFP expression, indicating reporter stability.

EwS1 and EwS2 cells carrying Dual mirRep145 were sorted based on their RFP expression (fig. S3B) to select the most homogeneously infected cell population for in vivo tumor initiation assays (Fig. 3C). The selected Dual mirRep145–bearing EwS1 and EwS2 cells were transplanted beneath the kidney capsule of NSG mice, and following tumor formation, mice were administered Dox as before. After tumor dissociation at autopsy, cells were assessed for GFP and RFP expression by flow cytometry (Fig. 3, D and E). EwS1 and EwS2 cells with comparable RFP expression were then sorted based on their GFP levels. The clonogenic and tumorigenic properties of sorted GFP$^-$ and GFP$^+$ cells were assessed in vitro and in vivo, respectively. GFP$^+$ cells displayed higher clonogenicity than their GFP$^-$ counterparts (Fig. 3F and fig. S3C), as well as greater tumor-initiating ability (Fig. 3G and fig S3, D to F). Our observations using Dual mirRep145 were therefore consistent with those obtained using the single-color mirRep145.

Identification of candidate genes that underlie EwS aggressiveness and bear potential prognostic value

To gain insight into the mechanisms underlying the difference in GFP$^+$ (miR-145^{low}) and GFP$^-$ (miR-145^{high}) EwS cell subpopulation behavior, we compared the transcriptome of primary GFP$^+$ and GFP$^-$ cells derived from freshly dissociated EwS1-PDX and EwS2-PDX carrying mirRep145 or Dual mirRep145. All cells sorted according to GFP expression were included into a single statistical mode in which the covariate of interest was GFP expression, denoted as GFP$^+$ and GFP$^-$. The other covariates used for adjustment were the tumor origin (EwS1 or EwS2) and the type of reporter (mirRep145 or Dual mirRep145). DEseq2 was used to fit the model and differentially expressed genes were defined by $|\log FC| > 1$ and a nominal $P < 0.01$. Using these parameters, we found 55 and 29 significantly up- and down-regulated genes, respectively, in GFP$^+$ compared to GFP$^-$ cells (tables S2 and S3). To address a possible link between miR-145 and EWS-FLI-1 expression levels, we compared differentially expressed genes between GFP$^+$ and GFP$^-$ EwS1 cells to those that displayed a change in expression upon *EWSR1-FLI1* depletion by short hairpin RNA (shRNA) in the same model (*23*). However, the observation that the same EWS-FLI-1–dependent gene expression signature was enriched in both GFP$^+$ and GFP$^-$ populations (fig. S4A) does not support the notion of variable EWS-FLI-1 expression between GFP$^+$ and GFP$^-$ cells. In addition, expression of 106 previously described EWS-FLI-1 direct target genes (*23*) was not found to be significantly different between GFP$^+$ and GFP$^-$ cells (fig. S4B), indicating that their distinct behavior was not related to differences in *EWSR1-FLI1* expression or function. Last, no significant enrichment for direct miR-145 targets was identified among differentially expressed genes between GFP$^+$ and GFP$^-$ cells (fig. S4, C and D), suggesting that the signatures distinguishing GFP$^+$ from GFP$^-$ subpopulations are not merely the effect of miR-145 expression but the result of complex transcriptional programs that may define different cell phenotypes.

To determine whether these gene expression signatures may bear any prognostic value, we asked whether the significantly up- and down-regulated genes in the GFP$^+$ subpopulation (miR-145^{low}) are

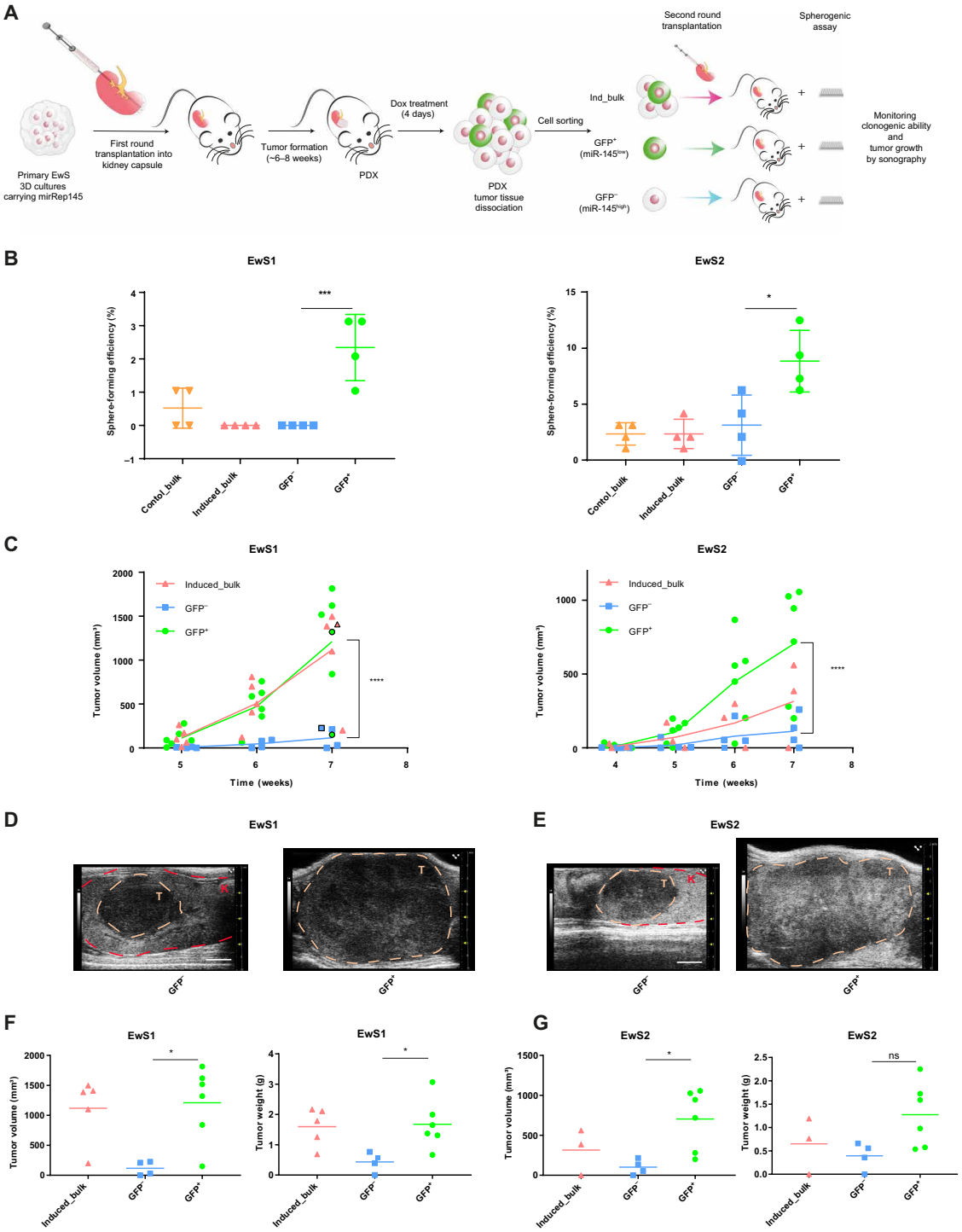

Fig. 2. Primary EwS 3D cultures with low miR-145 expression display high clonogenic capacity in vitro and tumor-initiating capacity in vivo. (**A**) Schematic diagram of the experimental design of in vivo studies. (**B**) GFP$^+$ (miR-145^{low}) subpopulations of EwS1-PDX (left) and EwS2-PDX (right) have higher clonogenic capacity than their GFP$^-$ (miR-145^{high}) counterparts (mean ± SD values of four technical replicates are shown). Control bulk and induced bulk (IB) cells were obtained from PDX-derived tumor tissues of control (drinking water devoid of Dox) and Dox-treated mice (2 mg/ml, 96 hours), respectively. (**C**) In vivo tumorigenicity of GFP$^+$ and GFP$^-$ cells obtained from EwS1-PDX (right) and EwS2-PDX (left). (Average tumor volumes were measured weekly by ultrasonography. EwS1: IB, $n = 5$ mice; GFP$^-$, $n = 4$ mice; GFP$^+$, $n = 6$ mice. EWS2: IB, $n = 3$ mice; GFP$^-$, $n = 4$ mice; GFP$^+$, $n = 6$ mice. Mean ± SD values of technical replicates are shown. Primary tumors whose symbols are outlined in black are shown in Fig. 4G.) (**D** and **E**) Ultrasonograms of GFP$^-$ and GFP$^+$ tumors from EwS1-PDX (D) and EwS2-PDX (E) 6 weeks after injection of cells beneath the kidney capsule (T, tumor tissue; K, kidney tissue; scale bars, 2 mm). (**F** and **G**) The GFP$^+$ subpopulation of EwS1-PDX (F) and EwS2-PDX (G) gave rise to larger tumors than the GFP$^-$ subpopulation (mean ± SD values of technical replicates are shown). [One-way analysis of variance (ANOVA) was used to perform the statistical analysis of (B), (F), and (G), and two-way ANOVA was used for the analysis of (C); ns, not significant; *$P \leq 0.05$; ***$P \leq 0.001$; ****$P \leq 0.0001$.]

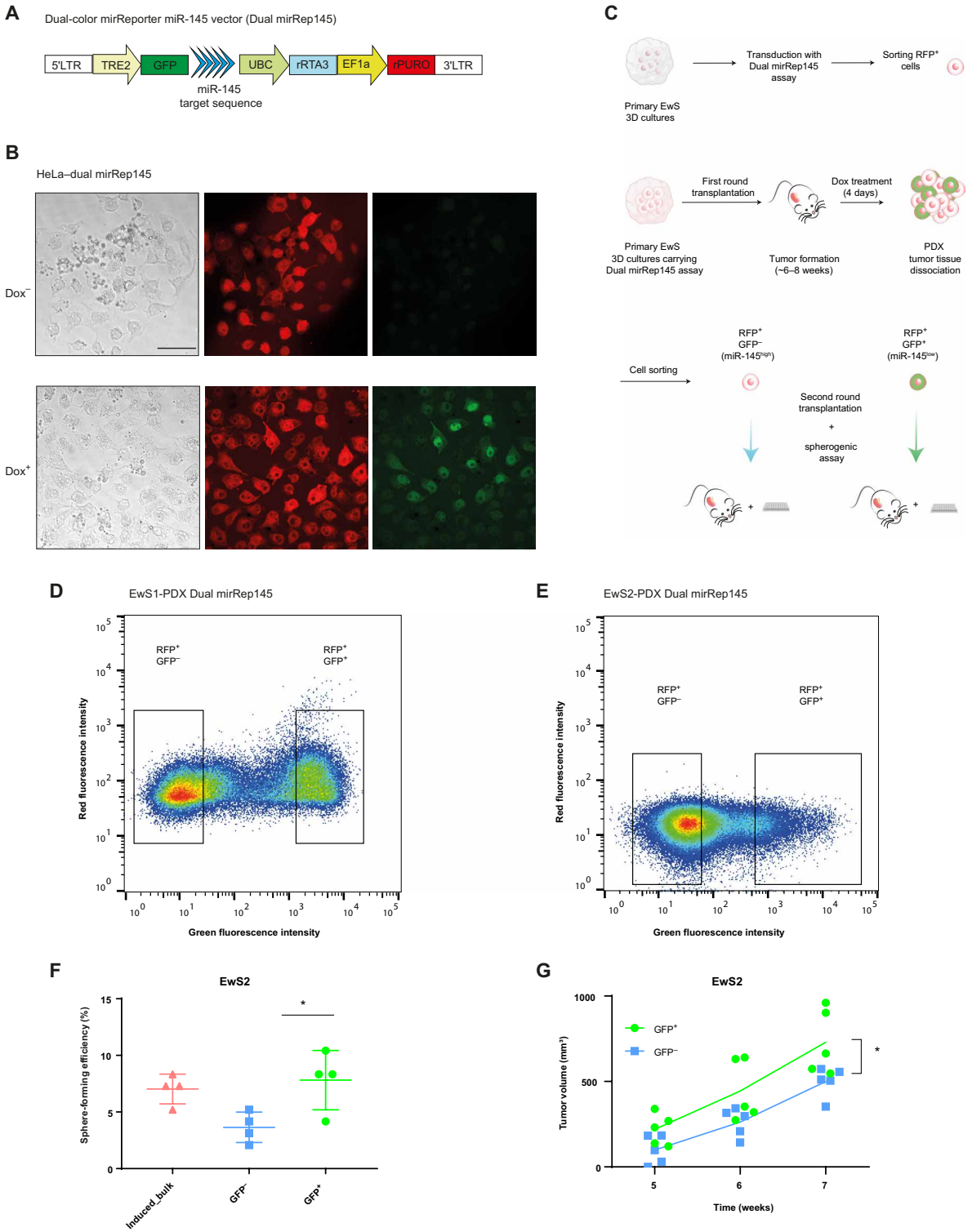

Fig. 3. A dual-color mirReporter allows monitoring cell infection homogeneity. (**A**) Diagram showing the dual-color mirReporter miR-145 construct (Dual mirRep145). (**B**) Representative confocal microscopy images showing Dox-induced (1 μg/ml, 48 hours) GFP expression (green) in HeLa cells carrying the Dual mirRep145 (bottom) compared to PBS-treated control cells (top) [middle: RFP expression (red) indicating the distribution of Dual mirRep145 infection; 40× objective; scale bar, 50 μm]. (**C**) Schematic illustration of the Dual mirRep145 assay design in vitro and in vivo. (**D** and **E**) FACS acquisition of RFP and GFP in Dual mirRep145 carrying EwS1-PDX (D) and EwS2-PDX (E) cells after in vivo induction of reporter expression [mice received Dox (2 mg/ml) for 96 hours before sacrifice and tumor dissociation]. (**F**) GFP$^+$ EwS2-PDX–Dual mirRep cells are more clonogenic than their GFP$^-$ counterparts. [Mean ± SD values of four technical replicates are shown. IB: dissociated tumor cells from mice treated with Dox (2 mg/ml) for 96 hours.] (**G**) Tumors derived from EwS2-PDX GFP$^+$ cells grow faster than tumors originating from the corresponding GFP$^-$ cells ($n = 5$ mice per group). [One-way ANOVA test was used to perform the statistical analysis of (F) and two-way ANOVA was used for the analysis of (G); *$P \leq 0.05$.]

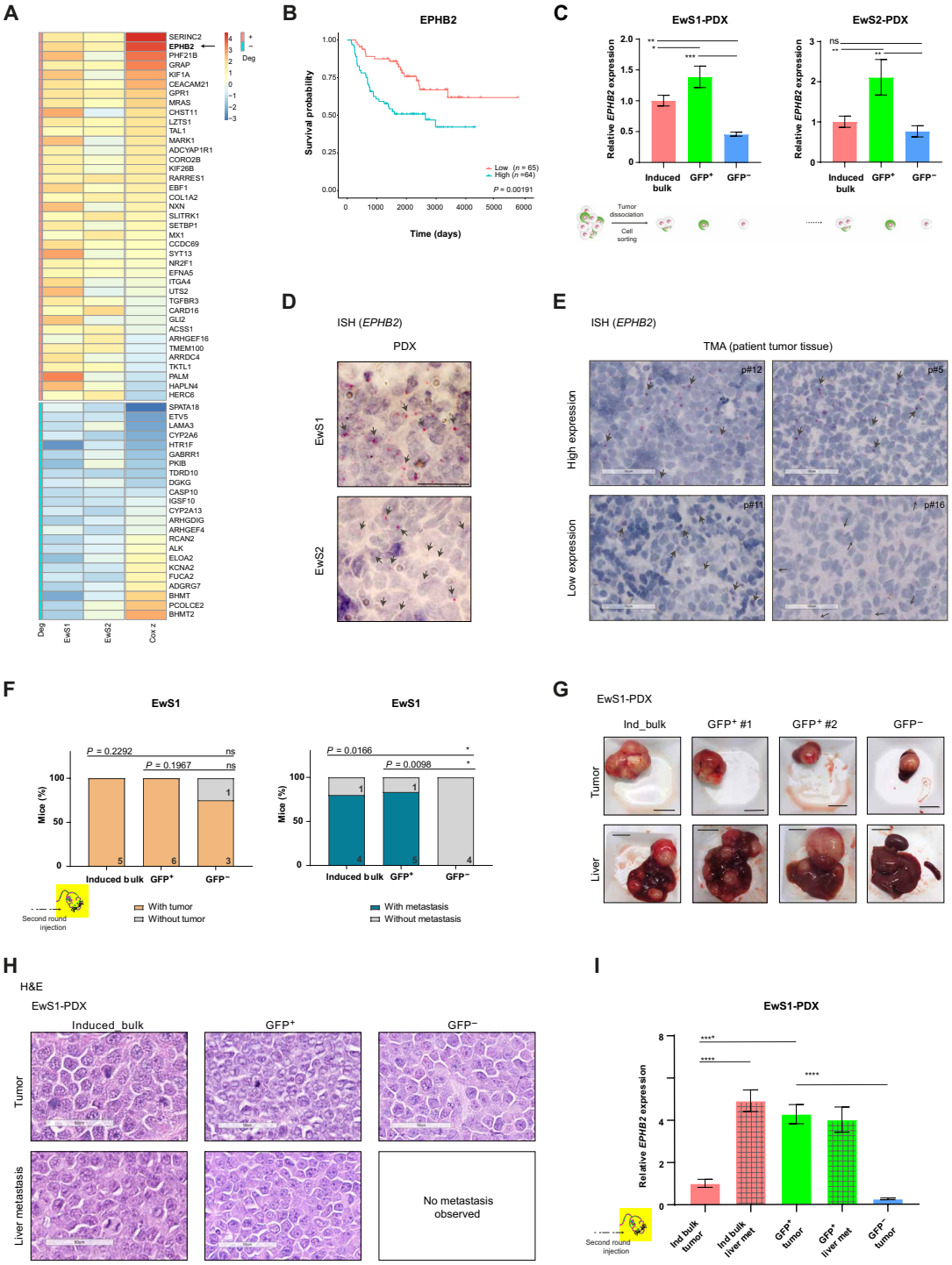

Fig. 4. Identification of EPHB2 as a candidate gene that underlies EwS aggressiveness with a potential prognostic value. (**A**) Heatmap of differentially expressed genes in the GFP$^+$ subpopulation of EwS-PDXs (compared to GFP$^-$ counterparts). The Cox *z* values (and sign) indicate the strength of the positive correlation between the expression level of a gene and patient survival. (**B**) Kaplan-Meier curves showing overall survival of patients with high and low *EPHB2* expression. (**C**) Relative *EPHB2* expression in IB, GFP$^+$, and GFP$^-$ subpopulations of EWS1 and EWS2 PDX (mean ± SD values of three technical replicates are shown). (**D**) RNA in situ hybridization (ISH) assessment of *EPHB2* expression in EwS-PDX tissues (scale bar, 25 μm) and (**E**) in primary EwS tumors (scale bars, 50 μm; arrows indicate ISH signals). (**F**) Distribution of local tumor– and metastasis-bearing mice following injection of the indicated cell subpopulations (IB, $n = 5$; GFP$^+$, $n = 6$; GFP$^-$, $n = 4$) with (**G**) representative pictures of primary tumors and matched livers (scale bars, 1 cm). (Corresponding primary tumor volume symbols are outlined in Fig. 2C. Photo credit: Tugba Keskin, CHUV.) (**H**) Representative H&E (hematoxylin and eosin)–stained sections of local tumors and matched liver metastases (scale bars, 50 μm). (**I**) qRT-PCR assessment of *EPHB2* transcripts in primary tumors and their matched liver metastases (mean ± SD values of three technical replicates are shown). [One-way ANOVA test was used to perform the statistical analysis of (C) and (I), log-rank (Mantel-Cox) was used for (B), and chi-square (Fisher's exact test) was used for (F). ns, not significant; *$P \leq 0.05$; **$P \leq 0.01$; ***$P \leq 0.001$; ****$P \leq 0.0001$.]

predictive of survival for patients with EwS. We combined five different primary EwS microarray datasets into a single dataset containing survival details of 129 patients. To assess putative predictive values of significantly down- and up-regulated genes in GFP$^+$ cells on overall EwS patient survival, we performed univariate Cox analysis of the correlation between the gene expression level and survival duration. Such analysis produces a *z* value, which indicates the strength and sign of the correlation for significantly up- and down-regulated genes in the highly tumorigenic miR-145^{low} EwS cells. We found that up-regulated genes had mostly positive *z* values (Fig. 4A), indicating correlation between their expression and adverse prognosis, whereas the opposite was true of down-regulated genes. To validate these observations, Kaplan-Meier survival analysis was performed in the same cohort by comparing two clusters of patients with individual gene expression below (n = 65) and above (n = 64) the median value. A significant negative correlation was observed between expression of the up-regulated gene *EPHB2* (P = 0.00191) and survival (Fig. 4B).

EPHB2 encodes a transmembrane RTK that binds ephrin ligands and mediates intercellular communication through bidirectional signaling (*24*). Several arguments support its functional implication in promoting EwS cell aggressiveness. First, its expression in GFP$^+$ cells was about four times higher than in GFP$^-$ cells (table S2). Second, EwS patients bearing tumors with high *EPHB2* expression levels have worse overall survival rates (Cox z = 4.102, Cox $P = 4.09 \times 10^{-5}$, Kaplan Meier P = 0.00191) than patients with tumors expressing low levels of the gene (Fig. 4, A and B). Third, EPHB2 plays a well-established role in both maintaining cell pluripotency and promoting carcinogenesis (*25*) and is implicated in tumor metastasis (*26*).

We therefore assessed *EPHB2* expression in EwS1 and EwS2 PDX-derived cell fractions and observed significantly higher expression of *EPHB2* in GFP$^+$ than in GFP$^-$ and IB cells in both 3D culture models (Fig. 4C). RNA in situ hybridization (ISH) analysis of EwS1 and EwS2 xenografts showed a marked difference in their *EPHB2* expression pattern, with relatively diffuse expression in EwS1 xenografts versus paucicellular expression in EwS2 (Fig. 4D). These observations reflect *EPHB2* expression heterogeneity in EwS, in terms of both level and cell percentage, as illustrated by *EPHB2* RNA ISH analysis of a cohort of 16 primary EwS patient samples (Fig. 4E and fig. S4E).

On the basis of the prognostic value of EPHB2 in patients with EwS and the notion that the major clinical determinant of EwS patient survival is their metastatic burden, we reasoned that EPHB2 may be involved in EwS dissemination. Consistent with our hypothesis, we observed a notable difference in metastatic spread among sorted cell populations. Following the second round of injection, tumors developed in all mice injected with GFP$^+$ and IB cells from EwS1 PDX and in 75% of the mice injected with GFP$^-$ cells (Fig. 4F). However, whereas large liver metastases formed in 80 and 83.33% of mice injected with IB and GFP$^+$ cells, respectively, none of the mice injected with GFP$^-$ cells developed visible metastases (Fig. 4F). This discrepancy did not appear to be due to differences in tumor growth at the site of injection because one EwS1 GFP$^+$ tumor whose size was comparable to those of GFP$^-$ tumors was associated with large liver metastases (Figs. 4, G and H, and 2C). Expression of *EPHB2* was elevated in the liver metastases derived from both IB and GFP$^+$ tumors, as well as in GFP$^+$ tumors at the site of injection. By contrast, it was low in IB tumors at the injection site and undetectable in GFP$^-$ tumors (Fig. 4I).

EPHB2, a candidate marker of EwS cells with self-renewing and metastatic properties

To determine its functional role in EwS self-renewal and tumor initiation, we partially depleted EwS1 cells of EPHB2 using lentiviral vectors bearing two different EPHB2-specific shRNAs (Fig. 5, A and B). Compared to controls, cells depleted of EPHB2 exhibited a dramatic decrease in spheroid formation in vitro (Fig. 5C) and a correspondingly impaired ability to initiate tumor growth in vivo (Fig. 5, D to F). ISH and qPCR assessment of tumors that emerged from EPHB2-depleted cell xenografts revealed their expression of *EPHB2* at levels comparable to those of control cells, suggesting that they originated from cells that had evaded *EPHB2* depletion (Fig. 5, G and H). To circumvent the technical limitations inherent to shRNAs, we generated CRISPR-mediated EPHB2 knockout (KO) EwS1 cells using three different single guide RNAs (sgRNAs) targeting *EPHB2*. The resulting EPHB2-depleted EwS1 cells displayed markedly reduced clonogenicity (Fig. 6, A to C). To address the possible involvement of EPHB2 in pro-metastatic properties of GFP$^+$ EwS1 cells, we addressed the invasiveness of EPHB2 KO cells in vitro, as assessed by Matrigel transwell assays. We observed that invasiveness was strongly impaired in the absence of EPHB2 (Fig. 6D).

To determine whether our functional observations reflect a general property of EwS, we interrogated the Cancer Cell Line Encyclopedia for EPHB2 expression levels in EwS cell lines and selected two, A673 and RD-ES, for further investigation based on their robust expression of the receptor. Both cell lines were grown as spheroids in ultralow attachment plates to mimic the primary models. After validation of its expression by FACS analysis (fig. S5, A and B), we depleted EPHB2 from both lines by shRNA and measured the ensuing changes in their clonogenicity and invasiveness in vitro. We observed a significant decrease in the clonogenicity and invasiveness of both cell lines upon EPHB2 depletion, supporting our findings in the primary EwS1 model (Fig. 6, E to H, and fig. S5, C to F).

In contrast to EwS1, EwS2 bulk and GFP$^+$ cells formed only microscopic metastases (fig. S6, A to C). A possible explanation for the difference in behavior between EwS1 and EwS2 cells may lie in their origin: Unlike EwS1 cells, which were derived from a metastatic tumor to the lung following chemotherapy, EwS2 cells originated from a primary, untreated tumor and only few expressed EPHB2 (Fig. 4D and table S1). We reasoned that if EPHB2 is involved in fueling the metastatic properties of EwS cells, enhancement of its expression in weakly metastatic primary tumor cells may promote their dissemination, similar to EwS1. Exogenous overexpression of EPHB2 in EwS2 cells (Fig. 7, A and B, and fig. S6D) did not alter their self-renewal or tumor-initiating ability (Fig. 7, C to F, and fig. S6E). In contrast, whereas EwS2 control cells did not form macroscopic metastases, EwS2 cells expressing exogenous EPHB2 formed multiple large metastases in several organs, particularly the liver, lung, contralateral kidney, and peritoneum (Fig. 7, G to J, and fig. S6, F and G). Careful histological examination revealed that control EwS2 cells were able to form a small number of micrometastases in the lung and kidney, often centered by blood vessels (Fig. 7J, left). However, in the absence of EPHB2 overexpression, no macro-metastases arose for the duration of the experiments. Together, our results indicate that EPHB2 promotes the metastatic properties of primary EwS cells, raising the possibility that pharmacological targeting of its signaling pathway may provide a candidate strategy to blunt EwS dissemination.

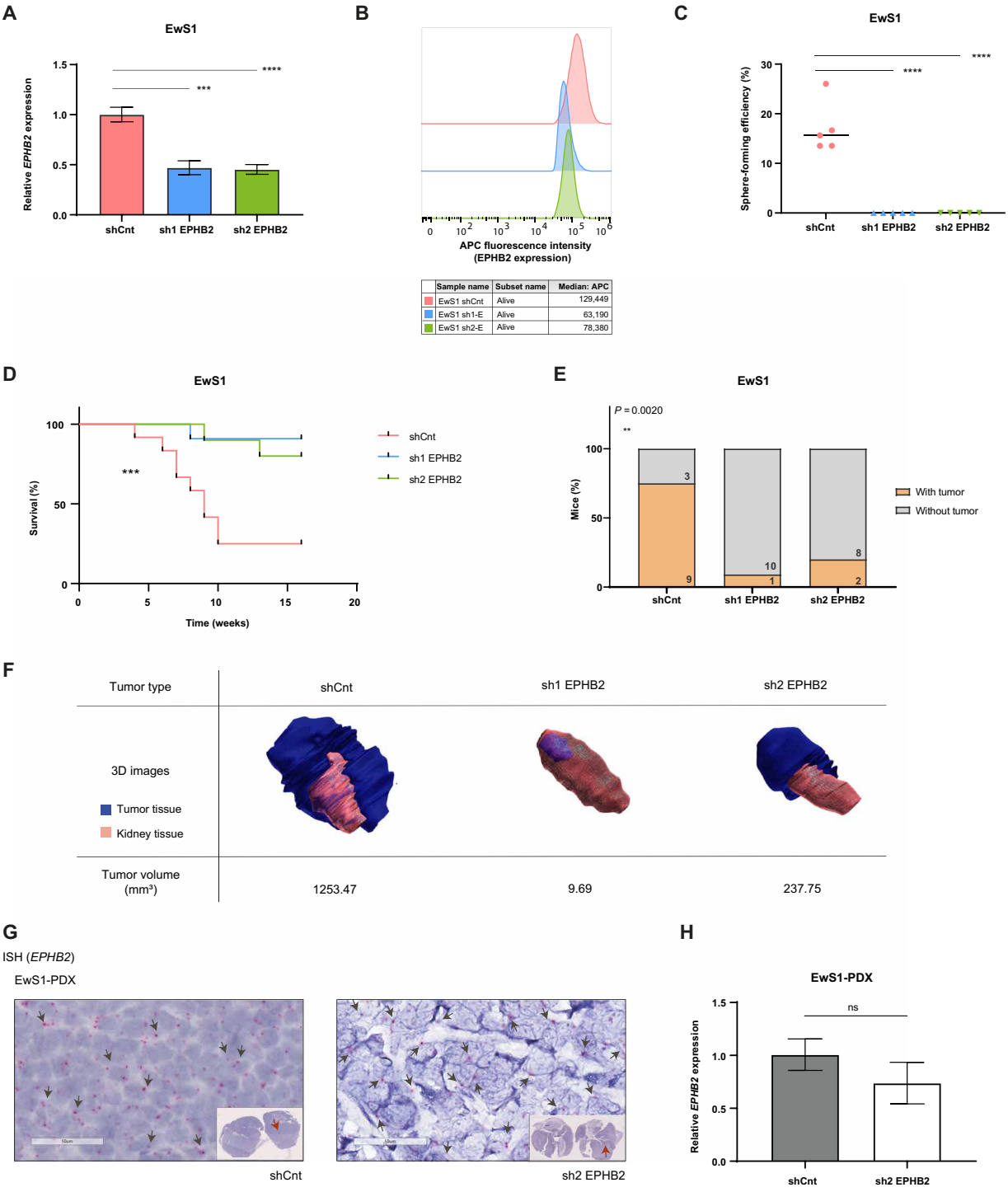

Fig. 5. EPHB2 depletion impairs tumor growth in vivo. (**A**) Relative *EPHB2* expression of EwS1 3D culture infected with EPHB2-targeting shRNAs (sh1 EPHB2 and sh2 EPHB2) compared to those in EwS1 control cells transduced with GFP-targeting shRNA (shCnt) as measured by qRT-PCR (mean ± SD, $n = 3$). (**B**) EPHB2 expression, as assessed by flow cytometry, in EwS1 3D cultures following shRNA-mediated EPHB2 depletion compared to EwS1 control cells (shCnt). (**C**) Clonogenic assay of EwS1 3D cultures depleted of EPHB2 (mean ± SD, $n = 5$). (**D**) Survival of mice injected with EwS1 3D cultures depleted of EPHB2 compared to mice injected with EwS1 control 3D culture (shCnt) (shCnt, $n = 12$; sh1 EPHB2, $n = 11$; sh2 EPHB2, $n = 10$). (**E**) EPHB2 depletion reduces the tumorigenic capacity of EwS1 3D culture (corresponding mouse numbers in each group are indicated in the graph bars). (**F**) Representative 3D ultrasonography reconstruction images of tumors at week 7 with corresponding tumor volumes (in cubic millimeters) below. (**G**) RNA ISH and (**H**) qRT-PCR assessment of *EPHB2* transcript expression in tumors derived from EwS1-shCnt and EwS1-sh2 EPHB2 xenografts indicate that the tumors initially depleted of EPHB2 regain its expression (scale bars, 50 μm; arrows indicate ISH signals. qRT-PCR: mean ± SD, $n = 3$). [One-way ANOVA test was used to perform the statistical analysis of (A), (C), and (H); log-rank (Mantel-Cox) was used for (D); and chi-square (Fisher's exact test) was used for (E). ns, not significant; $^{**}P \leq 0.01$; $^{***}P \leq 0.001$; $^{****}P \leq 0.0001$.]

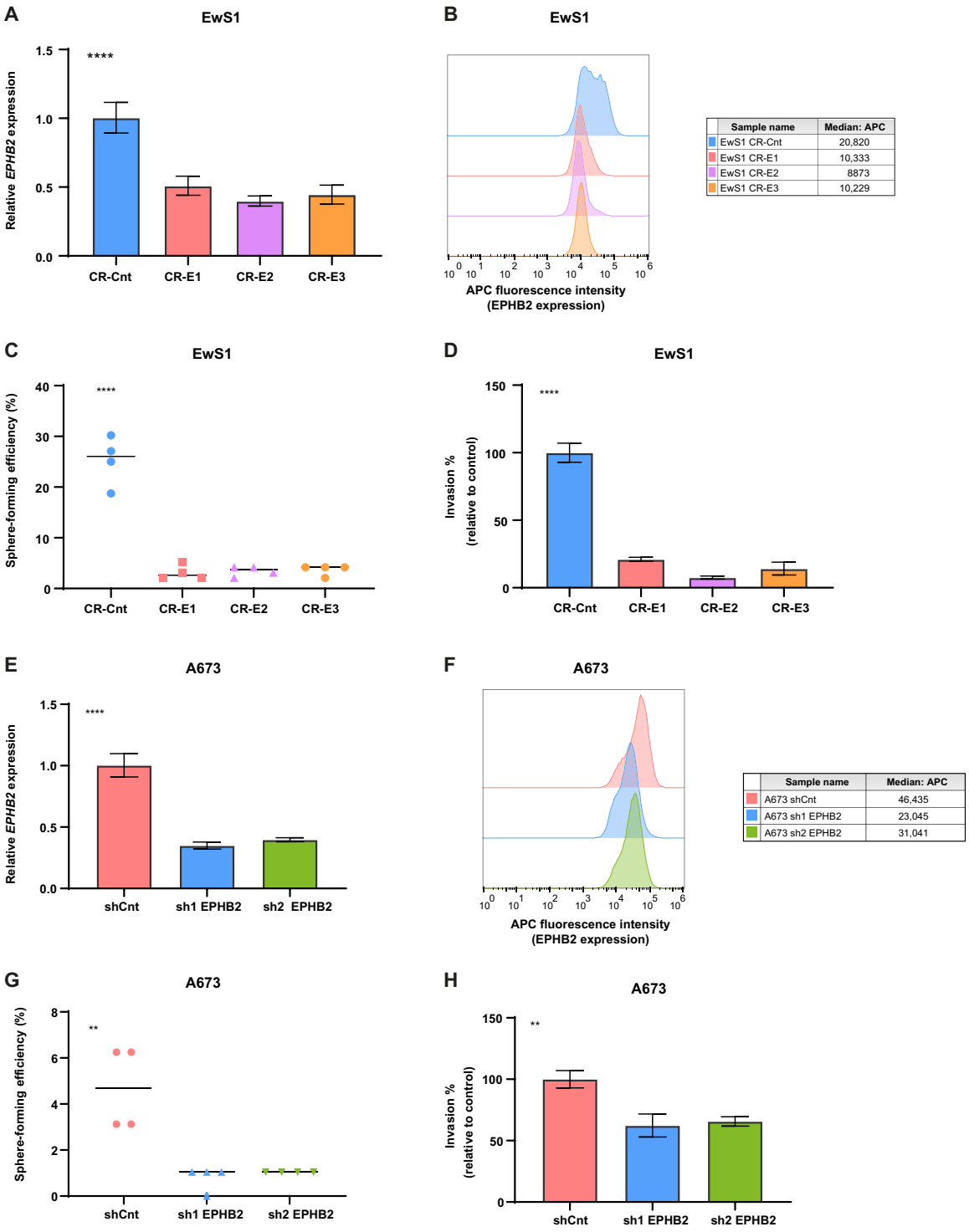

Fig. 6. EPHB2 depletion reduces clonogenicity and invasiveness of EwS cells. (**A**) Relative *EPHB2* expression of EwS1 3D culture infected with EPHB2-targeting sgRNAs (CR-E1, CR-E2, and CR-E3) compared to EwS1 control cells (CR-Cnt) as measured by qRT-PCR (mean ± SD values of three technical replicates are shown). (**B**) EPHB2 expression, as assessed by flow cytometry, in EwS1 3D cultures following sgRNA-mediated EPHB2 depletion in (A). (**C**) Clonogenic and (**D**) transwell-invasion assays for EwS1 tumor 3D cultures depleted of EPHB2 (CR-E1, CR-E2, and CR-E3) compared to control cells (CR-Cnt) (mean ± SD values of four and three technical replicates are shown for clonogenic and invasion assays, respectively). (**E**) qRT-PCR and (**F**) FACS analysis of EPHB2 expression in the EwS A673 cell line transduced with *EPHB2* targeting shRNAs (sh1 EPHB2 and sh2 EPHB2) compared to control cells (shCnt). (**G**) Clonogenic and (**H**) transwell-invasion assays for A673 cells depleted of EPHB2 (sh1 EPHB2 and sh2 EPHB2) compared to control cells (shCnt) (mean ± SD values of four and three technical replicates are shown for clonogenic and invasion assays, respectively). [One-way ANOVA test was used for statistical analysis of (A), (C), (D), (E), (G), and (H); $^{**}P \leq 0.01$; $^{****}P \leq 0.0001$.]

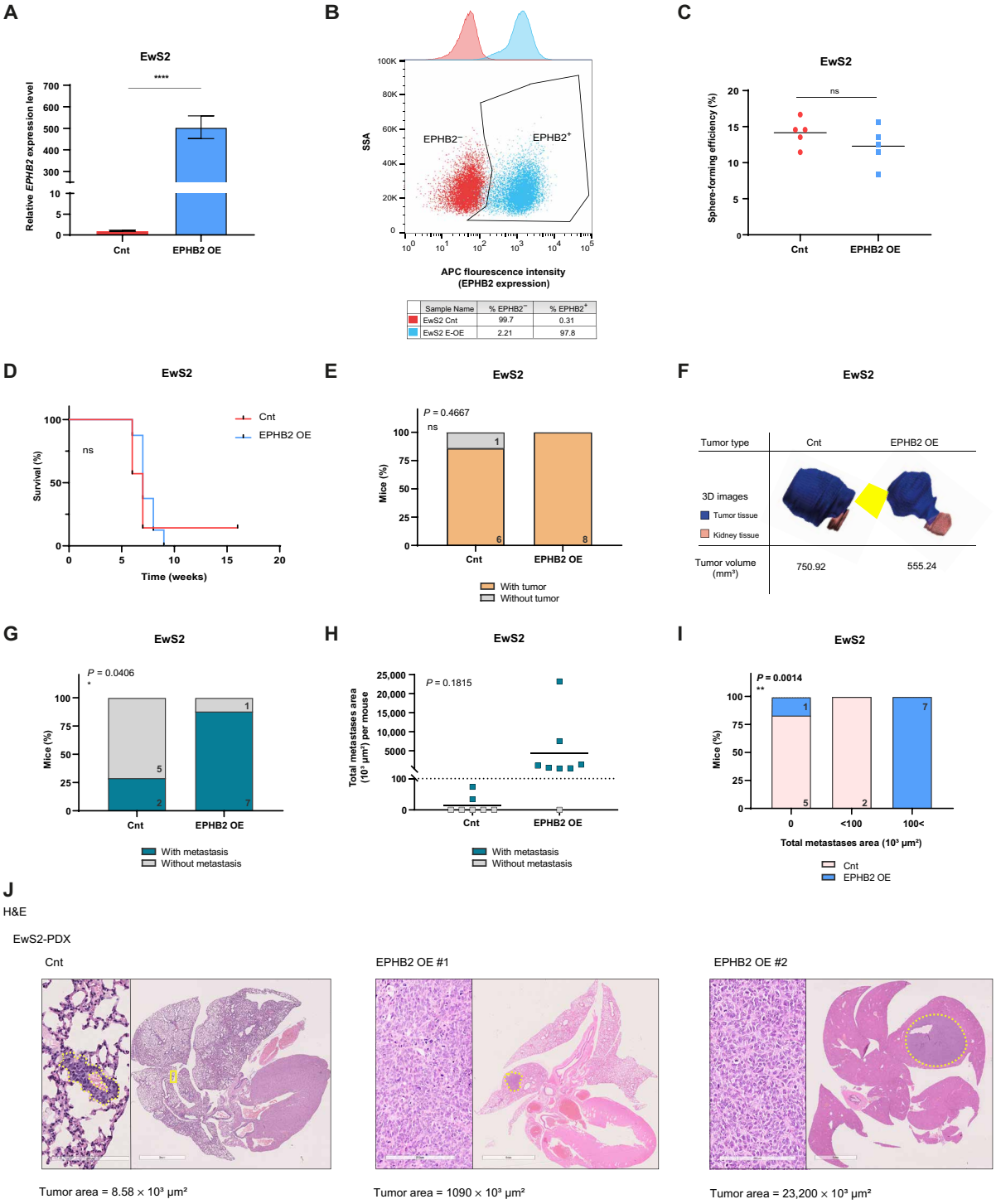

Fig. 7. EPHB2 overexpression increases EwS2 3D culture invasiveness. (**A**) qRT-PCR and (**B**) FACS assessment of EPHB2 expression in EwS2 cells overexpressing EPHB2 (EPHB2 OE) compared to control cells (Cnt). (**C**) Clonogenic assay of EwS2 EPHB2 OE and Cnt cells (mean ± SD values of five technical replicates are shown). (**D**) Survival of mice injected with EwS2 EPHB2 OE or EwS2 control 3D cultures (Cnt) (Cnt, $n = 7$; EPHB2 OE, $n = 8$). (**E**) Percentage of mice developing tumors following injection with the indicated EwS2 3D cultures (Cnt, $n = 7$; EPHB2 OE, $n = 8$). (**F**) Representative 3D sonography reconstruction images of EwS2 EPHB2 OE and EwS2 Cnt tumors. (**G**) Overexpression of EPHB2 significantly increased metastasis of EwS2 cells (Cnt, $n = 7$; EPHB2 OE, $n = 8$). (**H**) The total area of EwS2 metastases per mouse increased as a result of EPHB2 overexpression (mean ± SD. Cnt, $n = 7$; EPHB2 OE, $n = 8$). (**I**) Mice injected with EwS2 EPHB2 OE had a significantly higher metastatic burden than mice injected with control EwS2 cells (Cnt, $n = 7$; EPHB2 OE, $n = 8$). (**J**) Representative H&E sections of lung and liver metastases in mice injected with EwS2 EPHB2 OE compared to animals injected with control EwS2 cells (scale bars, Cnt: 200 µm, 3 mm; EPHB2 OE#1: 200 µm, 4 mm; EPHB2 OE#2: 200 µm, 5 mm). [One-way ANOVA test was used to perform the statistical analysis of (A), (C), and (H); log-rank (Mantel-Cox) was used for (D); and chi-square (Fisher's exact test) was used for (E), (G), and (I). ns, not significant; $*P \leq 0.05$, $**P \leq 0.01$, $****P \leq 0.0001$.]

DISCUSSION

Elucidation of the biological properties of cells responsible for tumor initiation, maintenance, and progression is key for the development of effective cancer therapies. However, in most cancer types, identification of these cells has been limited by reliance on predefined, largely nonspecific cell surface markers (*27*). Although helpful in uncovering subpopulations of cells enriched in those endowed with pluripotency and tumor-initiating ability, currently used markers fall short of accurately identifying the cells that actually display such properties. To overcome these limitations and isolate cells that represent the driving force of tumorigenesis, we developed a functional reporter assay, using as a model, EwS, in which a small fraction of cells display pluripotency and hold at least part of the responsibility for tumor initiation and phenotypic heterogeneity (*21*, *22*).

In EwS (*16*–*18*), and probably most pediatric cancers (*28*–*32*), cellular heterogeneity is generated primarily by epigenetic forces, which include histone modifications, DNA methylation, and miRNA expression. Because they are key players in the fine-tuning of cancer cell phenotypes by regulating pluripotency and differentiation, miRNAs are well suited to generate powerful candidate reporter systems. The level of their expression may not only be a reliable reflection of cell phenotypes that are pertinent to aggressive or indolent tumor behavior but also associate with gene expression networks that contribute to that behavior and help identify the relevant genes. On the basis of the dynamics of its expression according to the degree of tumor cell pluripotency or differentiation, we selected miR-145 to generate a reporter designed to reflect a spectrum of cancer cell phenotypes and identify those of interest. Using the reporter to target cells with low miR-145 expression in EwS, we identified highly tumorigenic subpopulations with metastatic properties.

Of the small number of deregulated genes shared by miR-145^{low} cell subpopulations from two independent primary tumors, *EPHB2* appeared immediately relevant, as its expression is associated with poor prognosis in EwS according to existing databases. The expression pattern was divergent between our two 3D culture models, being relatively diffuse in EwS1, which was derived from a metastatic tumor, but limited to only a small number of cells in EwS2, obtained from a primary tumor. Reminiscent of their tumors of origin, EwS1 formed macroscopic metastases following subcapsular renal injection of NSG mice, whereas EwS2 formed micrometastases composed of only a small number of cells, preferentially located around blood vessels in the lung and contralateral kidney in a fraction of mice. Overexpression of EPHB2 in EwS2 cells drove them to form macrometastases in several organs, providing a clear indication that EPHB2 expression participates in driving EwS metastatic proclivity.

EPHB2 expression is associated with the development and progression of diverse tumor types (*33*–*35*) and may facilitate metastasis by enhancing angiogenesis (*36*), modifying tumor cell adhesion and migration (*35*, *37*) and promoting invasion (*38*). Our present observations raise the possibility that the level of EPHB2 expression among metastatic tumor cells may determine their emergence from dormancy and/or adaption to the newly colonized microenvironment.

Our study suggests that diverse and complementary approaches may be required to dissect tumor heterogeneity at a functional level. Single-cell studies of EwS suggested that fluctuations in *EWSR1-FLI1* expression levels might underlie diverse biological properties among tumor cell subpopulations, including proliferation and metastatic proclivity (*39*, *40*). These observations, coupled to the notion that *EWSR1-FLI1* is a miR-145 target (*18*), would be consistent with variable EWS-FLI-1 expression levels as an explanation for the differences in tumorigenic behavior of GFP$^+$ and GFP$^-$ populations within our primary models. However, our comparative gene expression analysis of EWS-FLI-1 targets and GFP$^+$/GFP$^-$ signatures did not support this hypothesis. The absence of a clear miR-145 target gene signature in the differential transcriptional profile between GFP$^+$ and GFP$^-$ cells suggests that complex transcriptional programs, to which miR-145 expression is associated, govern the biological properties of these subpopulations and underlie their phenotypes. In support of this notion, expression of the miR-145 target *SOX2*, an important player in cell pluripotency, was elevated in GFP$^+$ cells. EPHB2, on the other hand, is not a miR-145 target but rather an effector component of the expression profile of EwS cells with low miR-145 levels, which in turn reflects a cellular phenotype associated with high metastatic proclivity.

A potential limitation of the present study is the use of only two primary tumor-derived EwS 3D cultures. Generation of primary 3D cultures from sarcomas, and EwS in particular, has been challenging, which explains the small number of currently available 3D EwS cultures. However, we confirmed our observations using two established cell lines grown as spheroids. Another limitation is the current lack of pharmacological inhibitors of the EPHB2 receptor, which restricted our assessment of the effect of its inhibition to observations based on its shRNA-mediated depletion. Given that EPHB2 is an RTK, however, development of pharmacological inhibitors should be possible.

These limitations notwithstanding, we have shown that combining a miRNA-based functional reporter system with primary tumor 3D culture technology provides a powerful and reliable method to isolate and characterize tumor cells that display aggressive behavior, including the formation of metastasis. MirRep145 allowed us to identify EPHB2 as a mediator of EwS metastasis that can be used both as a predictor of tumor behavior and as a potential therapeutic target to eliminate the most aggressive cells. The instructive role of miR-145 in cell fate transitions during cancer initiation and progression supports our strategy as an unbiased approach to explore and target tumor heterogeneity in diverse cancer types without the requirement of a predefined marker.

MATERIALS AND METHODS

Plasmid construction

Tet-On inducible mirReporter expression vectors were constructed using the Gateway LR Clonase II Enzyme Mix (Thermo Fisher Scientific). pINDUCER20 (Addgene, #44012) and pENTR/D-TOPO (Thermo Fisher Scientific) were the destination and entry vectors, respectively.

The coding sequence of enhanced GFP (EGFP) was amplified by PCR using pcDNA3-EGFP (Addgene, #13031) as template and EGFP-F and EGFP-R primers. The amplified EGFP cDNA sequence, which included a 3′UTR containing three miR-145 recognition sites, was cloned into the Bst BI and Mlu I restriction sites of the pLIV lentiviral vector (*23*). An EGFP cDNA containing five miR-145 recognition sites was subsequently generated by inserting two more miR-145 target sequences (oligo DNA A and oligo DNA B; table S4) into the Mlu I and Bam HI cloning site in the pLIV-EGFP vector containing the three miR-145 target sequence repeats. The resulting sequence was PCR-amplified using the primer pairs TOPO-F and TOPO-R (table S4), and the PCR product was cloned into the

pENTR/D-TOPO plasmid for subsequent pInducer20 gateway cloning. The target sequence of hs-mir-145-5p was obtained from the online tool mirbase.org (MIMAT0000437). MirReporter-Control was created by replacing the hs-mir-145-5p target sequence with the 3′UTR sequence of glyceraldehyde-3-phosphate dehydrogenase [National Center for Biotechnology Information (NCBI) Reference Sequence: NM_001256799.3; sequence position: 1186-1313].

The dual-color mirReporter–miR-145 vector was obtained by replacing the neomycin cassette and the internal ribosome entry site sequence with the coding sequence of rPuro and the EF (elongation factor)-1α promoter, respectively. The double-stranded synthetic DNA fragment (IDT) containing the rPuro coding sequence taken from the pLV-mir-control plasmid (catalog no. mir-p000, Biosettia) was inserted into the Nde I and Ssp I cloning site of mirReporter-145. Next, a DNA synthetic fragment (IDT) bearing the EF-1α promoter sequence was cloned into the Nde I and Spf I site. The synthetic DNA fragment sequences are available upon request.

Establishment of primary tumor 3D cultures and cell culture

EwS tumor samples were obtained from consenting patients with the approval of the ethics committee of the Canton de Vaud (Authorization No. 260/15). Primary tumor 3D cultures were established following immediate mechanical and enzymatic dissociation of the tumor samples. Red blood cells (RBCs) were removed using RBC lysis buffer (Miltenyi Biotec), and tumor cells were resuspended in Iscove's modified Dulbecco's medium (Gibco) containing KO serum (20%; Gibco), recombinant human EGF (10 ng/ml; Invitrogen), recombinant human FGF (10 ng/ml; Invitrogen), and penicillin-streptomycin (1%; Gibco) in ultralow attachment flasks (Corning). Once established, tumor cell 3D cultures were disrupted into single-cell suspensions manually with a P1000 pipette, and early passages were cryopreserved. EwS1 and EwS2 cultures were passaged every 7 and 4 days, respectively. In this study, EwS1 and EwS2 3D cultures ranged between passages 4 to 15 and 15 to 30, respectively.

HeLa cells [American Type Culture Collection (ATCC)] and A673 cells (ATCC) were cultured in Dulbecco's modified Eagle's medium (DMEM) (Gibco) whereas RD-ES cells (ATCC) were grown in RPMI (Gibco) supplemented with fetal bovine serum (FBS) (10%, PAN-Biotech) and penicillin-streptomycin (1%; Gibco). Human embryonic kidney (HEK) 293T cells (ATCC) were cultured in DMEM (Gibco) supplemented with FBS (10%; PAN-Biotech), MEM nonessential amino acid (Gibco), and penicillin-streptomycin (1%; Gibco). Cell cultures were maintained at 37°C in humidified, 5% CO_2 chambers. Spheroids of A673 and RD-ES cells were grown in ultralow attachment plates (Corning) and used in clonogenic and Matrigel-invasion assays.

Lentiviral infection and in vitro induction

For lentiviral production, HEK 293T cells (ATCC) were transfected using FuGENE 6 Transfection Reagent (Promega). pMD2G (Addgene, #12259) and pCMVΔR8.74 (Addgene, #12263) vectors were used as envelope and packaging plasmids, respectively. Lentiviral harvest was performed using Lenti-X Concentrator (TAKARA). Single-cell suspensions from primary EwS 3D cultures were infected with lentivirus expressing mirReporter-Control, mirReporter–miR-145, or dual-color mirReporter–mir-145. HeLa cells were infected for overexpression of mock-miRNA-rPuro (catalog no. mir-p000, Biosettia), mir-let7a-rPuro (catalog no. mir-p001, Biosettia), and mir-145-rPuro (catalog no. mir-p116, Biosettia). Transduced cells were selected by geneticin (1 mg/ml; Gibco) and puromycin (1 μg/ml; Invivogen) for 7 and 3 days, respectively, before further analysis.

EPHB2 depletion was achieved using pLKO.1 lentiviral shRNAs purchased from the RNAi Consortium (sh1 ref.: TRCN0000006423; sh2 ref.: TRCN0000006425), and sgRNAs targeting *EPHB2* (CR-E1, CR-E2, and CR-E3) were designed using the online CRISPR tool box CHOPCHOP (*41*) and cloned into the lentiCRISPRv2 vector. sgRNA target sequences were as follows: CR-E1: ACCAAGTTTATCCGG-CGCCGTGG; CR-E2: AGAAGACACGCACGGCGATGAGG; and CR-E3: GTCCGGCTGGGACCACGACA-GGG. In EPHB2 knockdown studies, control cells were infected with shRNA or sgRNA sequences targeting the GFP transcript (GCAAGCTGACCCT-GAAGTTCAT). For EPHB2 overexpression, a plasmid carrying EPHB2 cDNA sequence under the EF-1α promoter (catalog no. EX-E2379-Lv156) and its control plasmid expressing EGFP cDNA (catalog no. EX-EGFP-Lv156) were purchased from GeneCopoeia.

Light and fluorescent microscopy

Primary EwS 3D cultures were treated with Dox (100 ng/ml) (Sigma-Aldrich) for 48 hours and cultured for 10 days. Representative images were acquired using a Nikon Eclipse TS100 inverted epifluorescence microscope with ultraviolet lamp and filters set to 488 and 561 nm to detect GFP and RFP, respectively. HeLa cells seeded on coverslips (10 mm, VWR) were treated with Dox (1 μg/ml) for 48 hours. After fixation (4% formaldehyde, 10 min at room temperature) and mounting, slides were imaged by Zeiss Confocal Fluorescent Microscope LSM710 at 40×/1.30 numerical aperture oil immersion.

RNA extraction and real-time PCR

Total RNA extraction was performed using a miRCURYTM RNA Isaltion Kit (Exiqon). Five hundred nanograms of RNA template was used for cDNA synthesis (miRCURYTM LNA Universal RT miRNA PCR, Universal cDNA Synthesis Kit II, Exiqon).

Real-time PCR amplification was done using Power SYBR Green PCR Master Mix (Applied Biosystems) in a QuantStudio 5 System instrument (Thermo Fisher Scientific). PCR conditions included an initial holding period at 50°C for 2 min and 95°C for 10 min followed by 95°C for 15 s and 60°C for 1 min for 40 cycles. RNA LNA (Exiqon) primer sets were used for hsa-mir-145-5p and endogenous control Snord49a amplification. The EPHB2 primer pair was selected according to PrimerBank (http://pga.mgh.harvard.edu/primerbank) (PrimerBank ID: 111118977c1; table S4). Ribosomal protein lateral stalk subunit P0 transcript expression was used as the endogenous control (table S4). Relative quantitation of gene expression data was conducted according to the $2^{-\Delta\Delta Ct}$ method.

Flow cytometry

After 48 hours of Dox treatment, the culture medium of the induced cells was replaced with fresh medium and cells were kept in culture for 10 days [after 48-hour induction, halting Dox treatment at D0 (Day 0) and verifying GFP expression at D2, D5, and D10]. To assess EPHB2 levels, cells were labeled with APC (AlloPhycoCyanin) Mouse Anti-Human EPHB2 (BD Pharmingen). APC Mouse Immunoglobulin G1 (IgG1), K isotype antibody was used for control cell labeling. Calcein violet 450 acetoxymethyl (AM) (Thermo Fisher Scientific) labeling dye was used to detect live cells. The fluorescence intensity of GFP, violet AM, and APC was acquired by a Gallios (B43618, Beckman Coulter) cytometer with FL1, FL9, and FL6.

In vivo experiments, cell sorting, and tumor monitoring

All animal experiments were approved by the Animal Experimentation Ethics Committee of the Veterinary Service of the Canton of Vaud (Etat de Vaud, Service Vétérinaire), under authorization number VD2488.1. Ten thousand cells derived from dissociated EwS1 and EwS2 3D cultures in 20 µl of medium were injected beneath the renal capsule of 4- to 8-week-old, female NSG-KO mice. Tumor growth was monitored by ultrasound imaging using a 40-MHz probe and the Vevo 2100 ultrasound machine (VisualSonics). Tumor volumes were calculated by $V = 4/3\ p(\mathrm{Dd} \times \mathrm{Ds} \times \mathrm{Dt})/8$ (Dd: tumor height; Ds: tumor length in long axis; Dt: tumor length in short axis), and animals were euthanized when the tumor volume reached 1 cm^3. Mice received Dox (2 mg/ml) (Sigma-Aldrich) and 5% sucrose (Sigma-Aldrich) in drinking water starting 96 hours before sacrifice. After dissection, tumor fragments removed from each tumor bulk were fixed in 4% paraformaldehyde and processed for hematoxylin and eosin (H&E) staining and RNA ISH. The remaining tumor tissue was dissociated using a tumor dissociation kit (Miltenyi Biotec) by gentleMACS dissociator (Miltenyi Biotec). RBCs were removed by RBC lysis buffer (Miltenyi Biotec), and human tumor cells were enriched by depletion of mouse cells using a mouse cell depletion kit (Miltenyi Biotec). Before sorting GFP^+ and GFP^- cell populations by a Moflo Astrios EQ cell sorter (Beckman Coulter), dissociated tumor cells were treated with Calcein AM (Thermo Fisher Scientific) live-cell labeling dye and 4′,6-diamidino-2-phenylindole (DAPI) (Biotium) to remove dead cells. The sorted GFP^+ and GFP^- cell populations were injected beneath the renal capsule of NSG mice, and tumor growth was monitored by ultrasonography weekly.

Clonogenic and invasion assay

Spheroids generated from freshly dissociated patient-derived xenografts (PDX) and EwS cell lines A673 and RD-ES were sorted as single cells into 96-well plates (ultralow attachment; Corning) at one cell per well using a Moflo Astrios EQ cell sorter (Beckman Coulter). Calcein AM (Thermo Fisher Scientific) and DAPI (BIOTIUM) were used for live-cell detection. Sphere formation was monitored and scored 4 weeks after sorting.

Invasion assays were done according to the manufacturer's instructions (Corning Biocoat Matrigel Invasion Chamber). Briefly, 50,000 single cells were cultured in serum-free medium in the upper chamber of the transwell, whereas the lower chamber was filled with medium supplemented in KO serum. After 48 hours of culture, the cells in the upper chamber were removed and those in the lower layer of insert membranes were stained, and the membranes were mounted onto glass slides. Cells were counted using a Fiji-ImageJ program.

IHC and RNA ISH

Formalin-fixed, paraffin-embedded PDX tumors and mouse organs were sliced into 5-µm sections and subjected to standard H&E staining or IHC to detect GFP expression. RNAscope technology [Advanced Cell Diagnostics (ACD)] was used for RNA ISH according to the manufacturer's instructions as described previously (*42*). Briefly, tissue sections on slides were baked for 1 hour at 60°C, deparaffinized, and dehydrated. The tissues were pretreated with hydrogen peroxide for 10 min at room temperature and with target retrieval reagent for 15 min at 98°C. Protease Plus was then applied for 30 min at 40°C. EPHB2 probe (ACD) was hybridized for 2 hours at 40°C, followed by signal amplification. Tissue was counterstained with Gill's hematoxylin followed by mounting with VectaMount mounting media (Vector Laboratories). Images were taken with a Hamamatsu NanoZoomer S60 Digital slide scanner, at ×40 magnification.

Analysis of RNA sequencing data and relevance to survival

RNA sequencing (RNA-seq) library preparation was performed according to the Illumina TruSeq protocol by IGE3 genomic platform of University of Geneva. RNA-Seq was performed using HiSeq 4000 Illumina.

Reads were aligned to the human genome (NCBI-hg38) using hisat2 with default parameters. Gene-level counts for each sample were obtained with featureCounts against the hg38 RefSeq transcriptome. DeSeq2 was used to determine genes differentially expressed between GFP^+ and GFP^- cells, correcting for tumor 3D culture of origin and type of reporter. Differentially expressed genes were defined by $|\mathrm{logFC}| > 1$ and nominal P value < 0.01.

Five microarray datasets of primary EwS [GEO accession numbers: GSE12102 (*43*), GSE17618 (*44*), GSE34620 (*45*), and GSE63155 and GSE63156 (*46*)] were combined into a single dataset using the brainarray CDFs (Chip Definition Files) and ComBat from the sva package to remove batch effects. Normalization was performed with the SCAN.UPC package that provides a convenient interface for normalization with alternative CDFs and batch correction with ComBat.

For the differentially expressed genes for which expression data from the integrated dataset were available, we performed two types of survival analysis: Cox univariate analysis using expression as a continuous variable and Kaplan-Meier analysis after dividing the samples in two groups. [The median expression of *EPHB2* was used as the cutoff to divide the patients ($n = 129$) into high ($n = 64$) and low ($n = 65$) expressors.]

The heatmap in Fig. 4A shows, for all differentially expressed genes for which Cox univariate analysis was performed, the logarithmic fold change in the two primary tumor 3D cultures [difference in log2(RPKM + 1) between GFP^+ and GFP^- cells, averaged over all experiments on each tumor 3D culture] and the Cox z value. Up-regulated (down-regulated) genes are ordered by decreasing (increasing) Cox z.

Overlaps of differentially expressed genes with gene lists obtained from the literature or databases were statistically assessed using Fisher's exact test, with all genes analyzed by DeSeq2 as the universe. The list of direct EWS-FLI1 targets was obtained from (*42*), while predicted targets of miRNAs were obtained from TargetScan through the targetscan.Hs.eg.db Bioconductor package. For miRNA targets, no overlap was significant after correcting for multiple testing (Benjamini-Hochberg false discovery rate).

Statistical analysis and software used

GraphPad Prism (version 7) program was used to generate graphs and to perform one-way analysis of variance (ANOVA), Student's t test, two-way ANOVA, and log-rank (Mantel-Cox) test analyses. Analyses of flow cytometry acquisition data were done by FlowJo (version 10) program. qRT-PCR data were collected by QuantStudio design and analyses software (version 1.4.2). IHC and RNA ISH images were analyzed by AperioImageScope (v12.1.0.5029) and NDP. View2 Viewing software (U12388-01). biorender.com and Adobe illustrator (2020) programs were used to create the figures. Bioinformatic analysis was performed with R and its packages "survival," "SCAN.upc" (*47*), "sva," "Rsubread" (*48*), and "DESeq2" (*49*).

SUPPLEMENTARY MATERIALS

Supplementary material for this article is available at http://advances.sciencemag.org/cgi/content/full/7/27/eabf9394/DC1

View/request a protocol for this paper from *Bio-protocol*.

REFERENCES AND NOTES

1. J. A. Magee, E. Piskounova, S. J. Morrison, Cancer stem cells: Impact, heterogeneity, and uncertainty. *Cancer Cell* **21**, 283–296 (2012).
2. E. Batlle, H. Clevers, Cancer stem cells revisited. *Nat. Med.* **23**, 1124–1134 (2017).
3. K. Hinohara, K. Polyak, Intratumoral heterogeneity: More than just mutations. *Trends Cell Biol.* **29**, 569–579 (2019).
4. S. Yuan, R. J. Norgard, B. Z. Stanger, Cellular plasticity in cancer. *Cancer Discov.* **9**, 837–851 (2019).
5. A. Marusyk, M. Janiszewska, K. Polyak, Intratumor heterogeneity: The Rosetta Stone of therapy resistance. *Cancer Cell* **37**, 471–484 (2020).
6. D. Nassar, C. Blanpain, Cancer stem cells: Basic concepts and therapeutic implications. *Annu. Rev. Pathol.* **11**, 47–76 (2016).
7. J. E. Visvader, G. J. Lindeman, Cancer stem cells: Current status and evolving complexities. *Cell Stem Cell* **10**, 717–728 (2012).
8. O. Kopper, C. J. de Witte, K. Lõhmussaar, J. E. Valle-Inclan, N. Hami, L. Kester, A. V. Balgobind, J. Korving, N. Proost, H. Begthel, L. M. van Wijk, S. A. Revilla, R. Theeuwsen, M. van de Ven, M. J. van Roosmalen, B. Ponsioen, V. W. H. Ho, B. G. Neel, T. Bosse, K. N. Gaarenstroom, H. Vrieling, M. P. G. Vreeswijk, P. J. van Diest, P. O. Witteveen, T. Jonges, J. L. Bos, A. van Oudenaarden, R. P. Zweemer, H. J. G. Snippert, W. P. Kloosterman, H. Clevers, An organoid platform for ovarian cancer captures intra- and interpatient heterogeneity. *Nat. Med.* **25**, 838–849 (2019).
9. N. Sachs, H. Clevers, Organoid cultures for the analysis of cancer phenotypes. *Curr. Opin. Genet. Dev.* **24**, 68–73 (2014).
10. M. Bleijs, M. van de Wetering, H. Clevers, J. Drost, Xenograft and organoid model systems in cancer research. *EMBO J.* **38**, e101654 (2019).
11. J. Drost, H. Clevers, Organoids in cancer research. *Nat. Rev. Cancer* **18**, 407–418 (2018).
12. D. Tuveson, H. Clevers, Cancer modeling meets human organoid technology. *Science* **364**, 952–955 (2019).
13. T. Z. Minas, D. Surdez, T. Javaheri, M. Tanaka, M. Howarth, H.-J. Kang, J. Han, Z.-Y. Han, B. Sax, B. E. Kream, S.-H. Hong, H. Çelik, F. Tirode, J. Tuckermann, J. A. Toretsky, L. Kenner, H. Kovar, S. Lee, E. A. Sweet-Cordero, T. Nakamura, R. Moriggl, O. Delattre, A. Üren, Combined experience of six independent laboratories attempting to create an Ewing sarcoma mouse model. *Oncotarget* **8**, 34141–34163 (2017).
14. N. Riggi, M. L. Suvà, I. Stamenkovic, Ewing's sarcoma. *N. Engl. J. Med.* **384**, 154–164 (2021).
15. O. Delattre, J. Zucman, B. Plougastel, C. Desmaze, T. Melot, M. Peter, H. Kovar, I. Joubert, P. de Jong, G. Rouleau, A. Aurias, G. Thomas, Gene fusion with an ETS DNA-binding domain caused by chromosome translocation in human tumours. *Nature* **359**, 162–165 (1992).
16. N. Riggi, B. Knoechel, S. M. Gillespie, E. Rheinbay, G. Boulay, M. L. Suvà, N. E. Rossetti, W. E. Boonseng, O. Oksuz, E. B. Cook, A. Formey, A. Patel, M. Gymrek, V. Thapar, V. Deshpande, D. T. Ting, F. J. Hornicek, G. P. Nielsen, I. Stamenkovic, M. J. Aryee, B. E. Bernstein, M. N. Rivera, EWS-FLI1 utilizes divergent chromatin remodeling mechanisms to directly activate or repress enhancer elements in Ewing sarcoma. *Cancer Cell* **26**, 668–681 (2014).
17. C. De Vito, N. Riggi, S. Cornaz, M.-L. Suvà, K. Baumer, P. Provero, I. Stamenkovic, A TARBP2-dependent miRNA expression profile underlies cancer stem cell properties and provides candidate therapeutic reagents in Ewing sarcoma. *Cancer Cell* **21**, 807–821 (2012).
18. N. Riggi, M.-L. Suvà, C. De Vito, P. Provero, J.-C. Stehle, K. Baumer, L. Cironi, M. Janiszewska, T. Petricevic, D. Suvà, S. Tercier, J.-M. Joseph, L. Guillou, I. Stamenkovic, EWS-FLI-1 modulates miRNA145 and SOX2 expression to initiate mesenchymal stem cell reprogramming toward Ewing sarcoma cancer stem cells. *Genes Dev.* **24**, 916–932 (2010).
19. N. Xu, T. Papagiannakopoulos, G. Pan, J. A. Thomson, K. S. Kosik, MicroRNA-145 regulates OCT4, SOX2, and KLF4 and represses pluripotency in human embryonic stem cells. *Cell* **137**, 647–658 (2009).
20. K. L. Meerbrey, G. Hu, J. D. Kessler, K. Roarty, M. Z. Li, J. E. Fang, J. I. Herschkowitz, A. E. Burrows, A. Ciccia, T. Sun, E. M. Schmitt, R. J. Bernardi, X. Fu, C. S. Bland, T. A. Cooper, R. Schiff, J. M. Rosen, T. F. Westbrook, S. J. Elledge, The pINDUCER lentiviral toolkit for inducible RNA interference in vitro and in vivo. *Proc. Natl. Acad. Sci. U.S.A.* **108**, 3665–3670 (2011).
21. M. L. Suva, N. Riggi, J.-C. Stehle, K. Baumer, S. Tercier, J.-M. Joseph, D. Suvà, V. Clément, P. Provero, L. Cironi, M.-C. Osterheld, L. Guillou, I. Stamenkovic, Identification of cancer stem cells in Ewing's sarcoma. *Cancer Res.* **69**, 1776–1781 (2009).
22. S. Cornaz-Buros, N. Riggi, C. DeVito, A. Sarre, I. Letovanec, P. Provero, I. Stamenkovic, Targeting cancer stem–like cells as an approach to defeating cellular heterogeneity in Ewing sarcoma. *Cancer Res.* **74**, 6610–6622 (2014).
23. T. Keskin, A. Bakaric, P. Waszyk, G. Boulay, M. Torsello, S. Cornaz-Buros, N. Chevalier, T. Geiser, P. Martin, A. Volorio, S. Iyer, A. Kulkarni, I. Letovanec, S. Cherix, G. M. Cote, E. Choy, A. Digklia, M. Montemurro, I. Chebib, P. G. Nielsen, A. M. Carcaboso, J. Mora, R. Renella, M. L. Suvà, C. Fusco, P. Provero, M. N. Rivera, N. Riggi, I. Stamenkovic, LIN28B underlies the pathogenesis of a subclass of Ewing sarcoma LIN28B control of EWS-FLI1 stability. *Cell Rep.* **30**, 4567–4583.e5 (2020).
24. E. B. Pasquale, Eph receptors and ephrins in cancer: Bidirectional signalling and beyond. *Nat. Rev. Cancer* **10**, 165–180 (2010).
25. M. Genander, J. Frisen, Ephrins and Eph receptors in stem cells and cancer. *Curr. Opin. Cell Biol.* **22**, 611–616 (2010).
26. J. Potratz, A. Tillmanns, P. Berning, E. Korsching, C. Schaefer, B. Lechtape, C. Schleithoff, R. Unland, K.-L. Schäfer, C. Müller-Tidow, H. Jürgens, U. Dirksen, Receptor tyrosine kinase gene expression profiles of Ewing sarcomas reveal ROR1 as a potential therapeutic target in metastatic disease. *Mol. Oncol.* **10**, 677–692 (2016).
27. T. Klonisch, E. Wiechec, S. Hombach-Klonisch, S. R. Ande, S. Wesselborg, K. Schulze-Osthoff, M. Los, Cancer stem cell markers in common cancers—Therapeutic implications. *Trends Mol. Med.* **14**, 450–460 (2008).
28. C. Kadoch, G. R. Crabtree, Reversible disruption of mSWI/SNF (BAF) complexes by the SS18-SSX oncogenic fusion in synovial sarcoma. *Cell* **153**, 71–85 (2013).
29. M. F. Roussel, J. L. Stripay, Epigenetic drivers in pediatric medulloblastoma. *Cerebellum* **17**, 28–36 (2018).
30. J. Gojo, B. Englinger, L. Jiang, J. M. Hübner, M. L. Shaw, O. A. Hack, S. Madlener, D. Kirchhofer, I. Liu, J. Pyrdol, V. Hovestadt, E. Mazzola, N. D. Mathewson, M. Trissal, D. Lötsch, C. Dorfer, C. Haberler, A. Halfmann, L. Mayr, A. Peyrl, R. Geyeregger, B. Schwalm, M. Mauermann, K. W. Pajtler, T. Milde, M. E. Shore, J. E. Geduldig, K. Pelton, T. Czech, O. Ashenberg, K. W. Wucherpfennig, O. Rozenblatt-Rosen, S. Alexandrescu, K. L. Ligon, S. M. Pfister, A. Regev, I. Slavc, W. Berger, M. L. Suvà, M. Kool, M. G. Filbin, Single-cell RNA-seq reveals cellular hierarchies and impaired developmental trajectories in pediatric ependymoma. *Cancer Cell* **38**, 44–59.e9 (2020).
31. C. Savary, A. Kim, A. Lespagnol, V. Gandemer, I. Pellier, C. Andrieu, G. Pagès, M.-D. Galibert, Y. Blum, M. de Tayrac, Depicting the genetic architecture of pediatric cancers through an integrative gene network approach. *Sci. Rep.* **10**, 1224 (2020).
32. M. G. Filbin, I. Tirosh, V. Hovestadt, M. K. L. Shaw, L. E. Escalante, N. D. Mathewson, C. Neftel, N. Frank, K. Pelton, C. M. Hebert, C. Haberler, K. Yizhak, J. Gojo, K. Egervari, C. Mount, P. van Galen, D. M. Bonal, Q. D. Nguyen, A. Beck, C. Sinai, T. Czech, C. Dorfer, L. Goumnerova, C. Lavarino, A. M. Carcaboso, J. Mora, R. Mylvaganam, C. C. Luo, A. Peyrl, M. Popović, A. Azizi, T. T. Batchelor, M. P. Frosch, M. Martinez-Lage, M. W. Kieran, P. Bandopadhayay, R. Beroukhim, G. Fritsch, G. Getz, O. Rozenblatt-Rosen, K. W. Wucherpfennig, D. N. Louis, M. Monje, I. Slavc, K. L. Ligon, T. R. Golub, A. Regev, B. E. Bernstein, M. L. Suvà, Developmental and oncogenic programs in H3K27M gliomas dissected by single-cell RNA-seq. *Science* **360**, 331–335 (2018).
33. R. A. Johnson, K. D. Wright, H. Poppleton, K. M. Mohankumar, D. Finkelstein, S. B. Pounds, V. Rand, S. E. S. Leary, E. White, C. Eden, T. Hogg, P. Northcott, S. Mack, G. Neale, Y. D. Wang, B. Coyle, J. Atkinson, M. DeWire, T. A. Kranenburg, Y. Gillespie, J. C. Allen, T. Merchant, F. A. Boop, R. A. Sanford, A. Gajjar, D. W. Ellison, M. D. Taylor, R. G. Grundy, R. J. Gilbertson, Cross-species genomics matches driver mutations and cell compartments to model ependymoma. *Nature* **466**, 632–636 (2010).
34. C. Goparaju, J. S. Donington, T. Hsu, R. Harrington, N. Hirsch, H. I. Pass, Overexpression of EPH receptor B2 in malignant mesothelioma correlates with oncogenic behavior. *J. Thorac. Oncol.* **8**, 1203–1211 (2013).
35. A. H. Sikkema, W. F. A. den Dunnen, E. Hulleman, D. G. van Vuurden, G. Garcia-Manero, H. Yang, F. J. G. Scherpen, K. R. Kampen, E. W. Hoving, W. A. Kamps, S. H. Diks, M. P. Peppelenbosch, E. S. J. M. de Bont, EphB2 activity plays a pivotal role in pediatric medulloblastoma cell adhesion and invasion. *Neuro Oncol.* **14**, 1125–1135 (2012).
36. S. Sato, S. Vasaikar, A. Eskaros, Y. Kim, J. S. Lewis, B. Zhang, A. Zijlstra, A. M. Weaver, EPHB2 carried on small extracellular vesicles induces tumor angiogenesis via activation of ephrin reverse signaling. *JCI Insight* **4**, e132447 (2019).
37. S. D. Wang, P. Rath, B. Lal, J.-P. Richard, Y. Li, C. R. Goodwin, J. Laterra, S. Xia, EphB2 receptor controls proliferation/migration dichotomy of glioblastoma by interacting with focal adhesion kinase. *Oncogene* **31**, 5132–5143 (2012).
38. S. Chukkapalli, M. Amessou, A. K. Dilly, H. Dekhil, J. Zhao, Q. Liu, A. Bejna, R. D. Thomas, S. Bandyopadhyay, T. A. Bismar, D. Neill, L. Azoulay, G. Batist, M. Kandouz, Role of the EphB2 receptor in autophagy, apoptosis and invasion in human breast cancer cells. *Exp. Cell Res.* **320**, 233–246 (2014).
39. M.-M. Aynaud, O. Mirabeau, N. Gruel, S. Grossetête, V. Boeva, S. Durand, D. Surdez, O. Saulnier, S. Zaïdi, S. Gribkova, A. Fouché, U. Kairov, V. Raynal, F. Tirode, T. G. P. Grünewald, M. Bohec, S. Baulande, I. Janoueix-Lerosey, J.-P. Vert, E. Barillot, O. Delattre, A. Zinovyev, Transcriptional programs define intratumoral heterogeneity of Ewing sarcoma at single-cell resolution. *Cell Rep.* **30**, 1767–1779.e6 (2020).
40. G.-A. Franzetti, K. Laud-Duval, W. van der Ent, A. Brisac, M. Irondelle, S. Aubert, U. Dirksen, C. Bouvier, G. de Pinieux, E. Snaar-Jagalska, P. Chavrier, O. Delattre, Cell-to-cell

heterogeneity of EWSR1-FLI1 activity determines proliferation/migration choices in Ewing sarcoma cells. *Oncogene* **36**, 3505–3514 (2017).
41. K. Labun, T. G. Montague, M. Krause, Y. N. Torres Cleuren, H. Tjeldnes, E. Valen, CHOPCHOP v3: Expanding the CRISPR web toolbox beyond genome editing. *Nucleic Acids Res.* **47**, W171–W174 (2019).
42. T. Keskin, A. Bakaric, P. Waszyk, G. Boulay, M. Torsello, S. Cornaz-Buros, N. Chevalier, T. Geiser, P. Martin, A. Volorio, S. Iyer, A. Kulkarni, I. Letovanec, S. Cherix, G. M. Cote, E. Choy, A. Digklia, M. Montemurro, I. Chebib, P. G. Nielsen, A. M. Carcaboso, J. Mora, R. Renella, M. L. Suvà, C. Fusco, P. Provero, M. N. Rivera, N. Riggi, I. Stamenkovic, LIN28B underlies the pathogenesis of a subclass of Ewing sarcoma. *Cell Rep.* **31**, 107539 (2020).
43. K. Scotlandi, D. Remondini, G. Castellani, M. C. Manara, F. Nardi, L. Cantiani, M. Francesconi, M. Mercuri, A. M. Caccuri, M. Serra, S. Knuutila, P. Picci, Overcoming resistance to conventional drugs in Ewing sarcoma and identification of molecular predictors of outcome. *J. Clin. Oncol.* **27**, 2209–2216 (2009).
44. S. Postel-Vinay, A. S. Véron, F. Tirode, G. Pierron, S. Reynaud, H. Kovar, O. Oberlin, E. Lapouble, S. Ballet, C. Lucchesi, U. Kontny, A. González-Neira, P. Picci, J. Alonso, A. Patino-Garcia, B. B. de Paillerets, K. Laud, C. Dina, P. Froguel, F. Clavel-Chapelon, F. Doz, J. Michon, S. J. Chanock, G. Thomas, D. G. Cox, O. Delattre, Common variants near TARDBP and EGR2 are associated with susceptibility to Ewing sarcoma. *Nat. Genet.* **44**, 323–327 (2012).
45. S. Savola, A. Klami, S. Myllykangas, C. Manara, K. Scotlandi, P. Picci, S. Knuutila, J. Vakkila, High expression of complement component 5 (*C5*) at tumor site associates with superior survival in Ewing's sarcoma family of tumour patients. *ISRN Oncol.* **2011**, 168712 (2011).
46. S. L. Volchenboum, J. Andrade, L. Huang, D. A. Barkauskas, M. Krailo, R. B. Womer, A. Ranft, J. Potratz, U. Dirksen, T. J. Triche, E. R. Lawlor, Gene expression profiling of Ewing sarcoma tumors reveals the prognostic importance of tumor-stromal interactions: A report from the Children's Oncology Group. *J. Pathol. Clin. Res.* **1**, 83–94 (2015).
47. S. R. Piccolo, Y. Sun, J. D. Campbell, M. E. Lenburg, A. H. Bild, W. E. Johnson, A single-sample microarray normalization method to facilitate personalized-medicine workflows. *Genomics* **100**, 337–344 (2012).
48. Y. Liao, G. K. Smyth, W. Shi, The R package Rsubread is easier, faster, cheaper and better for alignment and quantification of RNA sequencing reads. *Nucleic Acids Res.* **47**, e47 (2019).
49. M. I. Love, W. Huber, S. Anders, Moderated estimation of fold change and dispersion for RNA-seq data with DESeq2. *Genome Biol.* **15**, 550 (2014).

Acknowledgments: We thank A.-C. Clerc of the Cardiovascular Assessment Facility for ultrasonography analysis, and the Cellular Imaging, Flow Cytometry, Mouse Pathology and Animal Facilities of UNIL, as well as the UNIGE IGE3 genomic platform for their support. **Funding:** This work was supported by Swiss National Science Foundation grant 310030-169563 (to I.S.), FNS Sinergia grant CRSII5-177266 (to I.S.), Swiss Cancer League grant KLS-4249-08-2017-R (to I.S.), Swiss National Science Foundation Professorship grant PP00P3-157468/1 (to N.R.), Swiss National Science Foundation Professorship grant PP00P3_183724 (to N.R.), Swiss Cancer League grant KFS-3973-08-2016 (to N.R.), Swiss Cancer League grant KFS4859-08-2019 (to N.R.), the Fond'Action Contre le Cancer Foundation (to N.R.), the FORCE Foundation (to N.R.), the Fondation Emma Muschamp (to N.R.), and National Science Foundation Graduate Research Fellowship DGE1745303 (to E.M.P.). **Author contributions:** Conception and design: C.F., N.R., and I.S. Investigation and methodology: T.K., S.C.-B., B.R., L.B., and P.M. Data analysis: T.K., K.C., E.M.P., P.P., and N.R. Visualization: T.K. and P.P. Resources: I.L., S.L.R., S.C., M.D., R.R., M.L.S., N.R., and I.S. Writing, review, and editing: T.K., N.R., and I.S. Study supervision: C.F., N.R., and I.S. Funding acquisition: N.R. and I.S. **Competing interests:** The authors declare that they have no competing interests. **Data and materials availability:** All data needed to evaluate the conclusions in the paper are present in the paper and/or the Supplementary Materials. Gene expression data generated in this project are available for the Gene Expression Omnibus repository under accession number GSE163699.

Submitted 30 November 2020
Accepted 21 May 2021
Published 2 July 2021
10.1126/sciadv.abf9394

Citation: T. Keskin, B. Rucci, S. Cornaz-Buros, P. Martin, C. Fusco, L. Broye, K. Cisarova, E. M. Perez, I. Letovanec, S. La Rosa, S. Cherix, M. Diezi, R. Renella, P. Provero, M. L. Suvà, I. Stamenkovic, N. Riggi, A live single-cell reporter assay links intratumor heterogeneity to metastatic proclivity in Ewing sarcoma. *Sci. Adv.* **7**, eabf9394 (2021).

ScienceAdvances

A live single-cell reporter assay links intratumor heterogeneity to metastatic proclivity in Ewing sarcoma

Tugba Keskin, Beatrice Rucci, Sandrine Cornaz-Buros, Patricia Martin, Carlo Fusco, Liliane Broye, Katarina Cisarova, Elizabeth M. Perez, Igor Letovanec, Stefano La Rosa, Stephane Cherix, Manuel Diezi, Raffaele Renella, Paolo Provero, Mario L. Suvà, Ivan Stamenkovic and Nicolò Riggi

Sci Adv **7** (27), eabf9394.
DOI: 10.1126/sciadv.abf9394